July 2018

Polymeric Peptide Mimics for Protein Delivery

Coralie Backlund

POLYMERIC PEPTIDE MIMICS FOR PROTEIN DELIVERY

A Dissertation Presented

by

CORALIE M. BACKLUND

Submitted to the Graduate School of the
University of Massachusetts Amherst in partial fulfillment
of the requirements for the degree of

DOCTOR OF PHILOSOPHY

May 2018

Polymer Science & Engineering

POLYMERIC PEPTIDE MIMICS FOR PROTEIN DELIVERY

A Dissertation Presented

by

CORALIE M. BACKLUND

Approved as to style and content by:

_____
Gregory N. Tew, Chair

_____
Lisa M. Minter, Member

_____
Murugappan Muthukumar, Member

_____
Shelly R. Peyton, Member

_____
E. Brian Coughlin, Department Head
Polymer Science & Engineering

DEDICATION

For my grandpa, Carl Geiser

The more you know, the more you are able to know.

ACKNOWLEDGMENTS

First and foremost, I would like to acknowledge my advisor Greg Tew for his support and guidance through my PhD. I appreciate the scientific freedom and many opportunities both at UMass and abroad that you afforded me. Additionally, I would like to thank Lisa Minter for her support in my struggles to learn more about the interface of materials and immunology. A special thanks to Muthu for continuously reminding me that science should be fun. I would also like to thank Shelly Peyton for inspiring me to achieve a higher level of science and a better understanding of the biological systems I work with.

This thesis is based on collaborations with the Futaki lab at Kyoto University in Japan, who made me feel at home in a foreign country and taught me new molecular biology techniques. A second set of collaborations with the Andresen lab at Denmark's Technical University allowed me to explore a new application, while also learning about a different academic system. My thesis would be incomplete without the support I received from both of these collaborations.

I would like to acknowledge my family for being there to listen to all of the ups and downs of PhD life and their continued support through this adventure. To my room mates, groupmates, and friends here at UMass and abroad, thank you for being a resource for both science and inspiration. Lastly, I would like to thank Thomas who has helped me keep it together for the last six years.

ABSTRACT

POLYMERIC PEPTIDE MIMICS FOR PROTEIN DELIVERY

MAY 2018

CORALIE M. BACKLUND, B.S., OREGON STATE UNIVERSITY

M.A., UNIVERSITY OF MASSACHUSETTS AMHERST

Ph.D., UNIVERSITY OF MASSACHUSETTS AMHERST

Directed by: Professor Gregory N. Tew

The plasma membrane is a major obstacle in the development and use of biomacromolecules for intracellular applications. Consequently, proteins with intracellular targets represent an enormous, yet under studied avenue for therapeutics. Extended research has aimed at facilitating intracellular delivery of exogenous proteins using protein transduction domains (PTDs), which allow transport of bioactive molecules into cells. Synthetic polymers, inspired by PTDs, provide a well-controlled platform to vary molecular architecture for structure activity relationship studies. Specifically, this thesis focuses on the use of ring-opening metathesis, a facile and efficient polymerization technique, through which we can vary structural parameters to optimize delivery of non-covalently encapsulated proteins. The aim was to characterize, optimize, and utilize PTD mimics (PTDMs) for functional protein delivery. Fluorescently labeled cargo were used to elucidate the predominant cellular entry mechanism for the PTDMs and were compared to their ability to deliver protein into cells. A series of polymers was designed around the most membrane active polymers to explore the incorporation of guanidine and hydrophobic moieties, yielding a PTDM capable of high protein delivery into a variety of cell types. The PTDM was then explored for use as a vaccine delivery reagent into immune cells. The

ability to have a specific response with the cargo of interest verifies cytosolic delivery using the PTDMs and provides valuable insight into their use to affect intracellular pathways.

TABLE OF CONTENTS

LIST OF TABLES

LIST OF FIGURES

GLOSSARY

7-AAD	7-Amino-actinomycin D
APC	Antigen Presenting cell
BMDC	Bone Marrow Dendritic Cell
CD11c	Dendritic cell surface marker
CD209	DC-sign: dendritic cell surface marker
CD4 T cell	Helper T cell
CD40	Surface marker on APCs
CD8 T cell	Cytotoxic T cell
CD80	Costimulatory surface marker on APCs
CD86	Costimulatory surface marker on APCs
CLSM	Confocal Laser Scanning Microscopy
CpG	TLR-9 agonist
CPP	Cell penetrating peptide
CPPM	Cell penetrating peptide mimic
CTL	Cytotoxic T Lymphocyte
DC	Dendritic Cell
DCM	Dichloromethane
dG	Di-guandine monomer
DMAP	4-Dimethylamnopryridine
dMe	Di-methyl monomer
DMF	N,N-dimethylformamide
DMSO	Dimethyl sulfoxide
DNA	Deoxyribonucleic Acid
dPh	Di-phenyl monomer
EDC	1-ethyl-3-(3-dimethylaminopropyl) carbodiimide
EGFP	Enhanced Green Fluorescent Protein
FBS	Fetal Bovine Serum
FSC	Forward Scatter
G3	Grubb's 3rd generation catalyst
GFP	Green Fluorescent Protein
GPC	Gel permeation chromatography
H-2K^b	Antibody against presentation of SIINFEKL in MHC I
HLA-DR	Human MHC class II subtype
iDC	Immature Dendritic Cell
IFN	Interferon
IL	Interleukin
LPS	Lipopolysaccharide

MeG	Methyl-guanidine monomer
MePh	Methyl-phenyl monomer
MFI	Median Fluorescence Intensity
MHC	Major Histocompatibility Complex
MHC class I	Present on every cell type, interacts with CD8 T cells
MHC class II	Only presented on APCs, interacts with CD4 T cells
MSC	Mesenchymal Stem Cells
NMR	Nuclear Magnetic Resonance
OVA	Ovalbumin
PBS	Phosphate Buffered Saline
PTD	Protein Transduction Domain
PTDM	Protein Transduction Domain Mimic
R9/R8	Nona-arginine, octarginine
RBCs	Red Blood Cells
ROMP	Ring-Opening Metathesis Polymerization
SEM	Standard Error of the Mean
SIINFEKL	MHC Class I specific Antigen from Ovalbumin
SSC	Side Scatter
TFA	Trifluoroacetic acid
THF	Tetrahydrofuran
THP-1	Human Monocyte Cell Line
TLR	Toll Like Receptor
TNF	Tumor Necrosis Factor

CHAPTER 1

INTRACELLULAR DELIVERY OF FUNCTIONAL PROTEINS

1.1 Introduction

Proteins and antibodies have the capacity to perform specific and complex functions making them promising candidates to probe molecular pathways within cells. Most proteins that would facilitate these specific interactions are generally incapable of passive diffusion across the cell membrane due to their size and polarity. Additionally, physical and chemical changes extracellularly and intracellularly can alter a proteins function *via* hydrolysis, oxidation, proteolysis, and denaturation.[1] To address these issues, a wide variety of delivery methods and vehicles have been designed for transporting and protecting these complex cargos.

Historically, introducing exogenous protein into the cell has been accomplished indirectly by delivering DNA that will express the protein of interest into the cell or by controlling protein synthesis through the delivery of RNA.[2] Despite the utility of these approaches, direct protein delivery has several advantages over recombinant genetic approaches. Instead of genetically manipulating cells to express a protein of interest, which can result in random insertion and mutation of endogenous genes, protein delivery allows for temporal control into specific areas of the cell. The delivery of proteins like Cre recombinase and the CRISPR-Cas9 system allow for specific gene editing with high specificity and low toxicity.[3,4] The transient nature of the protein within the cell also means that the amount of protein and its function can be controlled and is not indefinite. In comparison with small molecule drugs, the targeted effect can be exceptionally specific, such as in the case of using antibodies to promote or interrupt intracellular pathways.[5]

Currently, the overarching term attributed to methods of protein delivery is transduction which is rooted in its use for viral delivery of genetic material. While the field of protein transduction began with the use of physical membrane disruption such as electroporation and microinjection, it has shifted more towards the use of lipids, peptides, and synthetic nanocarriers to facilitate the transport of proteins across the membrane.[6] Additionally, a variety of inorganic carriers are also being developed as theranostic delivery reagents.[7–9] An overview of these methods is provided, with specific attention on their ability to deliver functional proteins into cells.

The major design principles of nanocarriers are three-fold: they need to (a) package and protect cargo, (b) deliver the protein intracellularly, and (c) release payload with appropriate spatiotemporal dynamics. One of the major areas of debate for transduction is the mechanism through which these carriers cross the membrane.[6,10,11] The mechanism of cellular entry directly dictates the availability of the cargo within the cell. If most of the nanocarrier assemblies are taken up through endocytosis, the cargo must overcome the endosomal membrane before being readily available in the cytosol or nucleus.

The field of nanocarriers is extremely complex and correct definitions of each carrier type are essential for comparing to other systems within the same class and for the translation of essential concepts to the next generation of carriers.[12] Here, we propose classification guidelines to help define carrier types. Although some overlap between the different categories is possible, as indicated in Figure 0.1, usually the distinction is clear enough to choose a predominant label.

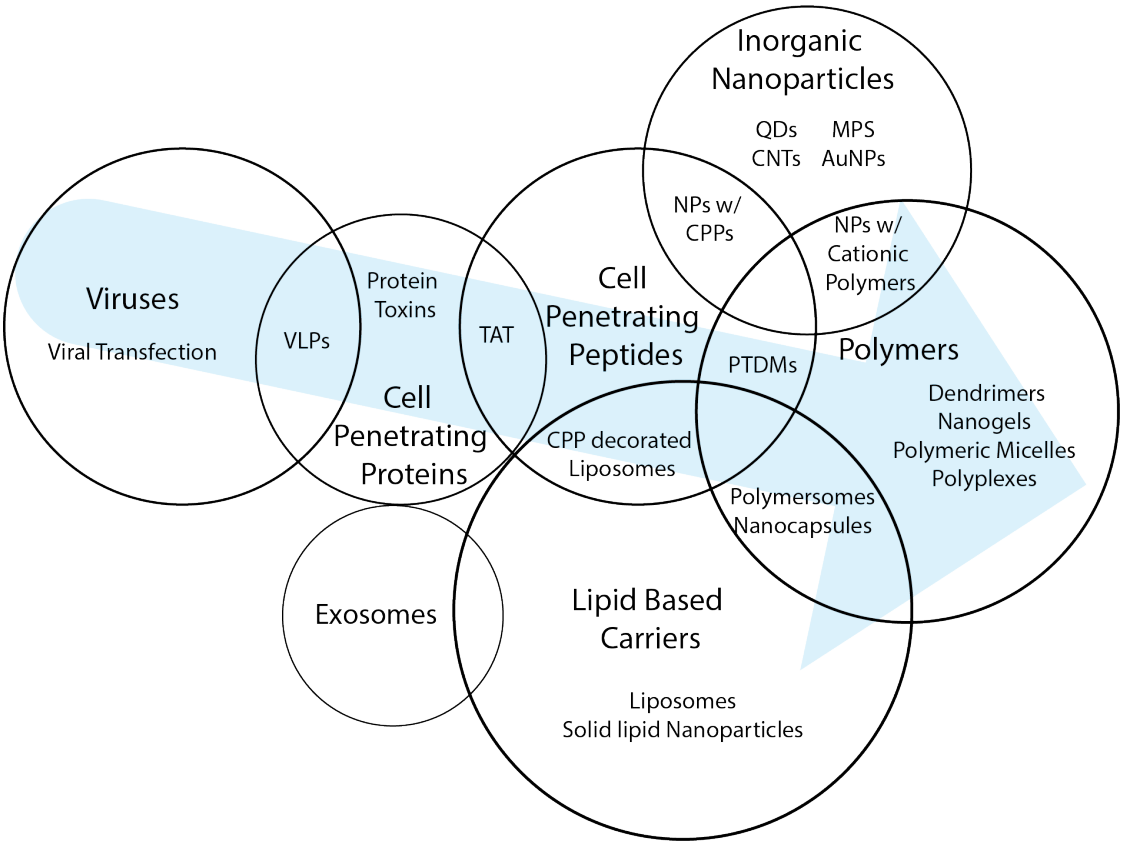

Figure 0.1. Categorization and progression of nanocarrier based protein delivery from viral transfection to synthetic nanocarriers. The circumference of the circle roughly indicates the volume of research directed toward protein delivery.

The scope of this introduction is to explore the methods that facilitate the transport of functional proteins across the cell membrane with special attention to nanocarrier types. While many methods explore protein delivery using fluorescently labeled cargo, the focus here is largely on *in vitro* experiments with functional protein cargo that has some measurable intracellular biological activity. This introduction highlights the current approaches to functional protein delivery along with the existing challenges and offers some perspective into future directions for the field.

1.2 Physical Delivery Methods

1.2.1 Microinjection

Microinjection involves the use of a glass micropipette to deliver foreign material with extremely precise spatial and temporal control into a variety of cell types.[13,14] A schematic of a single cell being microinjected is shown in Figure 0.2. Since the only exogenous material is the controlled amount of injected substance, it is theoretically the only independent variable in well controlled experiments.[15] Microinjections can be performed directly into both the cytosol and the nucleus, requiring much less protein than electroporation or carrier based methods.[14] Additionally, specific cell types can be transduced without using targeting motifs. Dosage of multiple cargos can also be controlled with current models of air-pressure-driven micro-injectors, which allow fine tuning of injection pressure and timing.[14]

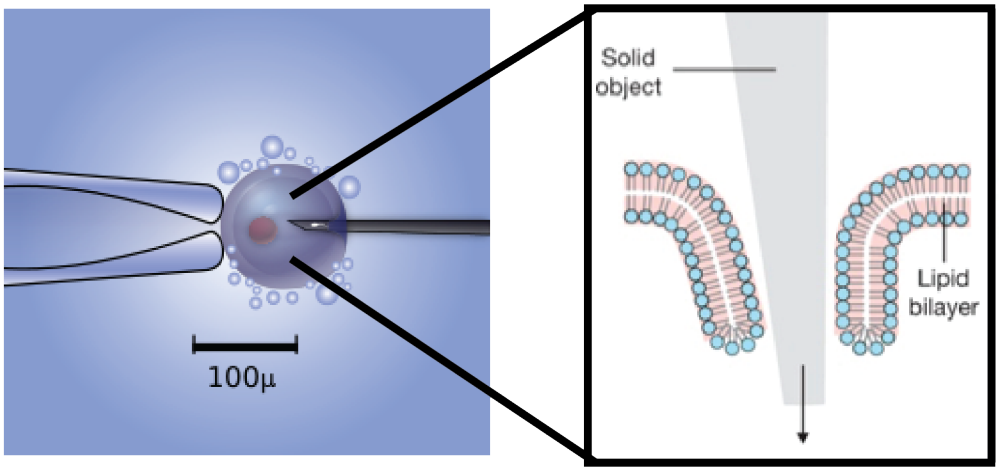

Figure 0.2. Single cell microinjection for introduction of exogenous proteins. Figure adapted from By KDS444 via Wikimedia Commons (left) and Stewart et. al.[6] (right).

Microinjection has been extensively used in studies with primary human neurons, since they are difficult to transfect by other methods. Several examples of functional protein delivery exist including recombinant caspases, heat shock protein 70 (Hsp70), and antibodies.[16–19]

Direct microinjection of recombinant active enzyme capsase-6 induces a protracted course of apoptosis in neurons. The results show that active caspase-6 induces significant cell death in neurons but not in astrocytes, where caspase-3 triggers cell death in astrocytes and not in neurons.[16]

Amyloid-β (Aβ), an intracellular peptide related to Alzheimer's disease is extremely toxic to human primary neurons when injected into the cytosol but not when applied in culture medium suggesting intracellular Aβ may contribute to cell death more significantly than extracellular Aβ.[17] Co-microinjection of Hsp70 with intracellular Aβ blocks the toxicity of the Aβ suggesting that estrogens and androgens protect neurons against Aβ toxicity by increasing the levels of Hsp70.

Microinjection of antibodies was used to study the importance of actin filaments for the regulation of gap junctional intracellular communication in astrocytes.[19] The injection of the antibody reduced spreading of neurobiotin suggesting that the actin cytoskeleton is involved in the regulation of intracellular communication.

Although microinjection has low cytotoxicity, only a few hundred cells can reasonably be transduced at a time limiting the overall efficacy of this technique.[16,17] Positive controls and immune-histochemical staining can be used to detect the transduction of injected proteins. Additionally, with division, delivered proteins will be diluted out with each cell cycle resulting in a lower readout for the injected protein in rapidly dividing cell types. Lastly, the injection causes physical stress to the membrane of the cell. Therefore a vehicle control is required to monitor assess the effect of the injection on viability.[20]

1.2.2 Electroporation

Electroporation uses an electric field to create short-lived pores through the cell membrane, which allow external molecules to cross.[6,21] Membrane disruption, as illustrated in Figure 0.3, allows small and large molecules such as antibodies, proteins, and DNA to be delivered through these reversible pores. There are several advantages to electroporation including its ease of use, as well as avoidance of endosomal entrapment. Additionally, it eliminates the cytotoxicity associated with foreign materials in the cases of chemical transduction or viral infection.

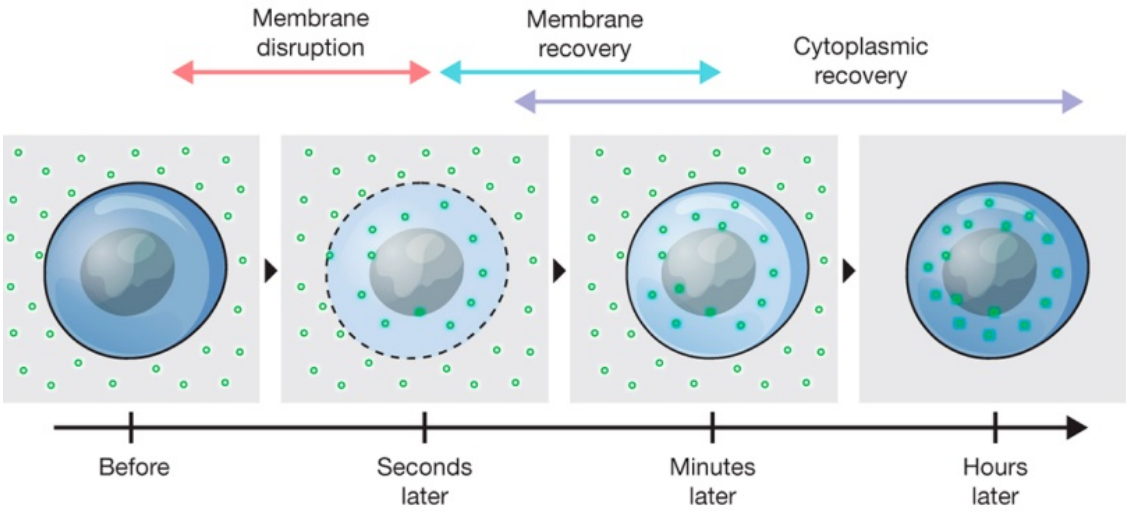

Figure 0.3. Membrane disruption leading to transient pores that allow protein to be delivered into the cytosol of cells. Illustration adapted from Steward et. al.[6]

Traditionally, a solution with suspended cells is dispersed between parallel plates that apply a series of electrical pulses of determinable voltage, frequency, and duration.[21] Microfluidic designs offer the ability to localize the electric field to the scale of the cell, reducing the required voltage, and providing better heat dissipation.[6,22]

A notable example is the transduction of Cas9:sgRNA complexes via electroporation into primary human hematopoietic stem cells and T cells resulting in specific nucleotide insertions in the CXCR4 and PD-1 surface receptor genes.[23] Direct

protein delivery via electroporation improved efficiency and reduced off target effects compared with endogenous expression of Cas9.[23,24] Other examples of proteins that have been transduced into a variety of lymphoid cells include cytochrome c, caspase-8, and granzyme B, all which showed functional status in the major apoptosis pathway of intact cells.[25]

When compared directly with a lipid-based system, transduction of rEGFP was approximately 10% at 18 hours after electroporation compared with about 20% efficiency from the lipid based system.[26] Increased voltage and protein concentration increased transduction efficiency, though never exceeded 30% in the study. While efficiency can be high for electroporation depending on the size of the cargo, it also results in membrane damage leading to excessive cell death, especially with sensitive cell, such as primary cells.[27] Additionally, the electric field can have detrimental effects such as aggregation and denaturation on both the biomolecules being delivered, as well as endogenous cellular proteins.[28,29]

1.2.3 Microfluidics

Cytosolic delivery has also been reported using rapid mechanical deformation on a microfluidic platform.[30] As the cell passes through a constriction with a minimum dimension smaller than the cell diameter, as seen in Figure 0.4, it results in the formation of transient pores.[31] The size and frequency of the pore is dependent on the shear and compressive forces caused by the microfluidic channel. The pores allow for material from the surrounding media to diffuse into the cytosol and cells can be processed at a rate of 20,000 cells/s.[31]

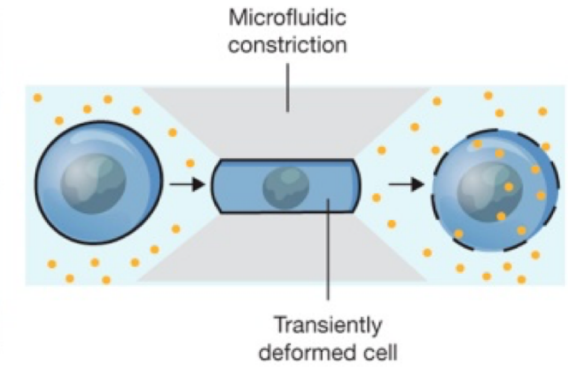

Figure 0.4. Membrane disruption using microfluidic squeezing. The intact cell is passed through a narrow channel which causes pores to form allowing exogenous protein (yellow) to cross the membrane. Image adapted from Stewart et. al.[6]

Transcription factors (Oct4, Sox2, c-Myc, and Klf-4) were delivered to human fibroblasts yielding higher levels of protein expression compared with other delivery methods that rely on endocytosis.[31] Cytoplasmic delivery of quantum dots can also be achieved using high throughput microfluidic devices.[32]

Microfluidic membrane disruption has most recently been use to load antigens into polyclonal B cells for use as cellular vaccines.[33] Post transduction, the B cells elicited robust priming of effector cells *in vitro* conferring cytosolic delivery OVA protein indicating successful transduction. Higher flow rates result in higher uptake, but also cause higher cytotoxicity. Microfluidics is only useful for transducing cells in suspension and has lower overall efficiency than Lipofectamine, but it does result in higher levels of cytosolic delivery.[31]

1.2.4 Insight

Physical membrane disruption addresses many challenges associated with protein delivery. Traditionally, key weaknesses of membrane disruption strategies have been the inconsistent extent of plasma membrane injury from cell-to-cell. In general, these methods render insufficient delivery and cause excessive cell damage. Membrane disruption also

suffers from poor throughput or scalability, loss of cytoplasmic content, and slow cell recovery resulting in inefficient protocols.[6] Methods that employ electric fields may denature proteins or damage cell components and many physical disruption techniques also require cells to be in suspension.

1.3 Lipid-Based Nanocarriers

1.3.1 Liposomes

Conventional liposomes are composed of phospholipids and cholesterol, forming a spherical vesicle with one or more bilayers (Figure 0.5). For several decades, liposomal carriers have been widely used for the delivery of various biomolecules including proteins, antibodies, peptides, and nucleic acids either through encapsulating cargo in the liposome or embedded it on the membrane surface.[34–37] The liposomal bilayer stabilizes the cargo by preventing degradation and facilitates internalization into cells generally through incorporation of cationic charge in the lipid membrane. Compatibility of constituent lipid components with the cell membrane make liposomes attractive for many applications.[34,38]

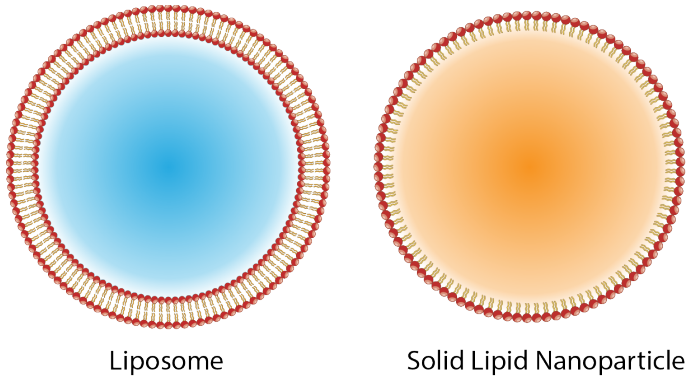

Figure 0.5. A simplified representation of liposomes that have one or more lipid bilayers with an aqueous core, and solid lipid nanoparticles which have a solid hydrophobic core.

Cellular uptake of liposomes is generally believed to be mediated by endocytic processes resulting in entrapment in endosomal compartments within the cell.[39] To

overcome the endosomal barrier, several strategies have been used including pH sensitivity and the addition of cell penetrating peptides to the surface of the liposome.[40]

An example of functional protein delivery mediated by a cationic lipid is the use of RNAiMAX™ to deliver CRISPR-Cas9 proteins along with their single guide strand RNA with over 50% gene editing efficiency.[3] Another bio-reducible lipid system has also shown delivery of the CRISPR-Cas9 complex and subsequent genome editing.[41]

Liposomes with protein suspended in the membrane, known as proteoliposomes, have also been used to deliver mitochondrial VDAC and Bak, which are important stimuli in the release of cyt-c and caspase activation, ultimately resulting in apoptosis.[36] A potent primary CTL response against soluble protein can be achieved through the delivery of antigen, such as OVA, in pH-sensitive liposomes to dendritic cells.[42] Efficient MHC class I presentation of antigens has also be shown using liposomes decorated with octa-arginine.[35,43]

Liposomal systems are widely studied and tend to be a benchmark in the field of biomolecule delivery due to their tunability and ease of use. In addition to their high endosomal entrapment, liposomal preparation methods which use solvents, sonication, and detergents can lead to protein denaturation and loss of activity. High cellular toxicity may also occur due to treatment in the serum free conditions which are required for efficient delivery, making liposomes an unfavorable candidate for sensitive cell types such as primary cells.[44]

1.3.2 Solid Lipid Nanoparticles

Solid lipid nanoparticles (SLNs) are submicron colloidal particles with a rigid core composed of hydrophobic solid lipids stabilized by an emulsifying layer in an aqueous

dispersion (Figure 0.5). In general, SLNs are solid at room or body temperature and both hydrophobic and hydrophilic proteins can be incorporated or adsorbed to their surface resulting in improved stability and sustained release of the cargo.[45] The main factors influencing peptide and protein release from solid lipid particles are the physiochemical characteristics of the loading, particle size, lipid matrix composition, and choice of surfactants.[46] Functional proteins including insulin, somatostatin, and thymocartin have been incorporated into SLNs through solvent evaporation, micro-emulsion, or melt dispersion with varying rates of loading and subsequent release.[47,48]

The hydrophilic nature of most proteins reduces their ability to be microencapsulated into the hydrophobic matrix of SLNs as they tend to partition in the water phase during the emulsion preparation.[46] Additionally, processing conditions can lead to aggregation or denaturation of cargo like their liposome counterparts. Lipid carriers with several lipids and emulsifying agents generally exhibit low cytotoxic effects *in vitro* compared with their polymeric counterparts, even at high concentrations. The cytotoxicity of SLNs can be mainly attributed to components of the aqueous phase, especially non-ionic emulsifiers and preservatives.[49]

1.3.3 Insight

Although protein encapsulation within lipid delivery systems can protect peptides and proteins from proteolytic enzymes, low protein loading efficiency and slow endosomal escape remain major hurdles for lipid delivery systems. Due to their synthetic simplicity and wide spread use, lipid-based carriers remain one of the most predominant carriers in the field of delivery. In the future, we can expect an increasing number of lipid-based carrier systems, especially for proteins with poor aqueous solubility.

1.4 Inorganic Nanocarriers

1.4.1 Carbon Nanotubes

Carbon nanotubes (CNTs) are cylindrical allotropes of carbon that have a long hollow structure with walls formed by a single layer of carbon, also known as graphene. Their orbital hybridization imparts distinct properties including exceptional strength and allows for an exceptionally high length to diameter ratio.[50,51] CNTs offer several appealing features such as large surface areas with well-defined physical and chemical properties, as well as unique optical and electrical properties.[52] Biomolecules can be conjugated non-covalently or covalently to the surface, helping to reduce their toxicity and immunogenicity.[50–54] While there have been significant advances in the field of CNT-based drug delivery, there are only a few examples of biomolecules being delivered into cells.

Kam et al. delivered streptavidin, a protein with clinical applications in anticancer therapies, conjugated to single walled nanotubes (SWNTs) into 3T3 fibroblasts, CHO, HL60, and Jurkat T cells, showing uptake through endocytosis. Additionally, they report streptavidin concentration dependent cytotoxicity, but negligible cell death caused by the SWNTs without streptavidin.[51]

Experiments exploring the binding, intracellular transporting, and release of cytochrome c (cyt-c) with SWNT carriers were carried out in an investigation of biological function. Due to its low molecular weight, SWNTs have a high loading of cyt-c, which is known to activate apoptosis and activity was monitored using Annexin V staining. HeLa and NIH-3T3 cells showed increased rates of apoptosis in the presence of cyt-c SWNTs suggesting that cyt-c was still functional after being transported into the cell.[55]

Additional reports have investigated functionalization with peptide chains to show delivery of shorter sequences. Although peptide function is not explicitly demonstrated,

high levels of cell death are shown after delivery of a peptide known to block the beta adrenergic receptor conjugated to CNTs.[54]

CNTs face challenges regarding (1) synthesis: purity, bioconjugation, functionalization, and modification that allow biocompatibility; (2) a thorough understanding of mechanism and interaction with cells; (3) development of toxicity guidelines and analysis; and (4) demonstration of advantages compared with existing technologies.[50] Cytotoxicity associated with CNTs remains a major concern both *in vitro* and *in vivo*. Conflicting reports may be attributed to variability in the dose, purity, functionalization, cell type, and treatment methods.[50] The use of metal catalysts remains the main source of cytotoxicity followed by their tendency to aggregate.[51,54] More guidelines and systematic testing are required to determine toxicity and the life cycle of functionalized CNTs within cells to further their viability for use in biomolecule delivery.

1.4.2 Quantum Dots

Quantum dots (QDs) are nanocrystals on the order of 2 to 10 nm made of semiconducting materials that can fluoresce to produce distinctive colors dependent on the size of the particle.[56] The distribution of colors and sizes are shown in Figure 0.6A. Due to their small size, QDs have been widely used as fluorescent probes to visualize biological processes both *in vitro* and *in vivo* due to their narrow tunable emission spectra, excellent thermal stability, and resistance to photo-bleaching.[57]

The delivery of QDs and their protein cargos can be roughly divided into passive endocytosis or carrier facilitated uptake, the latter of which involves conjugation to a peptide, protein, or polymer.[58,59] Most QD-protein conjugates without an endosomal escape motif are distributed in endosomal compartments making their cargo not readily

accessible in the cytosol.[57] QDs are not the most efficient functional protein nanocarrier, but do allow for dynamic tracking and detection of exogenous proteins and peptides within cells.[60]

QD-based transduction has been explored using the exogenous thin filament protein cardiac troponic C (cTnC) into myofibrillar cells.[61] To facilitate membrane crossing and endosomal escape, a peptide linker TAT-HA2 was conjugated to the QD-cTnC. Internalization and distribution through the cell, specifically in association with myofibrils, as seen in Figure 0.6B, was achieved with post-functionalization with the peptide.

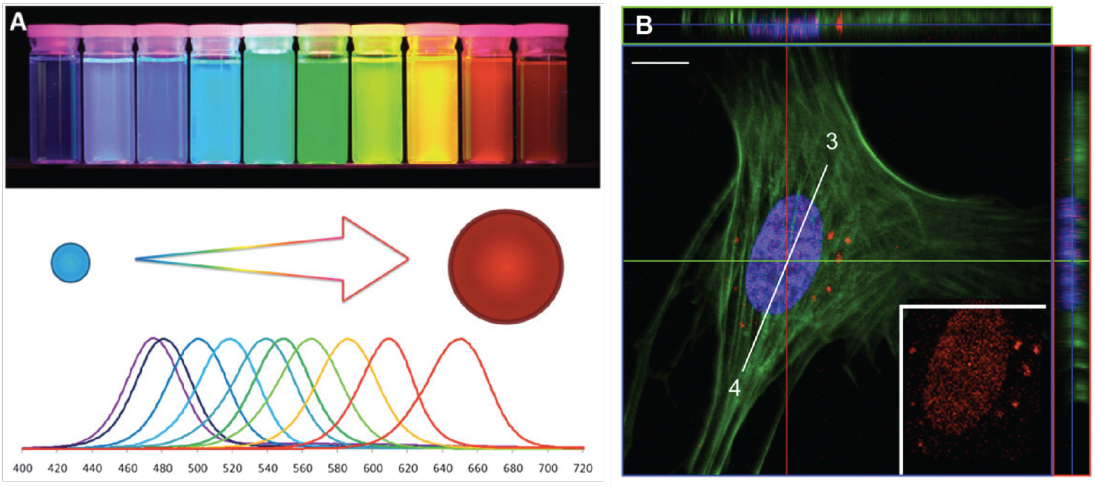

Figure 0.6. (A) Color dependence on size of QDs. (B) QDs (red) co-localized with myofibrils (green) within a cell. Figure adapted from Zrazhevskiy et. al.[57]and Koshman et. al.[61]

Intracellular delivery of QD-protein conjugates is highly dependent on the nature of the QD itself, as well as the cell type being investigated. Current techniques to functionalize QDs are dependent on the QD and are not easily translatable across cargos.[62] Additionally, conjugation as well as a shift in pH can increase the size of the QD substantially.[62] The toxicity of QD materials also remains a concern, arising from the semiconducting metals.[63] While there have been many accomplishments in the

development of controlled delivery of QDs into cells, progress in functionalization and cytotoxicity will help propel the use of QDs as visualization aids in cell culture.

1.4.3 Gold Nanoparticles

Gold nanoparticles (AuNPs) are easily functionalized yet bio-inert, facilitating cellular imaging with low cytotoxicity.[64,65] Similar to QDs, AuNPs require surface functionalization with cationic amines or peptides to promote endocytosis, or antibodies for receptor mediated endocytosis. Alternatively, reports of citrate capped AuNPs have also shown internalization by cells, possibly caused by protein adsorption.[66]

Recently, spherical hierarchical self-assemblies between proteins and AuNPs have been used to deliver functional proteins into cells.[67,68] Proteins were tagged with an oligo-glutamic acid (E10), which can self-assemble with arginine functionalized AuNPs resulting in direct cytosolic delivery of proteins with a variety of sizes and charges into mammalian cells while maintaining their function. Most notably, Cre recombinase, a gene modifying protein, was delivered into a LoxP modified human embryonic kidney cells resulting in knockout of an RFP gene and subsequent expression of GFP after 48 hours.[69] Additionally, granzyme A, a cytolytic enzyme produced by cytotoxic T cells, was delivered into HeLa cells via the same strategy, resulting in caspase 3/7 mediated cell death.[67]

In terms of vaccine development, Wang et. al. designed a multivalent antigen and adjuvant co-delivery platform using both click chemistry and chelation of AuNPs to attach the cargo.[64] Both types of conjugation induced production of pro-inflammatory cytokines and led to antibody production against the delivered antigen. AuNPs have also been used to deliver recombinant human VEGF, where the protein was attached by the thiol group of cysteine residues.[70] HUVECs treated with the AuNP-VEGF proliferated substantially

faster than those without the growth factor. While functionalization or protein modification is required, gold nanoparticles provide a useful tool for *in vitro* delivery, as well as intracellular imaging for protein tracking and dynamics.

1.4.4 Silica Nanoparticles

Mesoporous silica nanoparticles (MSNs) are prepared by an assembly of silicates and surfactant, in which the pore size and structure are easily controlled by the co-assembly conditions. In general, MSN materials have large surface areas and pore volumes and can by endocytosed by mammalian cells making them effective delivery vehicles for the controlled release of biomolecules.[71–73] Internalization studies suggest that the MSNs undergo nonspecific adsorptive endocytosis, and endosomal uptake was shown using FITC labeled cargos.[74] The addition of amine or guanidine groups, such as cell penetrating peptides, enhances energy dependent uptake and promotes endosome escape.[74,75]

To show functional protein delivery using MSNs, cyt-c was delivered into HeLa cells.[76] The protein was loaded using a diffusion driven process based on concentration and controlled release was measured with a drop in pH consistent with that which occurs in lysosomes. Delivery into HeLa cells revealed release of the functional protein into the cytoplasm. Loading and release of the cyt-c relied on its interactions with the silica surface and may not be easily applied to other proteins. Another example of functional protein delivery was MSNs functionalized with *n*-octadecyltrimethoxysilane were loaded with Ribonuclease A and anti-phospho-Akt antibody, which were subsequently delivered into MCF-7 human breast cancer cells resulting in controlled apoptotic cell death. [77]

A recently developed system involves a breakable hybrid organo-silica-nanocapsule where the protein cargo is encapsulated within a breakable hybrid shell

comprising of disulfide bridges embedded in a silica network.[78] The cytotoxic protein human TRAIL Apo2 ligand and onconase were delivered into C6 glioma cells where the active proteins were released by breaking the shell of the capsule. However, as shown through co-localization between lysotracker and GFP, much of the protein cargo remains sequestered in lysosomes with very little being available in the cytosol.

Although pores in MSNs can be used to encase proteins, there is a size limit restricting larger proteins from being successfully loaded and transported across the membrane.[79] Progress in controlling pore size and morphology will facilitate immobilization of a larger variety of cargos.

1.4.5 Magnetic Nanoparticles

The ability to tune the surface of magnetic nanoparticles (MNPs) makes them multifunctional, allowing synthesis with a variety of cargos.[80] Magnetically mediated protein delivery can enhance the therapeutic profile by increasing the localized concentration of target cargo and minimize non-specific interactions. Although MNPs have shown application in theranostics, there are very few cases of the use of MNPs for functional protein delivery *in vitro*.

Intracellular delivery of MNPs loaded with catalase, an antioxidant enzyme, was confirmed through the rescue of target cells that were undergoing toxicity due to hydrogen peroxide.[81] Experiments were performed in bovine aortic endothelial cells, where the MNPs were guided to these cells and increased their resistance to oxidative stress.

Iron oxide nanoparticles have been shown to cause cell membrane injury in both a concentration and time dependent manner.[82] Therefore, low concentrations of MNPs are

optimal to ensure mitigation of oxidative stress induced cell injury. Additionally, cargo must be functionalized to the MNP, potentially reducing the functionality of the protein.

1.4.6 Insight

Since inorganic nanoparticles are relatively new to the field of biomolecule delivery, many hurdles are still being addressed such as aggregation. Additionally, due to their inert nature many inorganic nanoparticles require functionalization with other delivery vehicles such as a cell penetrating peptide or cationic polymers to achieve internalization. The theranostic benefits of inorganics, especially when used as imaging agents has huge potential, but for now these particles are not able to deliver functional protein intracellularly.

1.5 Protein and Peptide Mediated Carriers

1.5.1 Engineered Proteins

Supercharged proteins are a class of engineered or naturally occurring proteins with unusually high net positive or negative theoretical charge.[83] The creation of supercharged proteins was first reported in 2007 as the product of extensive mutagenesis in which solvent exposed residues on the proteins surface are substituted with either acidic or basic amino acids.[84] The functionality of these proteins is preserved, but reduced in some cases.[83] Both positively and negatively supercharged proteins exhibit a remarkable ability to withstand thermal or chemical induced aggregation.[84,85] Superpositively charged proteins are also able to penetrate mammalian cell membranes and have shown utility in enabling the delivery of functional proteins.[83,85,86]

Positively supercharged GFP has been shown to deliver a variety of functional proteins directly into cells by translational fusion.[85,87] Cre recombinase functioned as a general measure of delivery as its enzymatic activity is only observed by its presence in

the nucleus. In addition to Cre recombinase, functional delivery of the CRISPR-Cas9 gene editing system has been shown using supernegatively charged GFP in conjunction with the cationic lipid system RNAiMAX.[3] The strategy for fusing functional proteins to the negatively charged GFP is illustrated in Figure 0.7.Recently, a diverse class of naturally occurring supercharged human proteins has been identified that potentially deliver functional proteins into mammalian cells.[83]

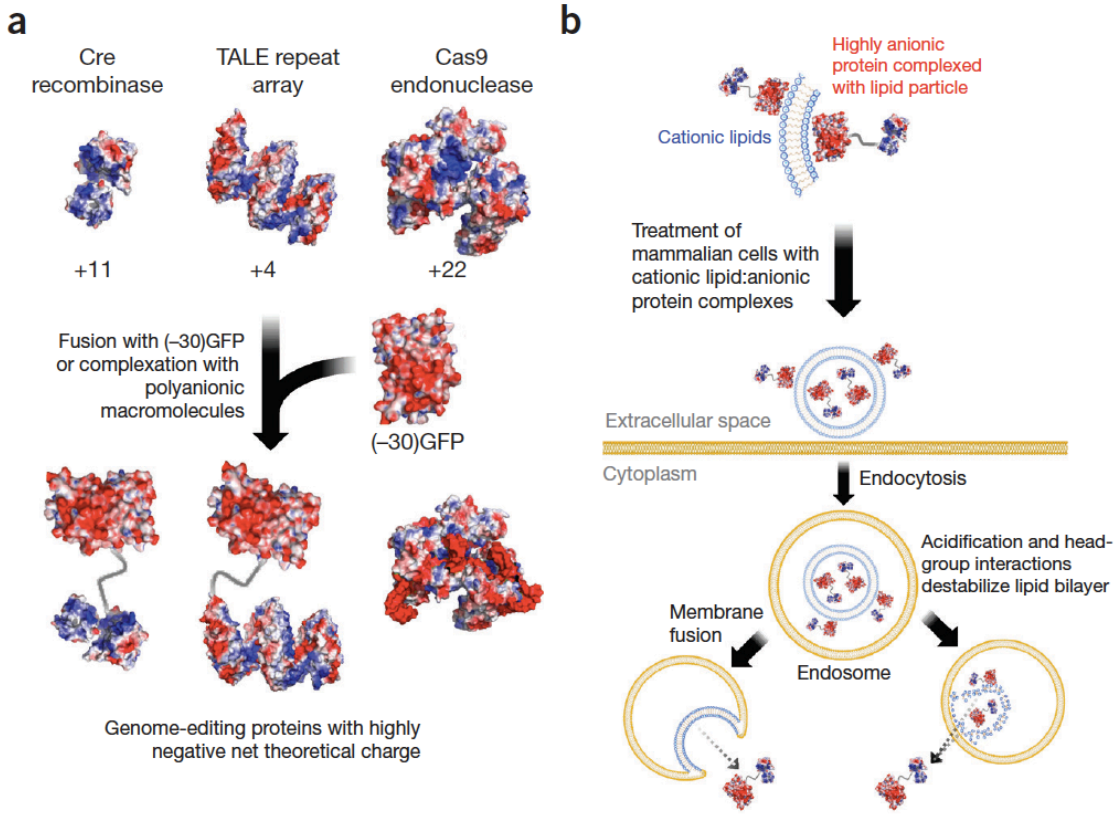

Figure 0.7. Functionalization of active proteins with super-negatively charged GFP (A) for intracellular delivery using cationic lipids commonly used to deliver RNA and DNA (B). Image adapted from Zuris et. al.[3]

In addition to supercharged proteins, intracellular delivery has been reported for engineered G proteins which contain a histidine affinity tag on the N- terminus and cell penetrating peptide sequence at the C-terminus.[88] The engineered G protein allows for capture of surface modified nanoparticles and antibodies through non-covalent interactions

with the histidine tag and non-invasively delivers the complex into cells using the CPP. Delivery of both cargos independently and combined was demonstrated in Hela cells.

The non-viral E2 subunit of pyruvate dehydrogenase has also been developed as a protein delivery platform.[89,90] E2 is a caged protein made of self-assembling monomers to form a hollow capsule which can be post modified with proteins. E2 was shown to co-deliver the MHC I restricted peptide SIINFEKL and CpG, an oligonucleotide into dendritic cells.[89]

Supercharged proteins are an interesting, new class of protein delivery vehicles. Understanding how these proteins are able to cross the membrane would facilitate the development of specific targeted carriers. Additionally, movement away from covalent attachment would enable these proteins to be easily used with a variety of cargos.

1.5.2 Exosomes

Exosomes are a family of vesicles secreted by most cell types with a diameter in the range of 30-120 nm.[91] The production of exosomes is a major route of cellular excretion allowing for the disposal for the removal of unwanted RNA and proteins and can also transport cargos between cells. Initially, an invagination of endosomal membranes creates a multi-vesicular body, they are then fused with the membrane and secreted.[91] Exosomes have shown utility in therapeutics due to their low immunogenicity and toxicity but high biological permeability and biocompatibility.[92]

Due to their intrinsic ability to carry endogenous proteins, exosomes seem to be suitable carriers for protein delivery. An example of this endogenous protein transfer was demonstrated by Shimoda et al. who reported the functional transfer of CagA into recipient cells inducing cell elongation.[93] Recently, the gene editing protein Cre recombinase was

loaded into exosomes by exploiting the evolutionarily conserved late-domain and showed functional gene knockdown.[94]

Loading and delivering small RNAs has been a major focus using exosomes for biological delivery.[91] There have been only a handful of reports on successful packaging of macromolecular proteins into exosomes due to the major challenge of low loading efficiency.[93–96] There is a need to explore more efficient protein loading approaches before exosomes will be widely applied for protein delivery.

1.5.3 Virus Like Particles

Virus like particles are derived from viral capsid proteins and resemble their native virus counterpart, but lack the genetic components.[28,97,98] They can be assembled to encapsulate a variety of non-viral biomolecules including proteins and engineered to express and display heterologous proteins. Many viruses can be used as VLPs including murine leukemia virus, lentivirus, retrovirus, Sendai virus, and their ability to deliver bioactive proteins such as antibodies, transcription factors, and enzymes has been demonstrated in a variety of cell types.[99–102] Although some viruses possess natural cell and tissue tropism,[103] broad cell specificity is exhibited by many VLPs making them viable candidates for protein delivery into a variety of cell types.[28]

Kaczmarczyk et. al. have shown that VLPs can be used to deliver a variety of functional proteins intracellularly, including Cre recombinase, cytotoxic enzymes, and human caspase 8.[97] Protein ligands such as TRAIL and IFN-γ can also be displayed on the outside of the VLP allowing for signaling control within cells during delivery.[97]

Similar to liposomes and exosomes, controlled loading of specific proteins into VLPs remains a challenge. Additionally, some knowledge of molecular biology is required to use this in a functional laboratory setting to load proteins of interest into the VLPs.

1.5.4 Protein Toxins

Plant and bacterial toxins can be potent inhibitors of intracellular processes and often contain their own translocation domain or complex.[39,104] While some toxins exploit cellular machinery to enter cells such as the cholera toxin, others can form pores for cytosolic entry like anthrax and diphtheria.[105–108] In general, pore forming toxins are an ensemble of an enzymatic moiety in conjunction with a cell surface receptor that mediates entry into the cytosol.[104] These protein complexes can be exploited for protein delivery, though the toxins themselves can have detrimental effects on cellular function, as well as viability.[104]

Anthrax has been shown to deliver a variety of cargos including peptides, proteins, and antibody-like molecules with varying degrees of success.[105] Ballard et. al. modified cytotoxic T cell epitopes derived from bacteria with an anthrax derivative to create immunogenic response for mouse CD8 T cells.[106] Additionally, the delivery of an antibody mimic into the cytosol of cells via conjugation with anthrax into has been demonstrated by co-immunoprecipitation of the affibody with its target, as well as interruption of several pathways.[109]

Auger et. al. demonstrated that a variety of proteins could be delivered using the diphtheria toxin.[110] The conjugation, targeting and endosomal escape of their strategy is depicted in Figure 0.8. To ensure that the protein cargo is functional after conjugation to

the diphtheria, alpha-amylase was delivered into HEK293 cells resulting in rapid glycogen degradation in treated cells.

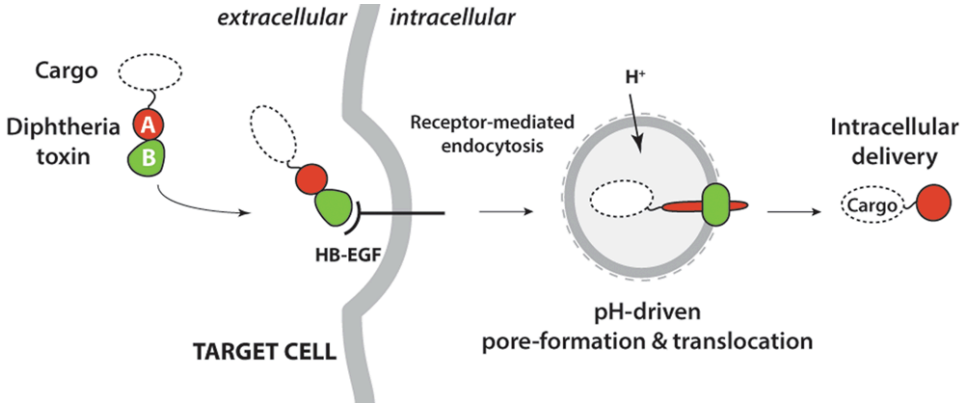

Figure 0.8. Diphtheria toxin can be conjugated to cargo and brought across the cell membrane through pH-driven pore formation releasing the cargo into the cytosol. Figure adapted from Auger et. al.[110]

Biological toxins provide a facile delivery platform for biomolecules with diverse structures and functionalities due to the promiscuity of their pore forming units. Investigations by several groups have demonstrated that the cargo must be able to adopt an unfolded or extended conformation in the endosome and cargos with low pK_a values that cannot be protonated in the endosome may inhibit translocation limiting the variety of cargo that can be efficiently transduced.[105] Lastly, further exploration in to the immunogenicity and cellular effects of using toxins would provide more insight into the practical use as protein carriers.

1.5.5 Cell Penetrating Peptides

Initially introduced into the field of delivery over two decades ago, cell penetrating peptides have become a staple for the intracellular delivery of proteins and other biomolecules.[111–113] The ability to transverse the membrane has transcended their use across a variety of systems including liposomes, engineered proteins, and polymers.[113–115] The hallmark discovery of HIV-1 Tat lead to the discovery and generation of an entire field

of short, cationic, and sometimes amphiphilic peptide sequences.[11,112,116,117] These can be loosely divided into naturally occurring sequences such as Antennapedia homeodomain and MAP; chimeric mimics like transportan and penetratin; along with their synthetic peptide mimics including R9 and Pep-1. [11,118]

Intracellular delivery can be achieved through direct conjugation of cell penetrating peptides to the cargo requiring post modification of the desired cargo. Some studies have reported non-covalent complexing with the desired cargo.[119–121] An inexhaustible list of protein delivery using cell penetrating peptides exists; a few highlights have been included here.

R9 has been used in to co deliver covalently linked Cas9 protein along with guide strand RNA to show efficient knockdown by the functional ribonuclear protein complex.[122] Additionally, oligo arginine attached to zinc finger nucleases as well as TALEN proteins have also shown gene editing capabilities suggesting their presence in the nucleus with low cytotoxicity.[123]

One major example of TAT and other CPPs is its use in delivering peptides and proteins for cancer treatments. Fusion of the apoptosis inducing protein apoptin to HIV-TAT resulted in high transduction efficiency in all cell types, but only apoptosis in cancer cells after migration to the cytoplasm and nucleus.[124] Other proteins include p53, anti-p21, and antitumor antibody fragments.[125] TAT fusion proteins have also been shown to deliver hsp70, required for protection against glutamate dehydrogenase deficiency disorders.[126,127]

Endosomal escape remains a major concern for many cell penetrating peptide systems. Akishiba et. al. demonstrated delivery of Cre recombinase, saporin, and IgG in addition to exosome encapsulated proteins using a modified endosomolytic peptide derived

from the spider venom.[96] Cytosolic delivery of bioactive protein was confirmed with gene recombination by Cre recombinase. The delivered anti-glucocorticoid receptor IgG blocked intracellular signaling and transcription suggesting functional activity of the antibody in the cytosol.

Conjugation of CPPs to biomolecular cargo has proven an effective tool for protein delivery, but there are still challenges within the field including toxicity, stability, and immune response.[128,129] Additionally, post modification of the cargo with CPPs can influence the functionality of the protein within the cell.

1.5.6 Insight

Natural sources of protein delivery such as CPPs and VLPs provide a biological answer to protein delivery. Since all the components are naturally synthesized by cells, degradation products are of minimal concern making these systems extremely biocompatible. Like all delivery systems, some assembly is required and in many cases knowledge of molecular biology methods is useful to facilitate conjugation or entrapment of the protein.

1.6 Synthetic Polymeric Nanocarriers

1.6.1 Protein Transduction Domain Mimics

Polymers can be used to mimic the functional transduction domains of proteins either by polymerizing cationic and hydrophobic monomers, or by incorporating active motifs into the backbone of the polymer chain.[114,115] Several groups have developed systems for protein transduction domain mimics (PTDMs), also referred to as cell penetrating peptide mimics (CPPMs).[130–132]

As a developing area of delivery, PTDMs have mostly been explored for uptake using a fluorescent label on the polymer itself. The Kolonko et. al. has demonstrated

cytosolic and endosomal uptake of FITC labeled artificial translocation domain.[133] Additionally, McKinlay et. al. show that uptake of guanidinium-rich oligophosphoesters is superior to their guanidinium-rich oligocarbonates and oligoarginines counterparts.[131]

Using a norbornene based amphiphilic block copolymer, Sgolastra et. al. demonstrated non-covalent delivery of functional Cre recombinase into a human T cell line using PTDMs resulting in gene knockout.[134] A similar polymer was used for delivery of functional anti-pPKCθ into primary human lymphocytes enabling the perturbation of intracellular pathways to dictate cell fate.[135]

Functional protein delivery has been shown for both covalent attachment as well as non-covalent delivery. While the polydispersity makes these systems difficult to fully characterize, they have shown promise in their ability to deliver proteins into cells at a higher efficiency than their peptide counterparts.[136]

1.6.2 Nanogels

Nanogels are a type of hydrogel on the order of 10-200 nm and are made of cross-linked soluble polymer chains. They can be modified to encapsulate proteins or to covalently attach cargo to the surface. The porous nature of hydrogels allows controllable release kinetics of their cargo based on crosslinking density. During synthesis, no organic solvents or harsh fabrication techniques are required; polymers that have been most widely evaluated for the preparation of nanogels include poly(N-isopropylacrylamide) (pNIPAM), poly(lactic acid) PLA, poly(lactic-co-glycolic acid) (PLGA), poly(caprolactone) (PCL), polyhydrobuterate, and polypropylene glycol.[137,138] Biological materials like dextran, hyaluronic acid, and chitosan are also used to form nanogels.[139] Nanogels, along with the

other nanocarriers described in this section have been illustrated in Figure 0.9 since many of them have similar components.

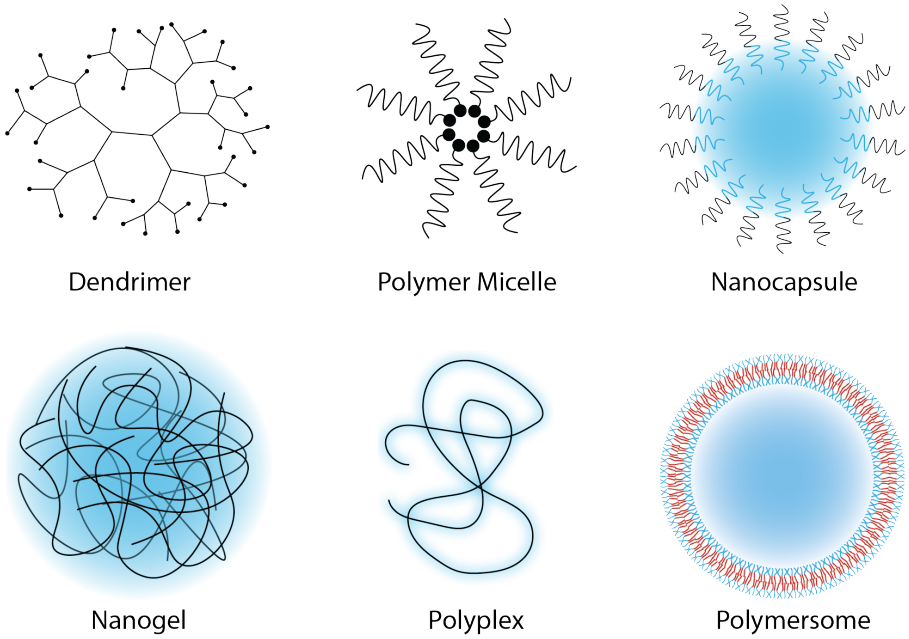

Figure 0.9. Schematic of synthetic nanocarriers.

Active enzymes, such as caspase-3, have been covalently attached to the surface as well as encapsulated inside polymeric redox sensitive nanogels through disulfide linkages.[140] Further modification with a CPP is required for internalization, and activity of caspase-3 was restored upon cleavage from the nanogel in the reducing environment of the cell.

Zhao et al. showed intracellular delivery of caspase-3 encapsulated in redox responsive nanogels which degrade at lowered pH due to their disulfide containing crosslinker. [141] Single encapsulation of the caspase-3 using the nanogel showed rapid uptake and trafficking into the cytosol, followed by induced apoptosis. Negative controls of the nanogel without the caspase-3 and the caspase-3 by itself showed low cytotoxicity in HeLa, U-87 MG, and MCF-7 cells.

Crosslinked nanoparticles were synthesized with a pH responsive PDEAEMA (polydimethyl amino ethyl methacrylate) core and hydrophilic PAEMA (polyazidoethyl methacrylate) charged shell to deliver OVA into dendritic cells.[142] The hydrophobic pH buffering component facilitated endosomal disruption and cytosolic delivery resulting in elevated IFN-γ production and cross presentation of antigen.

There are several advantages to nanogels as protein carries, including their biocompatibility due to their high water content, biodegradability, high loading capacity, and tunable crosslinking densities which allows controlled cargo release.[138] Additional modification can allow stimuli responsive release of cargo including degradation based on pH, temperature, or an applied electric field.[8]

1.6.3 Polymeric Micelles

The structure of amphiphilic molecules allows them to accumulate at the boundary of two non-miscible phases and to function as surfactants. With an increase in concentration, the free energy begins to rise and at the critical micelle concentration, the amphiphiles will self-assemble into colloidal sized particles illustrated in Figure 0.9.[12] Careful modulation of the relative block lengths and the composition of block copolymer affects the shape of the overall amphiphile, which affects the packing parameter, giving rise to micelles or higher order structures such as bilayers. Since assembly is a reversible process driven by thermodynamics, micelles are categorized as an amphiphilic colloid and not a solid nanoparticle.[143] Proteins can be loaded inside the hydrophobic core of the micelle for use as a delivery vehicle.

Coué et. al. describe a bioreducible poly(amidoamine) that associate with their protein cargo through charge reversibility.[144] For this system, the charge density of the

protein of interest was temporarily increased by the modification of the lysine residues to make them negatively charged carboxylic groups resulting in a strongly anionic surface. The cationic block copolymers were then associated with the cargo for rapid delivery into the cytosol. The modifying groups on the lysines are redox sensitive, degrading at a pH of 5.5 releasing the cationic polymer to allow endosomal escape. Functional antibody was stained for using a secondary antibody after cell fixation. Some activity was lost due to the initial modification, though presence was detected regardless of modification technique.

Polymer micelles face some inherent problems including low stability in aqueous environments, low loading capacity, low cellular uptake compared with liposome and polymersome counterparts, toxicity correlated with an increase in polymer required to deliver high concentrations of cargo, immunogenicity, and short half lives in biological environments.[12,139]

1.6.4 Dendrimers

Dendrimers are a specific type of highly branched, globular macromolecules which are composed of many arms emanating from a central core.[145] As depicted in Figure 0.9, the inner layers of the dendrimer have a homogeneous structure from every branch point stemming from the core. In some cases, dendrimers can be end capped with peripheral functional groups to change surface properties. The iterative nature of dendrimer synthesis leads to control over density and reactivity of surface functional groups, as well as control of overall size and molecular structure.[146]

In general, hydrophobic therapeutic substances are loaded in the non-polar core of the dendrimer and both positively or negatively charged surface functional groups can be

used to complex with cargo.[137] Only a few examples exist for protein delivery, and those are limited to cases of low numbers of protein bound per dendrimer.

Bayele et. al. used lysine rich dendrimers to deliver c-Myc monoclonal antibody into HeLa cells.[147] Dendrimers with guanidinium moieties at the end of each branch were capable of delivering the antibody IgG into HEp-2 cells.[148] Cargo with measurable intracellular function was not used in either of these studies, rather fluorescence was used to track the uptake. The multivalency of dendrimers make them excellent at interacting with cell receptors and subsequently being internalized by cells, though there is still much to be explored in their use to deliver biological cargos.[9,149] High cytotoxicity is associated with dendrimers after incubation for longer time periods.[147]

1.6.5 Nanocapsules and Polymersomes

Stable self-assembled polymeric shells are similar in morphology to liposomes in their colloidal nature with an outer layer made from amphiphilic block copolymers.[12] Depending on the polymeric component and the nature of the core, two variations exist: nanocapsules with an oily liquid core and a single outer layer of polymer and polymersomes with an aqueous core surrounded by a polymer bilayer. The difference between polymersomes and nanocapsules is depicted in Figure 0.9.

Nanocapsules have found utility in the encapsulation and delivery of hydrophobic drugs and proteins. Commonly used polymers include PLA, PLGA, and PCL in addition to poly(ethylene glycol) PEG. The Rotello group has developed a system using nanoparticles to stabilize nanocapsules for the delivery of biologics into cells.[68,150,151] The synthesis strategy can entrap a variety of cargos including proteins. Caspase-3 and Cas9 have been delivered in tandem with AuNPs using the nanoparticle stabilized emulsion.[69,150]

Polymersomes are analogous to liposomes with their ability to encapsulate and deliver hydrophilic substances but are instead made of block copolymers such as PEG-b-PBD (polybutadiene) and PEG-b-PEE (polyethylethylene). While both systems are inert, neither are biodegradable lending to the creation of PEG-b-PLA and PEG-b-PCL. Another study using the triblock PEG-PCL-PDEA (polydimethyl amine) polymersomes showed delivery of FITC labeled lysozyme, cyt-c, OVA, and IgG into HeLa and Raw cells.[152]

In terms of degradable carriers, anisamide decorated pH sensitive polymersomes showed efficient loading and delivery of apoptotic granzyme B into H460 lung cells.[153] The reducing environment within the cell dissembled the polymersomes allowing release of granzyme B into the cytosol. Cytosolic delivery induced apoptosis via delivery of granzyme B when the surface of the polymersomes were functionalized with high levels of anisamide on the surface. Nanocapsules and polymersomes provide a ripe area of research for protein delivery because of their ability to encapsulate a variety of cargos and to be environmentally responsive.

1.6.6 Polyplexes

Polyplexes have been traditionally labeled as a complex between polymers and DNA, though similar strategies are being applied to proteins.[9,154,155] Direct covalent attachment with polymers such as PEG has been used to improve stability and reduce the surface charge of proteins. Polymer attachment is easily achieved through well-established bioconjugation methods.[149] One of the most commonly used polymers is polyethyleneimine (PEI) which has been conjugated to the surface of various proteins to impart positive charge and enhance membrane permeability.[156–158] Murata et. al. functionalized denatured human tumor suppressor p53 with PEI using a reducible disulfide

bond to deliver the protein into Saos-2 cells. Reduction of the reversibly cationized complex in the cytosol allowed the p53 to refold into tetramers resulting in nuclear localization and induction of p53 target genes eventually leading to apoptosis.[125] The system was extended to allow delivery of functional anti-S100C antibodies into HFL-1 cells which could be seen in fluorescence images (Figure 0.10) as long filamentous structures as they bound to the S100C proteins on the actin filaments.[156]

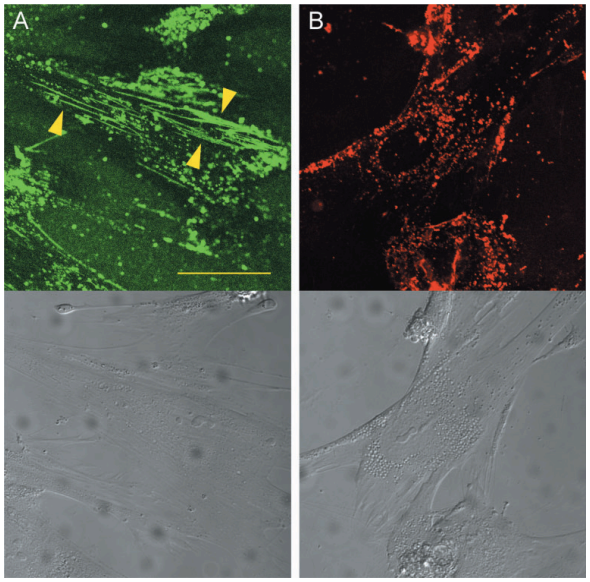

Figure 0.10. Confocal microscopy of distribution of FITC-labeled anti-S100C antibodies localized with actin (A) after delivery with the PEI cationized protein G into HFL-1 cells (scale bar 50 µm). Delivery of a non-specific protein with PEI-protein G resulted in unpatterned delivery (B). Lower images are differential interference contrast images corresponding to the upper panels. Arrowheads indicate filamentous structures. Image adapted from Kitazoe et. al.[156]

In another case, cytosolic delivery of MoAb 64.1 was demonstrated in Jurkat T cells using polypropylacrylic acid.[159] The antibody was conjugated to streptavidin which readily complexed with the biotinylated polymer allowing for release into the cytosol as determined by quantitative western blot.

1.6.7 Insight

Polymer nanocarrier systems are one of the fastest growing transduction methods due to facile synthesis and high uptake of detectable bioactive cargo. Synthetic carriers tout enhanced cargo stability in addition to permeability, though many studies do not look at the long term effects of the synthetic systems within cells. Additionally, there has been very few systematic comparisons between polymer systems probing how formulation and preparation effects protein delievery.[160] Expansion into structure activity relationships, as well as understanding how the protein cargos interact with their carriers is critical to improving polymer design for improved uptake and protein function.

1.7 Perspective

The intracellular delivery of functional proteins is an important task as it opens the doors to understanding and manipulating intracellular pathways with low toxicity and minimal interruption in normal cellular processes. Effective and safe delivery systems facilitate progress in multiple fields from cell bases therapies to molecular biology. Current demand for these delivery vehicles exceeds supply, especially in fields that are interested in treatment of primary and patient derived cells such as immune cells, neurons, and stem cells.

One major challenge that the field of protein delivery currently faces is the lack of standard experimental conditions to compare across all protein delivery methods. Many publications (not included in this review) only deliver fluorescently labeled cargos, which have no other detectable bioactivity, and rarely do the authors follow up with proteins that do show a bioactive readout. Model proteins that exhibit function either in the cytosol or nucleus easily demonstrate endosomal escape and the stabilizing capacities of the carriers.

Additionally, researchers have tendencies and preferences for certain cell lines which limits the diversity of cells studied and makes comparisons between methods even more challenging. Many of the reported cell lines, like HeLas, are known to be relatively easy to transfect and transduce, providing little barrier and less proof of concept. Here, the authors would like to encourage the field to begin to choose proteins that have a functional readout within the cells they are delivered into, and to deliver into cell lines or primary cells that have practical application such as immune cells or neurons.

An important, yet unanswered question that protein delivery faces is how much protein is required to have a biological response. Without quantification, or understanding of how concentration effects an intracellular pathway, it remains elusive whether one protein or many are needed to register a biological readout. Therefore, higher number of delivered proteins is not necessarily as important for functional protein delivery. Direct structure activity relationships would help elucidate this problem, furthering the development of more effective protein delivery.

The future of protein delivery is dependent on interdisciplinary research to facilitate the interface of biology and technology. Advances in delivering proteins across the membrane will lead to new challenges. Solving these next generation problems may hinge on our ability to understand current delivery mechanisms and implement analytical approaches necessary to characterize cellular response. Despite the barriers that remain, next generation technologies will translate beyond academic endeavors into personalized diagnostics and therapeutics.

1.8 Thesis Overview

The aim of the following thesis was to characterize, optimize, and utilize PTDMs for functional protein delivery. The PTDMs reported here provide a well-controlled platform to vary molecular composition for structure activity relationship studies to further our understanding of PTDs, their non-covalent association with cargo, and their cellular internalization pathways. Specifically, several polyoxanorbornene-based synthetic mimics were synthesized using ring-opening metathesis polymerization (ROMP) due to its relatively precise control over molecular weight and polydispersities. The living nature of ROMP allows for the formation of advanced architectures such as block copolymers which can be used to investigate the relationship between structure and internalization activity.

Elucidating the predominant cellular entry mechanism for protein transduction domains (PTDs) and their synthetic mimics (PTDMs) is a complicated problem that continues to be a significant source of debate in the literature. In Chapter 2, several guanidine rich homopolymers, along with an amphiphilic block copolymer were used to investigate the relationship between structure and internalization activity in HeLa cells, both alone and non-covalently complexed with EGFP by flow cytometry and confocal imaging. The findings indicate that while changing the amount of positive charge on our PTDMs does not seem to affect the endosomal uptake, the presence of hydrophobicity appears to be a critical factor for the polymers to enter cells either alone, or with associated cargo.

In Chapter 3, a series of polyoxanorbornene-based synthetic mimics, inspired by PTDs, with varying cationic and hydrophobic densities, and the nature of the hydrophobic chain and degree of polymerizations were investigated *in vitro* to determine their ability to non-covalently transport enhanced green fluorescent protein into HeLa cells, Jurkat T cells,

and hTERT mesenchymal stem cells. Polymers with high charge density lead to efficient protein delivery. Similarly, the polymers with the highest hydrophobic content and density proved to be the most efficient at internalization. The observed improvements with increased hydrophobic length and content were consistent across all three cell types, suggesting that these architectural relationships are not cell type specific. These results provide important design parameters for intracellular delivery of proteins and produced a candidate polymer for further investigation.

Delivery of a model protein, GFP, into several human cell types using the lead PTDM compared with four commercially available counterparts is explored in Chapter 4. This comparison reveals that while many of the protein delivery vehicles within the class of amphiphilic polymers are able to deliver into cells in serum free conditions, their delivery is severely hampered in the presence of serum. In contrast, the PTDM reported here is capable of high protein delivery into all tested cell types within 4 hours in the presence of complete media.

Lastly, to show functional protein delivery, in Chapter 5 we investigated the ability of these PTDMs to deliver a peptide into whole blood and subsequent stimulation of a directed immune response toward the specific peptide sequence. We have detected peptide delivery to over 90% of CD14+ monocytes in less than 15 minutes with nominal cytokine response and high cell viability. The co-delivery of an agonist to promote a specific immune response against the peptide in vitro allowed us to modulate monocyte differentiation and presentation of the specific peptide in association with MHC class I molecules. The ability to have a specific response with the cargo of interest verifies

cytosolic delivery using the PTDMs and provides valuable insight into their use to affect immune cells.

CHAPTER 2

RELATING STRUCTURE AND INTERNALIZATION FOR ROMP-BASED PROTEIN MIMICS

2.1. Introduction

Over the past decade, intracellular targeting has become an emerging area of research in drug delivery, diagnostics, and chemical biology. However, cell membranes are impermeable to most macromolecules and small molecules. One exception seems to be a class of cell-penetrating peptides (CPPs) known as protein transduction domains (PTDs) and their synthetic mimics (PTDMs). Intracellular delivery using PTDs remains a promising method for introducing exogenous macromolecules into cells.[161,162]

The Tat (transactivator of transcription) protein of the human immunodeficiency virus type 1 (HIV-1), discovered in 1988, was the first identified PTD.[163,164] Later, it was determined that an eleven amino acid residue sequence (YGRKKRRQRRR), rich in basic amino acids, was required for translocation of Tat through the plasma membrane.[165] In the last two decades, over 100 CPP sequences have been published and this number continues to expand as more is learned about these molecules.[166] These CPPs are usually small, cationic peptides, some of which contain a hydrophobic component. Their main feature is their ability to cross cell membranes either on their own or conjugated to a range of biomolecules, such as peptides, proteins, liposomes, and nanoparticles. This is possible at micro-molar concentrations without causing significant membrane damage.[58] Synthetic CPPs deviate from naturally occurring protein sequences and are either designed to mimic their structures and compositions or to produce amphipathic α-helical structures. Examples are the model amphipathic peptide (MAP) and oligoarginine sequences, such as **R8**. These

synthetic CPPs have also been covalently attached to various macromolecules and their internalization has been studied.[167,168]

Intracellular delivery of large molecules, including macromolecules and liposomes, often involves the uptake of PTD(M) complexes by endocytosis.[169] Arginine-rich PTDMs have been proposed to induce macropinocytosis, which in turn leads to accelerated internalization of cell surface adsorbed PTDMs and PTDM-cargo complexes.[170–172] Since macropinocytosis is considered a non-specific fluid phase endocytosis pathway, its induction should facilitate indiscriminate uptake.[173] The endosomal route usually finishes with the acidic and proteolytic degradation of the lysosomal content, thus preventing the delivered cargo from reaching its cytosolic targets.[174] The release of biologically active cargo from endosomes is a necessary step and is a major limitation for this type of uptake.[58]

A second mode of uptake is direct translocation, an energy-independent penetration pathway in which a transient destabilization occurs in the membrane, followed by the rapid intracellular localization of the peptide.[175–177] For drug delivery purposes, it is preferred that molecules enter cells by direct translocation, as this pathway does not incur endosomal entrapment. Changes in hydrophobicity have been implicated as the driving factor for arginine-rich molecules to cross cell membranes through direct translocation.[178] Additionally, cell surface concentrations of arginine-rich PTDMs may also play a role in peptide entry into cells.[179] Some peptides exceeding a threshold concentration have been observed to directly penetrate the membrane, while at lower concentrations uptake is primarily by endocytosis.[177,180,181]

A change in membrane curvature is required for both endocytosis and direct penetration, which can be facilitated by CPP–membrane interactions.[182] Decoupling

endocytosis from direct penetration remains largely unsolved. The use of endocytosis inhibitors may alter other cellular processes, making deconvolution of the treatments difficult.[183] Cooling cells to 4 ˚C provides another challenge in that cooler temperatures affect the membrane fluidity making it more rigid and therefore more permeable to larger molecules.[184]

While many CPPs and their mimics show high membrane permeability and efficient cargo delivery, the mechanisms by which PTDMs and PTDM-cargo complexes traverse cell membranes are not completely understood and are highly debated in the literature.[183] The methods by which arginine-rich PTDs are internalized depend on the physiochemical properties of the PTDs, the cargo molecules, and cell type, as well as a variety of other parameters. Therefore, it is not surprising that the predominant internalization mechanism may deviate depending on the attached cargo. Understanding this cellular uptake mechanism of CPPs under physiological conditions is important for the development of appropriate strategies for therapeutic applications both *in vitro* and *in vivo*. Since several routes may exist simultaneously, it is important to correlate the uptake pathway with the biological response associated with a specific cargo e.g. if the target of the cargo is cytosolic or endosomal. These parameters will enable the design of materials to target specific routes of internalization.

Creating polymeric scaffolds with CPP-like internalization and cargo delivery properties has recently emerged as a new research direction.[114–116] Polymers allow for the use of different, easily tailored chemistries and architectures for investigating structure activity relationships, while tuning for efficient cargo delivery. Using ring-opening metathesis polymerization (ROMP), which is functional group tolerant, well-controlled,

and versatile, a highly efficient set of synthetic PTDMs has been developed.[114,115,185–190] These designs, based on polyarginine, are guanidinium-rich and allow for non-covalent internalization of various biological cargos.[187,188,191] The ability to easily include diverse functional groups allows us to probe architecture, molecular composition, and molecular weight in a controlled manner, mimicking peptide synthesis.[114,191]

Polymeric mimics offer a controlled way to explore the effects of structure and macromolecular composition on internalization efficiency. Using **R8** as inspiration and a benchmark, a set of four homopolymers and one block copolymer (Figure 0.1) were chosen to investigate the impact of polymer structure and backbone on internalization efficiency in HeLa cells.

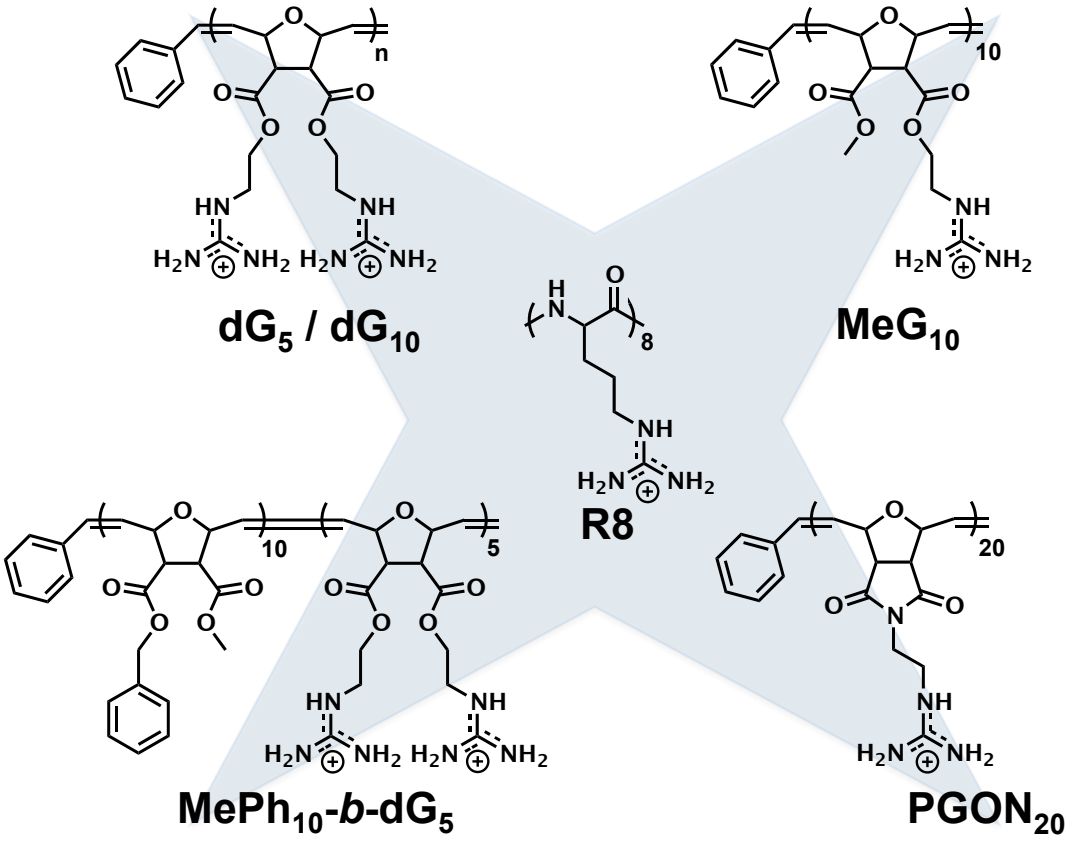

Figure 0.1. Polymers of interest: R8 **inspired the design of** dG_5 **(n=5),** dG_{10} **(n=10),** MeG_{10}**,** $PGON_{20}$**, and** $MePh_{10}$-b-dG_5**.**

Determining the parameters that dictate the predominant method of internalization is crucial to the understanding and optimization of CPPs and their mimics. In this work, we use the delivery of cargo by synthetic PTDMs as a handle for elucidating the intracellular pathways through which these molecules enter. More specifically, HeLa cells were treated with the chosen PTDMs, either with a FITC label or associated with fluorescent protein, allowing for confocal laser scanning microscopy (CLSM) and flow cytometry (FCM) analysis. Imaging explicates the predominant mode of uptake as endosomal uptake and allows us to address some of the more difficult questions regarding polymer-cell interactions, while flow cytometry generates quantitative results (on a much larger number of cells) that can be used to verify trends seen with imaging. From these results, we determined that concentration and polymer architecture have little effect on the mode of translocation into the cell, but rather play a more important role in how much cargo they are able to deliver.

2.2. Materials and Methods

2.2.1. Materials

Chemicals were obtained as reagent grade from Aldrich, Fluka, or Acros and used as received. 3rd generation Grubbs catalyst (Dichloro-di(3-bromopyridino)-N,N'-Dimesitylenoimidazolino-Ru=CHPh; G3) was synthesized as described previously by Grubbs et al. (1). The ACS reagent grade solvents, ethyl acetate, tetrahydrofuran (THF), N,N-dimethylformamide (DMF), and pentane, were purchased from Fisher Scientific and used as received. Dichloromethane (DCM) (ACS reagent grade, Fisher Scientific) was distilled from CaH_2 under nitrogen. Deuterated solvents for NMR were purchased from Cambridge Isotope Laboratories. Spectra/Por® Biotech cellulose ester dialysis membranes

with the molecular weight cut off of 100-500 were purchased from Spectrum Medical Industries. Media and supplements for cell culture were purchased from Lonza.

2.2.2. Instrumentation

^{1}H spectra were recorded at 300 MHz, using a Bruker DPX-300 NMR spectrometer. Chemical shifts (δ) are reported in ppm and coupling constants (*J*) in Hz. The abbreviations for splitting patterns are: s, singlet; d, doublet; dd, doublet of doublets; t, triplet; q, quartet; m, multiplet; br, broad. Gel permeation chromatography was measured on an Agilent 1260 series GPC setup with a PL Gel 5 μm guard column, two 5 μm analytical Mixed-C columns, and a 5 μm analytical Mixed-D column (Agilent), incubated at 40 °C, with RI detector. THF was used as the eluent at a flow rate of 1.0 mL/min. Polystyrene standards were used for the calibration and toluene was used as flow marker. Flow cytometry was performed on an LSRII flow cytometer and analyzed using the acquisition software FACSDiva™ (BD®). Analysis of flow cytometry data was performed using FlowJo™ (Tree Star®) software. Images were taken using a FV1000 Olympus® IX81 confocal laser scanning microscope (CLSM) at both 40 and 60X.

2.2.3. PTDM Synthesis

2.2.3.1. Monomer Synthesis

Monomers and PTDMs were synthesized according to established literature procedures.[185,187,189] The diester monomers were synthesized using the procedure introduced by Lienkamp et al.[192] In general, the Diels-Alder adduct **1** was obtained by the reaction of maleic anhydride with furan in toluene.

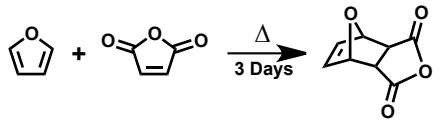

1

1 was dissolved in the minimum amount of dry DCM together with 2 eq. of 1,2-Di-Boc-2-ethyl guanidine, and 10 mol% 4-dimethylaminopyridine (DMAP). The temperature was lowered to 0°C with an ice bath and 1 eq. of 1-ethyl-3-(3-dimethylaminopropyl)carbodiimide (EDC) was added, then stirred over night at room temperature. After completion of the reaction, the solution was concentrated and the product was purified via column chromatography with silica gel using DCM/ethyl acetate (8:2) as eluent. Vacuum evaporation of the solvent yielded the pure product with a yield of ~80%.

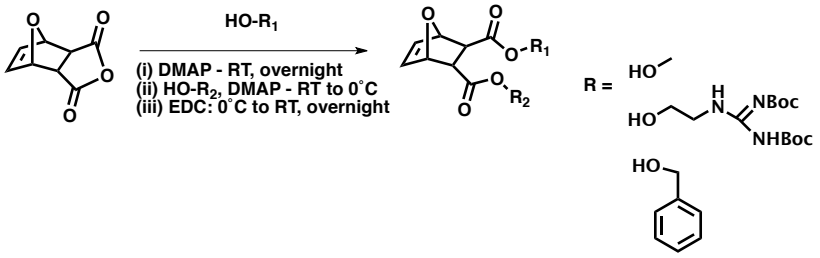

3 (dG): ^{1}H NMR (300 MHz, CD_3CN): δ 11.54 (s, 2H), 8.35 (s, 2H), 6.44 (s, 2H), 5.17 (s, 2H), 4.33 – 3.97 (m, 4H), 3.72 – 3.41 (m, 4H), 2.82 (s, 2H), 1.48 (s, 9H), 1.42 (s, 9H); ^{13}C NMR (75 MHz, CD_3CN): δ 172.43, 164.51, 157.35, 153.72, 137.56, 84.05, 81.41, 79.50, 63.72, 47.49, 40.21, 28.38, 28.09; HR-MS (FAB) *m/z* $[M+H]^+$: 755.3827 (calc.), 755.3824 (found).

Compound **1**, 1.5 equivalents of methanol, and 10 mol% DMAP were dissolved in dry DCM and the reaction was stirred for 3 days at room temperature. Solvent was evaporated and the product was crystalized in a 1:1 mixture of chloroform:hexanes with a yield of ~60%.The product was dissolved in dry DCM along with 1.5 equivalents of 1,2-

Di-Boc-2-ethyl guanidine, and 10 mol% DMAP and the solution was cooled to 0˚C. 1 equivalent of EDC was added and the reaction was stirred overnight at room temperature. The product was washed with brine, evaporated down, and purified using column chromatography with silica gel 9:1 DCM:ethyl acetate. The yield was ~70%.

4 (MeG): ^{1}H NMR (300 MHz, CD_3CN): δ 11.50 (s, 1H), 8.55 (s, 1H), 6.46 (s, 2H), 5.3 (d, 2H), 4.25 (m, 2H), 3.72(m, 5H), 2.84 (s, 2H), 1.49 (s, 18H). ^{13}C NMR (75 MHz, CD_3CN): δ 171.7, 171.5, 163.4, 156.3, 153.1, 136.6, 83.2, 80.7, 80.6, 79.4, 63.5, 52.4, 47.1, 46.4, 39.4, 28.3, 28.1; HR-MS (FAB) *m/z* $[M+H]^+$: 483.22 (calc.), 484.23 (found).

Compound **1**, 1.5 equivalents of benzyl alcohol, and 10 mol% DMAP were dissolved in dry DCM and the reaction was stirred for 3 days at room temperature. The product was precipitated out of DCM and was filtered and vacuum evaporated to yield the pure product with a yield of ~70%. The product was dissolved in 1:1 mixture of DCM:THF along with 2 equivalents of methanol and 10% DMAP and the solution was cooled down to 0˚C in an ice bath. 1 equivalent of EDC was added and the solution was stirred over night at room temperature. Solvent was evaporated off and the reaction mixture was dissolved in minimal DCM. Purification of monomer MePh was performed via column chromatography with silica gel using DCM:ethyl acetate (8:2) as eluent. Vacuum evaporation of the solvent yielded the pure product with a yield of ~80%.

(MePh): ^{1}H NMR (300 MHz, CD_3CN): δ 7.34 (d, J = 3.0 Hz, 10H), 6.44 (s, 2H), 5.16 (s, 2H), 4.97 (dd, J = 45.5, 12.4 Hz, 4H), 2.87 (s, 2H); ^{13}C NMR (75 MHz, CD_3CN): δ 172.37, 137.52, 137.03, 129.41, 129.14, 129.06, 81.30, 67.26, 47.58; HR-MS (FAB) *m/z* $[M+H]^+$: 365.1389 (calc.), 365.1398 (found).

The imide monomer was synthesized using a procedure previously developed by Gabriel et al.[2] In general, the Diels-alder adduct was obtained by the reaction of maleimide with furan in ethyl acetate at 90˚C for 3 hours. The product, 1,2-Di-Boc-2-ethyl guanidine, and triphenylphosphine were dissolved in THF and cooled to 0˚C. 1 equivalent of diisopropyl azodicarboxylate (DIAD) was added dropwise and reaction was stirred for 24 hours at room temperature. Solvent was removed by evaporation and recrystallized in methanol twice to yield 40% of the GON monomer.

5 (GON): ^{1}H NMR (300 MHz, CD_3CN): δ 11.44 (s, 1H), 8.35 (t, J = 6.0 Hz, 1H), 6.56 (s, 2H), 5.10 (s, 2H), 3.52 (m, 2H), 3.43 (m, 2H), 2.85 (s, 2H), 1.47 (s, 9H), 1.36 (s, 9H); ^{13}C NMR (75 MHz, CD_3CN): δ 176.3, 156.6, 153.0, 136.5, 83.3, 80.9, 47.6, 39.0, 38.4, 28.3, 28.1.

2.2.3.2. Activated Ester Synthesis

Activated ester was synthesized according to the procedure introduced by Madkour et al. Briefly, compound **B** was synthesized as described in the literature.[3] Compound **A**, pentafluorophenol, and DMAP were dissolved in 50 mL dry DCM under nitrogen. The resulting solution was then cooled to 0˚C, and EDC was added to the mixture in portions. The reaction mixture was then allowed to warm to room temperature and stirred for another 12 hours. The mixture was then washed with 10% $KHSO_4$ solution, saturated $NaHCO_3$ solution, and brine. The resulting DCM solution was dried using anhydrous Na_2SO_4, filtered, and the solvent was evaporated. The resulting residue was purified by filtration through a neutral alumina plug using DCM as the eluent.

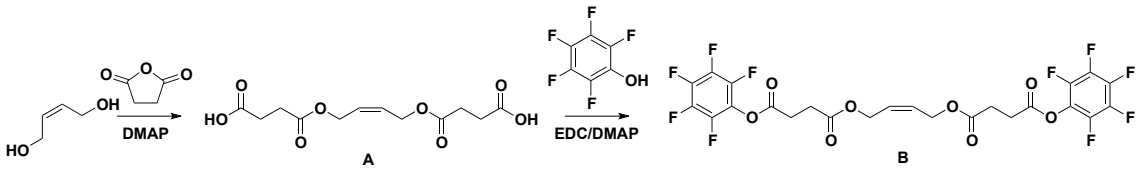

^{1}H-NMR (300 MHz, CDCl3): δ 5.77 (m, 2H), 4.75 (d, J = 5.6 Hz, 4H), 3.05 (t, J = 6.2 Hz, 4 H), 2.95 (t, J = 6.2 Hz, 4H); ^{13}C-NMR (75 MHz, CDCl3): δ 171.1 (C=O-O allylic), 168.4 (C=O-O-C6F5), 142.9, 141.7, 139.5,137.8 & 136.1 (m, F5C6), (CH2-C=C), 28.7 & 28.3 (CH2-CH2).

2.2.3.3. Polymer Synthesis

Example of reaction conditions for homopolymer synthesis: Monomer (MeG or dG) and G3 catalyst were dissolved in dry DCM in respective schlenk flasks, purged with nitrogen and subjected to three freeze-pump-thaw cycles. The monomer solution was added into the catalyst solution via syringe all at once. The brown solution was stirred for 2 hours (30 minutes for the $PGON_{20}$) at room temperature. The reaction was terminated with 1 mL of ethyl vinyl ether and stirred for 30 minutes. DCM was evaporated and the product dissolved in minimal DCM to be loaded on a short silica gel column (7 cm length, 3 cm diameter). The unreacted end-group and any side products were washed from the column with DCM, while polymer remained on the column and was recovered with ethyl acetate. Ethyl acetate was evaporated to yield the pure product.

MeG_{10}: ^{1}H-NMR (300 MHz, CDCl3): δ 11.55 (1H, br), 8.42 (1H, br), 7.39 (0.5H, br), 5.88 (trans) and 5.63 (cis) (2H total, br), 5.02 (cis) and 4.70 (trans) (2H total, br), 4.14 (2H, br), 3.65 (5H, br), 3.17 (2H, br), 1.49 (18H, s).

dG_5: ^{1}H-NMR (300 MHz, CDCl3): δ 11.56 (2H, br), 8.41 (2H, br), 7.35 (1H, br), 5.93 (trans) and 5.66 (cis) (2H total, br), 5.07 (cis) and 4.69 (trans) (2H total, br), 4.17 (4H, br), 3.59 (4H, br), 3.21 (2H, br), 1.53 (18H, s), 1.44 (18H, s).

dG_{10}: ^{1}H-NMR (300 MHz, CDCl3): δ 11.57 (2H, br), 8.40 (2H, br), 7.34 (0.5H, br), 5.93 (trans) and 5.65 (cis) (2H total, br), 5.10 (cis) and 4.69 (trans) (2H total, br), 4.20 (4H, br), 3.58 (4H, br), 3.19 (2H, br), 1.52 (18H, s), 1.44 (18H, s).

$PGON_{20}$: ^{1}H-NMR (300 MHz, CDCl3): δ 11.57 (1H, br), 8.39 (1H, br), 7.34 (0.25H, br), 6.00 (trans) and 5.81 (cis) (2H total, br), 5.00 (cis) and 4.43 (trans) (2H total, br), 3.60 (2H, br), 3.33 (2H, br), 2.09 (2H, br), 1.38 (18H, s).

Reaction conditions for block copolymer synthesis: Monomer **dG**, monomer **MePh**, and G3 catalyst were dissolved in dry DCM in respective schlenk flasks, purged with nitrogen, and subjected to three freeze-pump-thaw cycles. Monomer **dG** solution was added into the catalyst solution via syringe all at one time. The brown solution was stirred for 30 minutes at room temperature before monomer **MePh** was introduced. After stirring for an additional 2 hours, the reaction was terminated with 1 mL of ethyl vinyl ether and stirred for 30 minutes. DCM was evaporated and the product was dissolved in minimal DCM and loaded on a short silica gel column (7 cm length, 3 cm diameter). The unreacted end-group and any side products were washed from the column with DCM, while polymer remained on the column and was recovered with ethyl acetate. Ethyl acetate was evaporated to yield the pure product.

$MePh_{10}$-*b*-dG_5: ^{1}H-NMR (300 MHz, CDCl3): δ 11.57 (2H, br), 8.40 (2H, br), 7.37 (6H, br), 5.80 (trans) and 5.61 (cis) (4H total, br), 5.08 (2H, br), 5.00 (cis) and 4.77 (trans) (4H

total, br), 4.66 (2H, br), 4.17 (4H, br), 3.64 (4H, br), 3.49 (3H, br), 3.17 (4H, br), 1.46 (18H, s), 1.41 (18H, s).

Polymers were synthesized in a similar manner to that listed above but terminated with 20 mole equivalents activated ester (compound **B**) dissolved in a minimal amount of DCM and stirred overnight. DCM was evaporated and the product dissolved in minimal DCM to be loaded on a short silica gel column (7 cm length, 3 cm diameter). The unreacted end-group and any side products were washed from the column with DCM, while polymer remained on the column and was recovered with ethyl acetate. Ethyl acetate was evaporated to yield the pure product.

MeG_{10}: ^{1}H-NMR (300 MHz, CDCl3): δ 11.55 (1H, br), 8.42 (1H, br), 7.39 (0.5H, br), 5.88 (trans) and 5.63 (cis) (2H total, br), 5.02 (cis) and 4.70 (trans) (2H total, br), 4.14 (2H, br), 3.65 (5H, br), 3.17 (2H, br), 3.01 (cis) and 2.77 (trans) (0.4H total, br), 1.49 (18H, s).

dG_5: ^{1}H-NMR (300 MHz, CDCl3): δ 11.56 (2H, br), 8.41 (2H, br), 7.35 (1H, br), 5.93 (trans) and 5.66 (cis) (2H total, br), 5.07 (cis) and 4.69 (trans) (2H total, br), 4.17 (4H, br), 3.59 (4H, br), 3.21 (2H, br), 3.02 (cis) and 2.77 (trans) (0.8H total, br), 1.53 (18H, s), 1.44 (18H, s).

dG_{10}: ^{1}H-NMR (300 MHz, CDCl3): δ 11.57 (2H, br), 8.40 (2H, br), 7.34 (0.5H, br), 5.93 (trans) and 5.65 (cis) (2H total, br), 5.10 (cis) and 4.69 (trans) (2H total, br), 4.20 (4H, br), 3.58 (4H, br), 3.19 (2H, br), 3.01 (cis) and 2.77 (trans) (0.4H total, br), 1.52 (18H, s), 1.44 (18H, s).

$PGON_{20}$: ^{1}H-NMR (300 MHz, CDCl3): δ 11.57 (1H, br), 8.39 (1H, br), 7.34 (0.25H, br), 6.00 (trans) and 5.81 (cis) (2H total, br), 5.00 (cis) and 4.43 (trans) (2H total, br), 3.60 (2H, br), 3.33 (2H, br), 3.02 (cis) and 2.79 (trans) (0.2H total, br), 2.09 (2H, br), 1.38 (18H, s).

$MePh_{10}$-*b*-dG_5: ^{1}H-NMR (300 MHz, CDCl3): δ 11.57 (2H, br), 8.40 (2H, br), 7.37 (6H, br), 5.80 (trans) and 5.61 (cis) (4H total, br), 5.08 (2H, br), 5.00 (cis) and 4.77 (trans) (4H total, br), 4.66 (2H, br), 4.17 (4H, br), 3.64 (4H, br), 3.49 (3H, br), 3.17 (4H, br), 3.01 (cis) and 2.77 (trans) (0.3H total, br), 1.46 (18H, s), 1.41 (18H, s).

100 mg end-functionalized polymer was dissolved in 1 mL amine-free DMF. 2 mole equivalents of fluorescein-5-thiosemicarbazide were added. The reaction was allowed to stir at room temperature for three days. The solvent was evaporated, and the reaction product was purified by column chromatography using ethyl acetate.

MeG_{10}: ^{1}H-NMR (300 MHz, CDCl3): δ 11.55 (1H, br), 8.42 (1H, br), 7.39 (0.5H, br), 5.88 (trans) and 5.63 (cis) (2H total, br), 5.02 (cis) and 4.70 (trans) (2H total, br), 4.14 (2H, br), 3.65 (5H, br), 3.17 (2H, br), 3.01 (cis) and 2.77 (trans) (0.4H total, br), 1.49 (18H, s).

dG_5: ^{1}H-NMR (300 MHz, CDCl3): δ 11.56 (2H, br), 8.41 (2H, br), 7.35 (1H, br), 5.93 (trans) and 5.66 (cis) (2H total, br), 5.07 (cis) and 4.69 (trans) (2H total, br), 4.17 (4H, br), 3.59 (4H, br), 3.21 (2H, br), 3.02 (cis) and 2.77 (trans) (0.8H total, br), 1.53 (18H, s), 1.44 (18H, s).

dG_{10}: ^{1}H-NMR (300 MHz, CDCl3): δ 11.57 (2H, br), 8.40 (2H, br), 7.34 (0.5H, br), 5.93 (trans) and 5.65 (cis) (2H total, br), 5.10 (cis) and 4.69 (trans) (2H total, br), 4.20 (4H, br), 3.58 (4H, br), 3.19 (2H, br), 3.01 (cis) and 2.77 (trans) (0.4H total, br), 1.52 (18H, s), 1.44 (18H, s).

$PGON_{20}$: ^{1}H-NMR (300 MHz, CDCl3): δ 11.57 (1H, br), 8.39 (1H, br), 7.34 (0.25H, br), 6.00 (trans) and 5.81 (cis) (2H total, br), 5.00 (cis) and 4.43 (trans) (2H total, br), 3.60 (2H, br), 3.33 (2H, br), 3.02 (cis) and 2.79 (trans) (0.2H total, br), 2.09 (2H, br), 1.38 (18H, s).

$MePh_{10}$-*b*-dG_5: ^{1}H-NMR (300 MHz, CDCl3): δ 11.57 (2H, br), 8.40 (2H, br), 7.37 (6H, br), 5.80 (trans) and 5.61 (cis) (4H total, br), 5.08 (2H, br), 5.00 (cis) and 4.77 (trans) (4H total, br), 4.66 (2H, br), 4.17 (4H, br), 3.64 (4H, br), 3.49 (3H, br), 3.17 (4H, br), 3.01 (cis) and 2.77 (trans) (0.3H total, br), 1.46 (18H, s), 1.41 (18H, s).

2.2.4. Deprotection

The polymers were dissolved in 2 mL DCM and 2 mL trifluoroacetic acid (TFA) for deprotection. After stirring overnight, the excess acid was removed by azeotropic distillation with methanol. After complete evaporation of the acid, samples were dissolved in water/methanol mixture and dialyzed against RO water until the conductivity of water was ~0.1μS. The deprotected copolymer was recovered by lyophilization. Final deprotected polymer was stored at -20 ºC.

2.2.5. Internalization of FITC-Labeled Polymers

HeLa cells were seeded at $1x10^4$ cells/ 2 mL of α-MEM with 10% FBS on 35 mm glass bottom plates 48 hours prior to treatment and cultured at 37˚C and 5% CO_2. FITC-PTDMs were diluted 1:10 in PBS and then to a final concentration of 5, 10, and 20 μM in α-MEM with 10% FBS. Cells were washed with warm, fresh, complete media and 200 μL of PTDM solution was applied on top of the glass bottom. Cells were incubated for one hour and then washed three times with cold media to remove excess PTDM and to slow cellular function. Cells were covered in 1 mL of cold media and imaged at 60X with confocal laser scanning microscope (CLSM).

To investigate co-localization with lysosomes, cells were treated with 5 μM FITC-PTDM and 20 nM lysotracker red for 1 hour. Samples were analyzed in a similar manner to the internalization experiments using both red and green lasers on the CLSM. Correlation between the location of the lysotracker and the FITC-PTDM was determined by Pearson's co-localization coefficient (PCC) using Autoquant® software.

2.2.6. EGFP Delivery

HeLa cells were seeded at $1x10^6$ cells/ 2 mL of α-MEM with 10% FBS on 35 mm glass bottom plates and $1x10^5$ cells/ 1 mL on 12-well plates 48 hours prior to treatment and cultured at 37˚C and 5% CO_2. Polymer was complexed with 2 μg of EGFP using previously reported methods at a ratio of 20:1 PTDM to protein (unpublished). Cells were treated for four hours with the polymer/protein complexes in a total volume of 1 mL α-MEM with 10% FBS. Before imaging, cells were washed three times with cold media and covered in 1 mL fresh, cold α-MEM with 10% FBS. Cells were imaged using CLSM at 60X. To prepare for flow cytometry (FCM), the cells were lifted using trypsin and washed three times with a 20 U/mL heparin solution before being suspended in PBS with 0.2 wt% FBS.

To determine if the 30 minute incubation period was required for optimal uptake, cells were treated with PTDMs not incubated with protein at the same concentration. PTDMs and protein were diluted as stated above and added drop-wise without mixing into the media. Uptake was analyzed by flow cytometry to determine the percentage of cells that internalized the polymer, as well as the median fluorescence intensity (MFI) of the cells. Cell viability was determined using 7-aminoactinomycin D (7-AAD) staining.

2.3. Results and Discussion

2.3.1. Polymer Design and Synthesis

In this study, PTDMs were designed to resemble **R8** (Figure 0.1), with **MeG$_{10}$** containing one guanidinium group per repeat unit, yielding about 10 positive charges per polymer. The diguanidine (**dG**) series (**dG$_5$** and **dG$_{10}$**) was designed to create a higher density of guanidinium groups to better mimic the distribution of charge along the peptide backbone. **dG$_5$**, with about 10 positive charges, correlates to **R8** in that it has approximately the same number of guanidinium groups, but only half the number of repeat units, while **dG$_{10}$** has approximately the same number of repeat units as **R8**, but has twice as many guanidinium moieties, or about 20 positive charges. A second ROMP backbone, the imide-based poly-guanidinium oxanorbornene (**PGON**), was added to the series because of its high membrane activity with lipid vesicles.[189] Since **PGON$_{20}$** only contains one guanidinium group per repeat unit, a length of 20 was chosen for comparison to **dG$_{10}$**, resulting in about 20 positive charges along the length of the polymer. Lastly, a block copolymer with 10 hydrophobic and 5 diguanidinium monomers (**MePh$_{10}$-*b*-dG$_5$**) was included because of its efficient non-covalent protein delivery into Jurkat T Cells (unpublished), predominantly due to the added hydrophobicity that has been shown to be required for efficient protein delivery. Added hydrophobicity, which has been predicted to increase saddle splay curvature, combined with lipid head-group coordination by guanidinium groups, promotes membrane permeation.[182] These polymers were all synthesized with and without covalently attached FITC labels.

2.3.2. Internalization of FITC-Labeled Polymers

HeLa cells were treated with FITC-PTDMs for 1 hour and imaged using a CLSM, as shown in Figure 0.2A, and also analyzed using flow cytometry (Figure 0.2B and C).

Images revealed that **dG$_5$** and **MeG$_{10}$** exhibited low cell entry. **MeG$_{10}$** appeared to aggregate extensively and was dropped from further studies. This aggregation could be due to the overall charge density being too low, with one charge per monomer, allowing the PTDMs to have a greater self-affinity than for the solution or cell membranes. Both homopolymers with 20 guanidinium units (**PGON$_{20}$** and **dG$_{10}$**) demonstrated efficient internalization, particularly **PGON$_{20}$**. This is unsurprising, as previous reports have shown that it is highly membrane active in biophysical assays compared to other homopolymers produced in this group.[185] The block copolymer PTDM also showed punctate internalization throughout the cell with high efficiency for all imaged cells.

The median fluorescence intensities (MFIs), shown in Figure 0.2B, corroborate the confocal images. An artificially high MFI is expected from **MeG$_{10}$**, since large aggregates were seen in and on cells in the confocal images. **dG$_{10}$** and **PGON$_{20}$** showed high membrane activity (see Figure 0.2) and consequently result in a 3 to 4 fold higher MFI than **MePh$_{10}$-*b*-dG$_5$**. We speculate that efficient internalization with the dye requires a combination of a critical hydrophobic component and charge content that is not met with **dG$_5$**. Along this line of thought, the internalization of **PGON$_{20}$** could be attributed to its increased length. Although **MePh$_{10}$-*b*-dG$_5$** resulted in a low MFI, the punctate fluorescence was prevalent in all imaged cells, and more than 95% of the cell population was fluorescent.

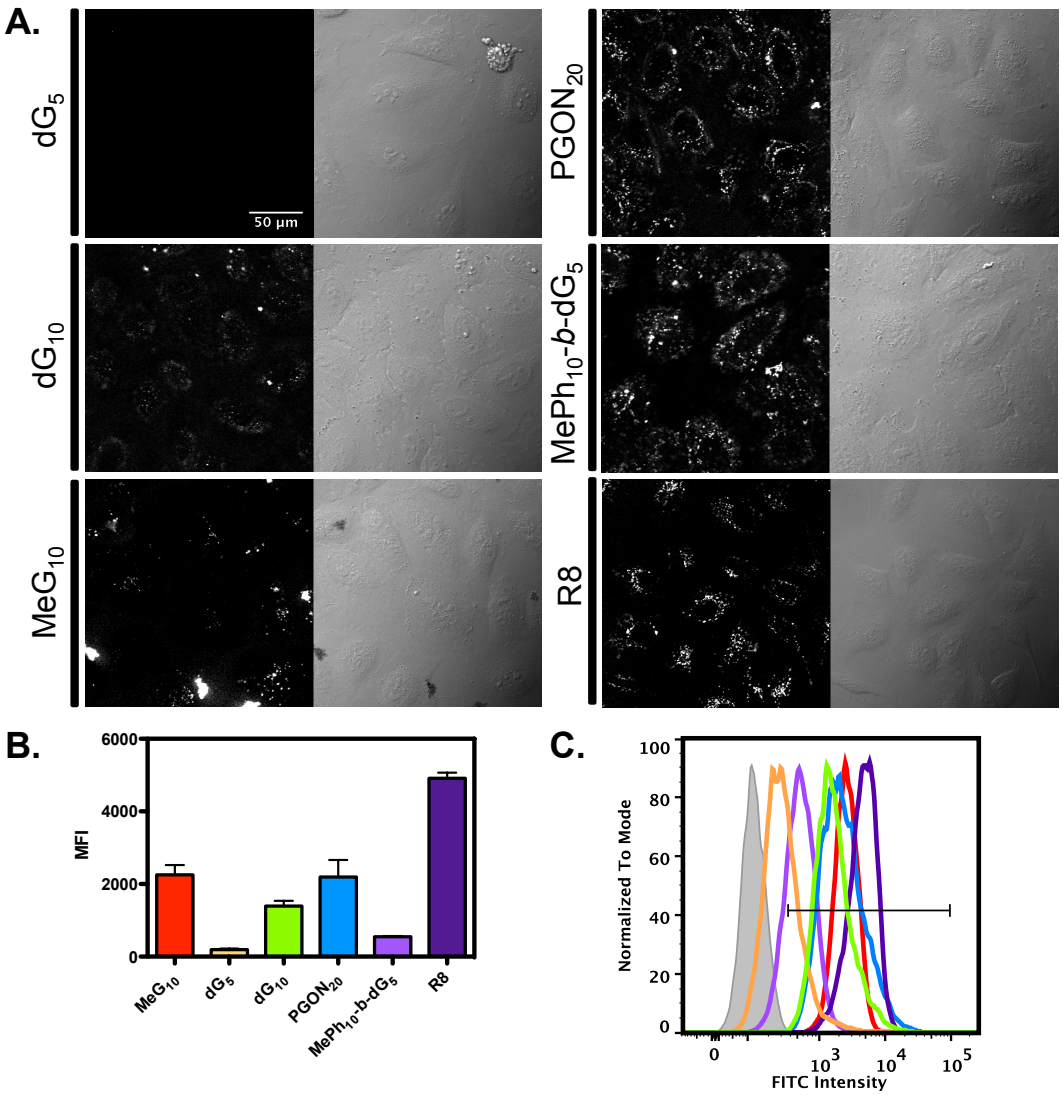

Figure 0.2. Internalization of FITC-labeled PTDMs into HeLa cells. Cells were treated with 5 µM PTDM for 1 hour and imaged with a CLSM (A) and assessed for fluorescence internalization using a flow cytometer for both MFI (B) and a positive shift in intensity from the blank (grey) in FCM histograms (C). Polymer colors in (B) correspond to their respective shifts in (C).

While punctate fluorescence is easily visible, the location and type of endosomal compartments was still in question. To determine if the PTDMs were trapped in endosomes and if those endosomes were bound for degradation, co-localization with lysotracker was investigated.

2.3.3. Co-localization with Lysosomes

To compare the location of internalized PTDMs with late endosomal compartments, cells were treated with lysotracker red during the treatment with FITC-PTDMs (Figure 0.3). FITC-PTDMs (green) trapped in late endosomes should co-localize with the lysotracker red, indicated by yellow.

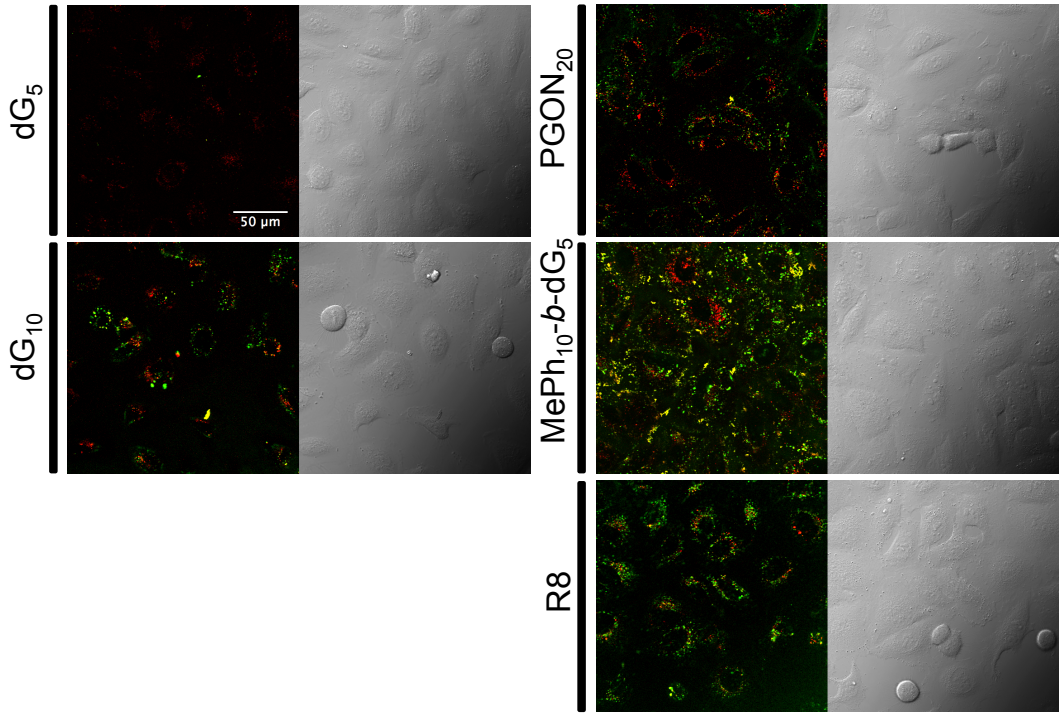

Figure 0.3. Internalization of FITC-PTDMs (green) in the presence of lysotracker (red) in HeLa cells. Cells were treated with 5 µM FITC-labeled polymer and lysotracker red for one hour and imaged using a CLSM.

While the diester homopolymers (**dG_5** and **dG_{10}**) proved less successful at internalization, **R8**, **$PGON_{20}$**, and **$MePh_{10}$-*b*-dG_5** showed robust internalization in punctate structures. Some of the **$MePh_{10}$-*b*-dG_5** appears to overlap with the lysotracker red, suggesting that endosomal entrapment is involved in internalization. The enlargement of **$MePh_{10}$-*b*-dG_5** with lysotracker red is overlapped (yellow), but mutual exclusion of the polymer (green) from the late endosomes (red) also exists. The Pearson's Correlation Coefficient (PCC) for the homopolymer PTDMs and **R8** was approximately 0.3 for all

samples, suggesting little to no correlation between the lysotracker and the polymer, while **MePh$_{10}$-*b*-dG$_5$** had a PCC of 0.8, suggesting high co-localization with the late endosomes. In other words, the hydrophobic PTDM was able to internalize in late endosomes but was not exclusively located there. This suggests that while some PTDM is permanently trapped in endosomes, it is not necessarily all destined for degradation. Additionally, escape from endosomal compartments cannot be dismissed. Longer time periods of this study with a more photo stable dye would allow for further investigation on the kinetics of our polymers within cells but was not the focus of this study.

2.3.4. Concentration Dependence

Since the mechanism of uptake can be dependent on the experimental conditions, an increase in concentration of **MePh$_{10}$-*b*-dG$_5$** and **R8** was used to investigate the effect of concentration on the predominant mode of internalization. Increasing the concentration appeared to increase the amount of **R8** and **MePh$_{10}$-*b*-dG$_5$** that entered the cell, although with increasing cytotoxicity (Figure 0.4A). Confocal images showed that at higher concentrations of both PTDMs, cells began to bleb and appeared unhealthy. More aggregated punctate fluorescence suggests compromise of the cellular membrane. The increase in fluorescence intensity and decrease in viability (using 7-AAD) with increasing concentration was quantified using flow cytometry. As shown in Figure 0.4, **R8** decreases to approximately 20% viability, while **MePh$_{10}$-*b*-dG$_5$** showed lower induced apoptosis even at higher concentrations of PTDMs despite considerable blebbing apparent in the CLSM images. There was no change in mechanism observed, as fluorescence remained punctate in all images, even after four hours. Although persistent punctate structures would suggest the inability of the PTDMs to escape endosomes over short periods of time, it is

difficult to exclude some PTDM endosomal escape since these fewer dispersed molecules would appear much dimmer by CLSM analysis.

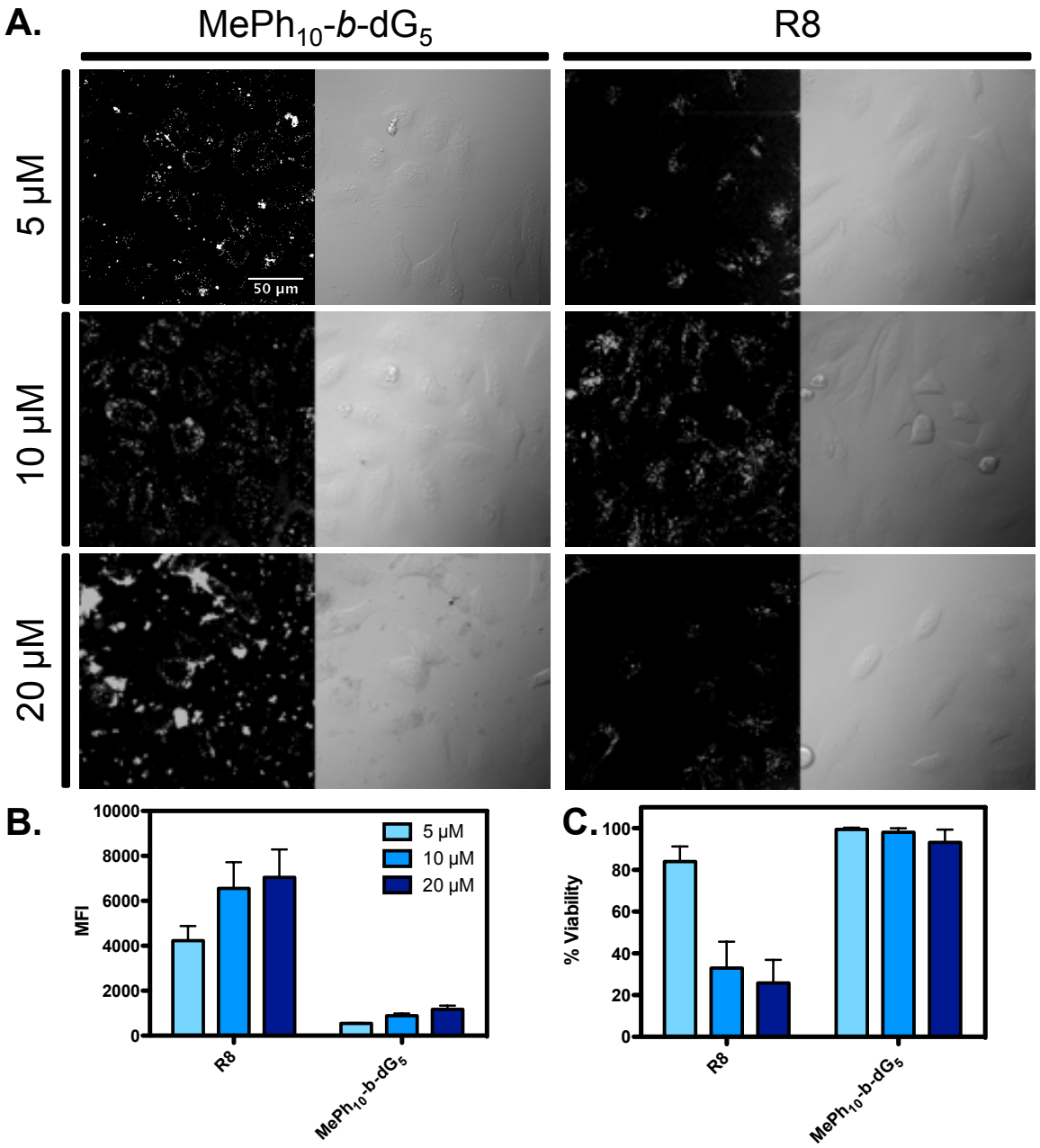

Figure 0.4. Effects of concentration on FITC labeled polymer internalization. Concentration dependence for $MePh_{10}$-b-dG_5 and R8 labeled with FITC at 5, 10, and 20 µM (A). HeLa cells were treated with 1 hour with PTDMs and imaged with a CLSM and assessed for MFI (B) and viability (C) using flow cytometry.

2.3.5. EGFP Delivery

Polymers were tested for transduction efficiency with enhanced green fluorescent protein (EGFP) as an indication of internal cell location and delivery efficiency. The PTDMs and protein were incubated for 30 minutes to allow for the formation of non-covalent complexes and then applied drop-wise to HeLa cells. At four hours, all homopolymer PTDMs and **R8** proved to be ineffective at delivering protein into the cell, showing limited uptake in both the microscope images and FCM data (Figure 0.5). The block copolymer showed significantly higher internalization, but was still punctate, suggesting entrapment in endosomes within the observed time periods. None of the PTDMs or **R8** showed any cytotoxic effects compared to the untreated sample, as determined by 7AAD during flow analysis. While the lack of delivery with the diester homopolymer PTDMs was unsurprising because of their poor internalization with the dye, it is interesting that **PGON$_{20}$** was unable to facilitate protein internalization. This could be attributed to its lack of a defined hydrophobic segment. **MePh$_{10}$-*b*-dG$_5$** was expected to have high delivery, as **R8** has been shown to be more effective with a hydrophobic component attached.[193] As demonstrated here and by others, the hydrophobic domain of the PTDM is important to protein internalization.[193,194] The block copolymer outperformed all other polymers tested at protein delivery yielding an MFI around 20 times higher, as determined by FCM (Figure 0.5B). This was corroborated with confocal images, which revealed both punctate and diffuse fluorescence within the imaged cells (Figure 0.5A).

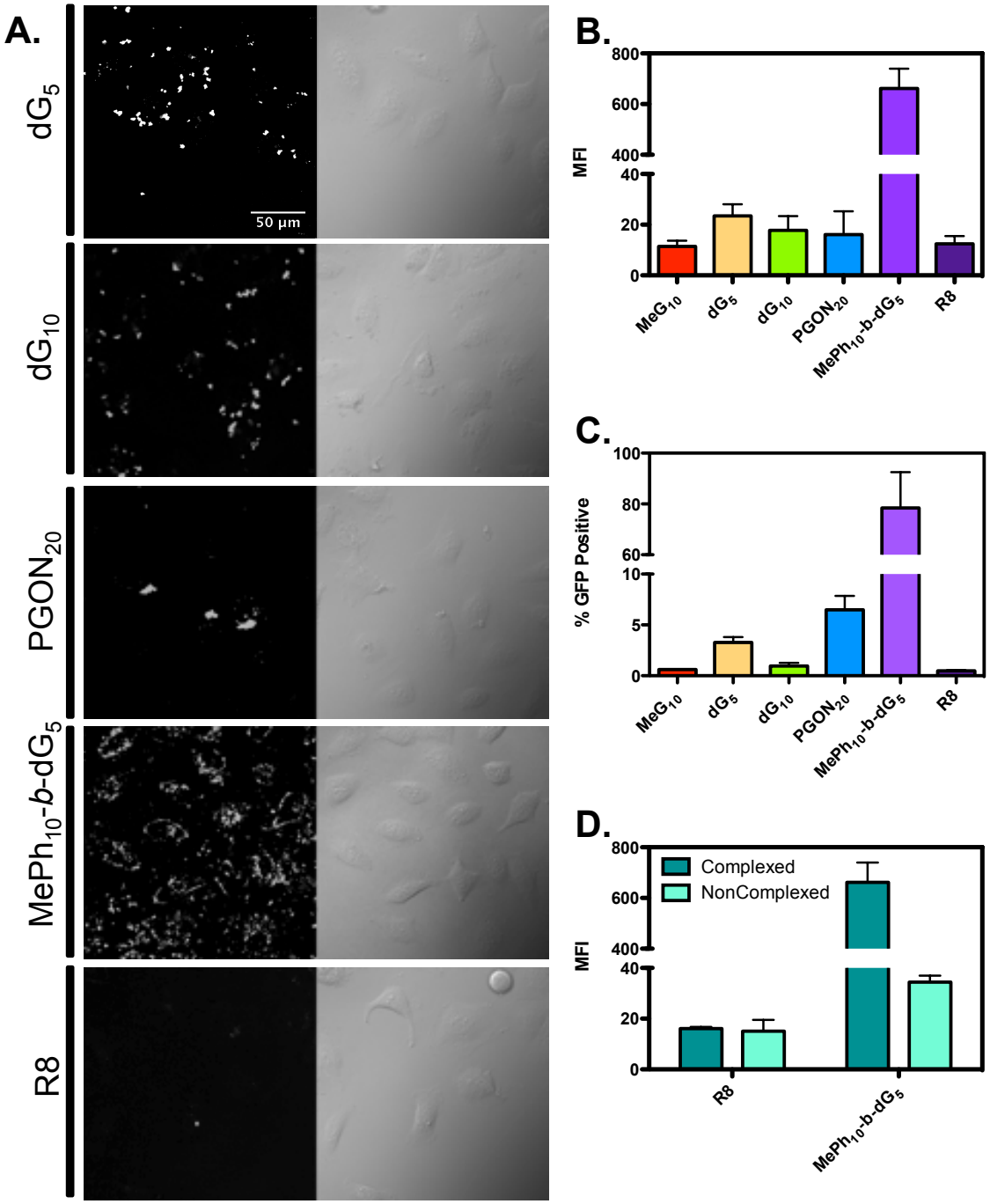

Figure 0.5. EGFP delivery into HeLa cells with unlabeled PTDMs. EGFP was complexed with PTDMs for 30 minutes at a molar ratio of 20:1. HeLa cells were treated with the complexes for four hours to observe internalization. Cells were imaged using a CLSM (A). Internalization efficiency as determined by MFI (B) and percent uptake (C) was confirmed using FCM to quantitate the delivery of EGFP. Complexed $MePh_{10}$-*b*-dG_5 with protein was tested in relation to non-complexed polymer and protein compared to R8 with and without the protein (D).

Additionally, complex formation was tested to determine if the PTDMs merely compromise the cell membrane allowing protein into the cytosol, or if they actively facilitate transport across the membrane. Cells were treated with **MePh$_{10}$-*b*-dG$_5$** and **R8** complexed with protein for 30 minutes at room temperature and were compared with cells treated directly with the PTDMs followed by protein, which were given no time to form a complex. The flow cytometry data, highlighted in Figure 0.5C, showed internalization for the cells treated with **MePh$_{10}$-*b*-dG$_5$** and protein complex, but not for those treated with the PTDMs and protein independently. This suggests that **MePh$_{10}$-*b*-dG$_5$** does not merely interact with the membrane to allow indiscriminant uptake of proteins in the cytosol, but rather an incubation time is required for the PTDMs to form complexes with the proteins.

2.4. Conclusion

While determining the predominant mode of internalization for CPPs remains a challenge, using PTDMs to advance the understanding of how structure influences uptake activity is critical to improving design parameters for efficient internalization. By examining changes in molecular composition in relation to their ability to enter cells when complexed with cargo, PTDMs can be enhanced to deliver specific molecules into the cell. Here, we performed common methods to assess internalization mechanisms and efficiency for guanidinium-containing PTDMs both alone and non-covalently complexed to cargo. This provides the first side-by-side studies for this class of PTDMs and **R8** with respect to cellular internalization. Homopolymer PTDMs proved to be inefficient at entering cells, with the exception of **PGON$_{20}$**, which was even able to enter cells at a higher capacity than the block copolymer PTDM **MePh$_{10}$-*b*-dG$_5$**. Increasing the concentration of the PTDMs led to improved internalization but also to higher cytotoxicity, a common observation

across PTDMs. None of the homopolymer PTDMs were able to facilitate the delivery of EGFP, while **MePh$_{10}$-*b*-dG$_5$** proved to be exceptionally efficient. Additionally, **MePh$_{10}$-*b*-dG$_5$** was the only polymer that also localized with late endosomes, suggesting endosomal entrapment for some of the complexes on the time scale used in this study. This finding highlights the importance of hydrophobic segments for efficient cargo delivery by PTDMs and that these structural changes influence the balance of pathways. These polymers remained punctate in the case of internalization for FITC-labeling and protein delivery, suggesting that endosomal uptake is the predominant mode of internalization. Findings will contribute to future design considerations for intracellular delivery systems and aid in our understanding of the modes of internalization for arginine-rich molecular transporters.

CHAPTER 3

INCREASED HYDROPHOBIC BLOCK LENGTH OF PTDMS PROMOTES PROTEIN INTERNALIZATION

3.1. Introduction

The plasma membrane plays a crucial role in cell survival, acting as a selectively penetrable barrier limiting large macromolecules from entering the cytoplasm.[195] As the field of molecular biology expands, investigation of intracellular processes is often hampered by the inability of biomacromolecules, such as proteins and antibodies, to efficiently and selectively cross the cell membrane.[11] The use of protein transduction domains (PTDs), sometimes referred to as cell penetrating peptides (CPPs), to facilitate the delivery of large biological cargo can be used to overcome this barrier.[10,11,196] PTDs are generally short, cationic protein segments with the ability to traverse the phospholipid bilayer.[197] The first protein discovered with this ability was the HIV-1 TAT protein.[163,164] Subsequent studies found that TAT's ability to translocate the membrane was largely due to the arginine rich domain between residues 48 – 60.[165] Guanidinium groups, such as those present in polyarginine, have since been shown to be important in facilitating translocation.[111,176] Through studying TAT and several other naturally occurring PTDs, along with their structural derivatives, it became apparent that secondary protein structure and peptide based backbones are not essential requirements for efficient cellular uptake, but that charge content is critical with guanidine functionality being particularly efficient.[111,112,165,198–200] Consequently, a large number of highly charged, cationic PTD mimics (PTDMs) have been reported.[167,201–207]

More recently, addition of a hydrophobic domain has been shown to improve membrane transduction activity.[208] Examples of this are N-terminal stearylation/acylation

of polyarginine,[24] and the use of supramolecular, hydrophobic counter ions,[176,209,210] which improve both membrane affinity and cellular internalization. Inherently amphiphilic CPPs, such as penetratin, have also provided a source of inspiration for chimera mimics like Pep-1.[119,161,211] Additionally, aromaticity has also been shown to play a role in membrane interactions and translocation;[212–214] oligoarginine activity has been enhanced with the use of aromatic counter ions, and with the incorporation of tryptophan or phenylalanine in the peptide sequences.[215–218]

Given the importance of aromatic amino acids in membrane proteins and their unique interactions with the bilayer, it was proposed that aromatic side chains would make better activators than other hydrophobic amino acids, given equal relative hydrophobicity.[111,219,220] We have previously reported the synthesis and preliminary investigations of oxanorbornene based guanidinium rich polymer mimics of polyarginine, which have shown higher membrane activity compared to their polyarginine counterparts.[187–189] Aromatic groups have been studied in peptide based CPPs and the role of hydrophobicity has been further explored for protein delivery using PTDMs.[186,221] More specifically, constitutional macromolecular isomers have been used to investigate the importance of sequence segregation for protein delivery, instilling the importance of a distinct hydrophobic domains.[134] Herein, we have designed and characterized eight different block-copolymer PTDMs inspired by polyarginine and amphiphilic peptides to deliver protein via non covalent complexes into HeLa cells, as well as two hard to transfect cell types, Jurkat T cells, and hTERT MSCs, thus providing critical information regarding the importance of hydrophobicity in PTDM delivery systems.

Polymer mimics offer distinct advantages over peptide derivatives of PTDs in that they are functionally and structurally versatile. In our previously reported synthetic approach, we achieved well-defined PTDMs with control over the spatial arrangement of positive charges and hydrophobic groups. These molecules were obtained using ring-opening metathesis polymerization (ROMP), a technique well known for its highly controlled nature, functional group tolerance, and rapid polymerization times. Here, we extend this platform to access a series of block copolymers with precise hydrophobic and cationic content and density.[134,185–187,191,221,222] Control over monomer hydrophobic content also enables deconvolution of side chain hydrophobicity from the hydrophobicity imparted by the polymer backbone. Using HPLC to determine the relative hydrophobicity of the monomers allows us to relate the hydrophobic content of each polymer, in terms of length, with their ability to deliver cargo.

Attachment of cargo via covalent linkage is often required for efficient use of PTDs.[128,223,224] The polymers studied here are able to form stable, non-covalent complexes with their associated cargos that are then internalized into cells.[188] In the context of promoting fundamental studies, non-covalent interactions are preferred due to their simplicity, delivery efficiency, and minimization of labor.[225] To evaluate the ability of these protein-containing complexes to enter cells, enhanced green fluorescent protein (EGFP) was chosen as a cargo. Flow cytometry was used to determine both the percentage of cells that receive the cargo, as well as the extent of uptake in the cells of interest. Additionally, cell viability was assessed after treatment, though very little toxicity was seen from any of the polymer-protein complexes.

In general, we found that a high density of cationic charge with a longer hydrophobic block led to higher levels of uptake. While some hydrophobic content threshold was required, the overall hydrophobic density seemed to have less of an impact than cationic density or length of the hydrophobic block on the ability of the block copolymers to efficiently internalize cargo. From this it has been hypothesized that increased hydrophobic block length creates a more stable interaction with the cargo protein. Similar results were found across all three cell types suggesting that this trend is applicable to all ROMP-based oxanorbornene block copolymers. The structure-activity study of these PTDMs provides guidance for building polymers that enable more efficient delivery of cargo, such as proteins, as tools to probe intracellular pathways.

3.2. Materials and Methods

3.2.1. PTDM Synthesis

3.2.1.1. Monomers

Similar to monomer synthesis in section **Error! Reference source not found.**, all f ive monomers were synthesized following the procedure introduced by Lienkamp et. al.[192] In general, the Diels-Alder adduct **1** was obtained by the reaction of maleic anhydride with furan in toluene. As following Lienkamp et al., the monomers were synthesized from **1** under similar conditions:

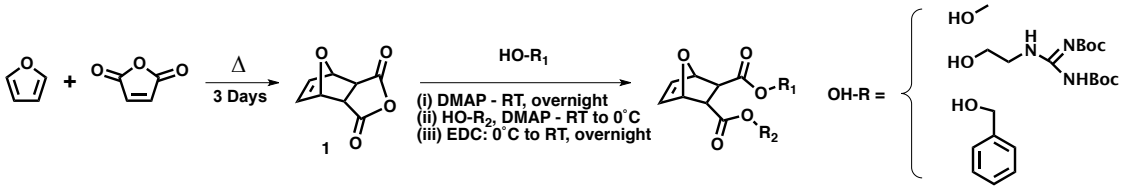

dG: 1 was dissolved in the minimum amount of dry DCM together with 2 eq. of 1,2-Di-Boc-2-ethyl guanidine, and 10 mol% 4-dimethylaminopyridine (DMAP). The temperature was lowered to 0°C with an ice bath and 1 eq. of 1-ethyl-3-(3-

dimethylaminopropyl)carbodiimide (EDC) was added, then stirred over night at room temperature. After completion of the reaction, the solution was concentrated and the product was purified via column chromatography with silica gel using DCM/ethyl acetate (8:2) as eluent. Vacuum evaporation of the solvent yielded the pure product with a yield of ~60%.

^{1}H NMR (300 MHz, CD3CN): δ 11.54 (s, 2H), 8.35 (s, 2H), 6.44 (s, 2H), 5.17 (s, 2H), 4.33 – 3.97 (m, 4H), 3.72 – 3.41 (m, 4H), 2.82 (s, 2H), 1.48 (s, 9H), 1.42 (s, 9H); 13C NMR (75 MHz, CD3CN): δ 172.43, 164.51, 157.35, 153.72, 137.56, 84.05, 81.41, 79.50, 63.72, 47.49, 40.21, 28.38, 28.09; HR-MS (FAB) m/z [M+H]+: 755.3827 (calc.), 755.3824 (found).

MeG: 1 was dissolved in the minimum amount of dry DCM together with 1 eq. of 1,2-Di-Boc-2-ethyl guanidine, and 10 mol% DMAP. The temperature was lowered to 0°C with an ice bath and 1 eq. of EDC was added, then stirred over night at room temperature. The half ester was precipitated from solution, isolated using vacuum filtration, and washed with cold DCM followed by drying on vacuum overnight. The half ester, one equivalent of MeOH. and 10% DMAP were dissolved in DCM and stirred at RT under nitrogen. After completion of the reaction, the solution was concentrated and the product was purified via column chromatography with silica gel using DCM/ethyl acetate (8:2) as eluent. Vacuum evaporation of the solvent yielded the pure product with a yield of ~80%.

^{1}H-NMR (300 MHz, CDCl3): δ=11.50 (1H, s), 8.55 (1H, s), 6.46 (2H, s), 5.3 (2H, d, J=6.0 Hz), 4.25 (2H, m), 3.72 (5H, m), 2.84 (2H, s), 1.49 (18H, s).13C-NMR (75 MHz, CDCl3): δ= 171.7, 171.5, 163.4, 156.3, 153.1, 136.6, 83.2, 80.7, 80.6, 79.4, 63.5, 52.4, 47.1, 46.6, 39.4, 28.3, 28.1. HR-MS (FAB): calc. 483.22, found 484.23.

dPh: 1 was dissolved in the minimum amount of dry DCM together with 2 eq. of benzyl alcohol, and 10 mol% DMAP. The temperature was lowered to 0°C with an ice bath and 1 eq. of EDC was added, then stirred over night at room temperature. After completion of the reaction, the solution was concentrated and the product was purified via column chromatography with silica gel using DCM/ethyl acetate (8:2) as eluent. Vacuum evaporation of the solvent yielded the pure product with a yield of ~88%.

^{1}H NMR (300 MHz, CD3CN): δ 7.34 (d, J = 3.0 Hz, 10H), 6.44 (s, 2H), 5.16 (s, 2H), 4.97 (dd, J = 45.5, 12.4 Hz, 4H), 2.87 (s, 2H); ^{13}C NMR (75 MHz, CD3CN): δ 172.37, 137.52, 137.03, 129.41, 129.14, 129.06, 81.30, 67.26, 47.58; HR- MS (FAB) m/z [M+H]+: 365.1389 (calc.), 365.1398 (found).

MePh: One equivalent of **1** and 1.25 equivalents of the corresponding substituted benzyl alcohol, and 10 mol% DMAP were dissolved in minimal amounts of distilled DCM and the reaction mixture was stirred under nitrogen at room temperature overnight. The half ester was precipitated from solution, isolated using vacuum filtration, and washed with cold DCM followed by drying on vacuum overnight. The half ester, one equivalent of MeOH. and 10% DMAP were dissolved in DCM and stirred at RT under nitrogen. The solution was then cooled down to 0˚C and one equivalent of EDC was added. The solution as stirred overnight under nitrogen at room temperature. The reaction mixture was then collected by rotoevaporation and purified by column chromatography with DCM/ethyl acetate (8:2). the sample was dried under vacuum over night to obtain a pure white solid (yield 82%).

^{1}H NMR (300 MHz, CD3CN): δ = 7.38 (comp, 5H), 6.44 (comp, 2H), 5.14 (d, 2H), 5.06 (comp, 2H), 3.50 (s, 3H), 2.84 (q, 2H).13C NMR (75 MHz, CD3CN): δ = 173.35, 172.84,

137.95, 137.91, 137.51, 129.84, 129.60, 129.50, 81.64, 81.63, 67.72, 52.75, 47.96, 47.89. HR-MS (FAB) m/z [M+H]+: 289.1076 (calc.), 289.1078 (found).

dMe: 1 was dissolved in the minimum amount of dry DCM together with 2 eq. of MeOH, and 10 mol% DMAP. The temperature was lowered to 0°C with an ice bath and 1 eq. of EDC was added, then stirred over night at room temperature. After completion of the reaction, the solution was concentrated and the product was purified via column chromatography with silica gel using DCM/ethyl acetate (8:2) as eluent. Vacuum evaporation of the solvent yielded the pure product with a yield of ~84% (6).

^{1}H NMR (500 MHz, DMSO): δ = 6.46 (s, 2H), 5.11 (s, 2H), 3.55 (s, 6H), 2.82 (s, 2H). 13C NMR (125 MHz, DMSO): δ = 171.70, 136.61, 79.74, 51.63, 46.23. HR-MS (FAB) m/z [M+H]+: 213.0763 (calc.), 213.0749 (found).

3.2.1.2. Polymers

Reaction conditions for block copolymer synthesis: Monomer **dG**, monomer **MePh**, and G3 catalyst were dissolved in dry DCM in respective schlenk flasks, purged with nitrogen, and subjected to three freeze-pump-thaw cycles. Monomer **dG** solution was added into the catalyst solution via syringe all at one time. The brown solution was stirred for 30 minutes at room temperature before monomer **MePh** was introduced. After stirring for an additional 2 hours, the reaction was terminated with 1 mL of ethyl vinyl ether and stirred for 30 minutes. DCM was evaporated and the product was dissolved in minimal DCM and loaded on a short silica gel column (7 cm length, 3 cm diameter). The unreacted end-group and any side products were washed from the column with DCM, while polymer remained on the column and was recovered with ethyl acetate. Ethyl acetate was evaporated to yield the pure product. Block co-polymers were characterized by ^{1}H NMR

along with THF GPC using a polystyrene standard (**Error! Reference source not found.**) t o determine block length and ratio.

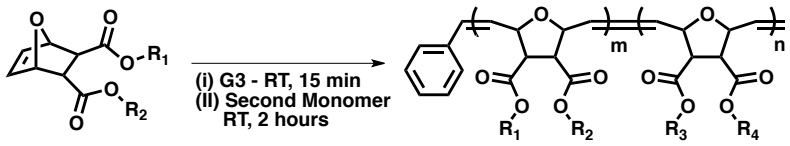

dPh$_5$-*b*-dG$_5$: ^{1}H-NMR (500 MHz, $(CD_3)_2CO$): δ 11.66 (2H, br), 8.47 (2H, br), 7.32 (12H, br), 5.98 (trans) and 5.68 (cis) (4H total, br), 5.21 (4H, br), 5.01 (cis) and 4.74 (trans) (4H total, br), 4.25 (4H, br), 3.69 (4H, br), 3.27 (4H, br), 1.46 (18H, s), 1.41 (18H, s).

MePh$_{10}$-*b*-dG$_5$: ^{1}H-NMR (500 MHz, CDCl3): δ 11.57 (2H, br), 8.40 (2H, br), 7.37 (6H, br), 5.80 (trans) and 5.61 (cis) (4H total, br), 5.08 (2H, br), 5.00 (cis) and 4.77 (trans) (4H total, br), 4.66 (2H, br), 4.17 (4H, br), 3.64 (4H, br), 3.49 (3H, br), 3.17 (4H, br), 1.46 (18H, s), 1.41 (18H, s).

dPh$_5$-*b*-MeG$_{10}$: ^{1}H-NMR (500 MHz, CDCl3): δ 11.52 (1H, br), 8.31 (1H, br), 7.33 (12H, br), 5.84 (trans) and 5.60 (cis) (4H total, br), 4.99 (4H, br), 4.90 (cis) and 4.60 (trans) (4H total, br), 4.17 (2H, br), 3.62 (3H, br), 3.49 (2H, br), 3.13 (4H, br), 1.44 (9H, s), 1.41 (9H, s).

MePh$_{10}$-*b*-MeG$_{10}$: ^{1}H-NMR (500 MHz, CDCl3): δ 11.55 (1H, br), 8.42 (1H, br), 7.34 (6H, br), 5.82 (trans) and 5.61 (cis) (4H total, br), 5.03 (2H, br), 5.00 (cis) and 4.76 (trans) (4H total, br), 4.59 (2H, br), 4.14 (6H, br), 3.62 (2H, br), 3.51 (4H, br), 3.14 (9H, br), 1.44 (9H, s), 1.40 (18H, s).

dPh$_{10}$-*b*-dG$_5$: ^{1}H-NMR (500 MHz, $(CD_3)_2CO$): δ 11.56 (2H, br), 8.39 (2H, br), 7.33 (12H, br), 5.88 (trans) and 5.62 (cis) (4H total, br), 5.10 (2H, br), 5.03 (cis) and 4.66 (trans) (4H total, br), 4.18 (2H, br), 3.60 (4H, br), 3.15 (4H, br), 1.46 (18H, s), 1.43 (18H, s).

$MePh_5$-*b*-dG_5: ^{1}H-NMR (500 MHz, $(CD_3)_2CO$): δ11.66 (2H, br), 8.47 (2H, br), 7.32 (6H, br), 5.98 (trans) and 5.68 (cis) (4H total, br), 5.21 (4H, br), 5.01 (cis) and 4.74 (trans) (4H total, br), 4.25 (4H, br), 3.69 (4H, br), 3.27 (4H, br), 1.46 (18H, s), 1.41 (18H, s).

dMe_5-*b*-dG_5: ^{1}H-NMR (500 MHz, $(CD_3)_2CO$): δ11.59 (2H, br), 8.39 (2H, br), 5.93 (trans) and 5.67 (cis) (4H total, br), 5.08 (4H, br), 4.90 (cis) and 4.70 (trans) (4H total, br), 4.23 (6H, br), 3.65 (4H, br), 3.18 (4H, br), 1.46 (18H, s), 1.41 (18H, s).

dMe_{10}-*b*-dG_5: ^{1}H-NMR (500 MHz, $(CD_3)_2CO$): δ 11.56 (2H, br), 8.38 (2H, br), 5.89 (trans) and 5.59 (cis) (4H total, br), 5.07 (4H, br), 5.96 (cis) and 4.69 (trans) (4H total, br), 4.21 (6H, br), 3.61 (4H, br), 3.22 (4H, br), 1.51 (18H, s), 1.47 (18H, s).

Table 0.1. Molecular weight of polymer series determined by gel permeation chromatography in tetrahydrofuran (THF) using a polystyrene standard.

Polymer	M_n	M_w	M_p	PDI
dPh_5-b-dG_5	9488	10123	10103	1.067
$MePh_{10}$-b-dG_5	5612	6071	6166	1.082
dPh_5-b-MeG_{10}	9965	10609	10782	1.065
$MePh_{10}$-b-MeG_{10}	11063	12060	12277	1.090
dPh_{10}-b-dG_5	9496	10265	10565	1.081
$MePh_5$-b-dG_5	5412	5744	5743	1.061
dMe_5-b-dG_5	5078	5392	5438	1.062
dMe_{10}-b-dG_5	6366	7011	7380	1.10

3.2.1.3. Deprotection

The polymers were dissolved in 2 mL DCM and 2 mL trifluoroacetic acid (TFA) for deprotection. After stirring overnight, the excess acid was removed by azeotropic distillation with methanol. After complete evaporation of the acid, samples were dissolved in water/methanol mixture and dialyzed against RO water until the conductivity of water

was ~0.1μS. The deprotected copolymer was recovered by lyophilization. Final deprotected polymer was stored at -20 ºC.

3.2.2. Characterization

3.2.2.1. Reverse Phase High Liquid Chromatography

Water and acetonitrile were each prepared with 0.1% TFA for the liquid phase. Monomers were prepared at 5 mg/mL in DMSO, which also served as the flow marker. Samples were loaded onto a C8 reverse phase column held at room temperature and run at a gradient of 100% water to 100% acetonitrile over 60 minutes. Each sample was followed by 15 minutes of equilibration back to water prior to loading of the next sample.

3.2.2.2. Dynamic Light Scattering

dPh$_{10}$-*b*-dG$_5$, **MePh$_{10}$-*b*-dG$_5$**, and **dMe$_{10}$-*b*-dG$_5$** were dissolved in DMSO and brought to a final concentration of both 5 mg/mL and 2.5 mg/mL. Samples were subjected to dynamic light scattering (DLS) at 10 degree intervals between 30 and 90 degrees. An exponential decay was fit to the data to calculate the R_g values of the polymers. Exponential fits can be found in Figure 0.4.

3.2.3. Protein Delivery

3.2.3.1. Suspension Cells

Jurkat T cells, a human T lymphocyte leukemia cell line (clone E6-1, ATCC TIB-152), were grown in RPMI 1640 supplemented with 10%(v/v) FBS, L-glutamine, non-Essential amino acids (NEAA), Na-pyruvate, 100 U/mL penicillin, and 100 U/mL streptomycin at 37˚C, 5% CO_2 and were passaged 24 hours before treatment. Polymers were mixed with 2 μg of EGFP at a ratio of 20:1 polymer to protein and allowed to complex for 30 minutes. Jurkats were harvested and suspended in fresh complete media and placed into a 12 well plate at $4X10^5$ cells/mL. PTDM – protein complexes were applied drop-wise

into each well. Cells were treated for 4 hours, then washed 3 times with 20 U/mL heparin in PBS before being suspended in 0.2% BSA FACS buffer and stained with 7-AAD. EGFP internalization and viability were assessed by flow cytometry using a BD® LSR-II. EGFP fluorophores were excited at 488 nm, and fluorescence was measured at 530 nm. The fluorescence signal was collected for 10,000 cells and viable cells were gated on to obtain a histogram of fluorescence intensity per cell. Live cells were assessed for their median fluorescence intensity (MFI) and their total positive shift in fluorescence (% positive). Internalization and delivery was repeated in three independent experiments. Statistical analysis was performed using the one way ANOVA and Tukey post hoc test to determine significance between polymers.

3.2.3.2. Adherent Cells

HeLa (human) and hTERT mesenchymal stem cells (MSCs) were grown at 37˚C with 5% CO_2 in DMEM supplemented with 10%(v/v) FBS, 100 U/mL penicillin, and 100 U/mL streptomycin. Cells were plated at $5X10^4$ cells/mL in a 12 well plate 48 hours before treatment for FACS analysis or $1X10^6$ cells in a 35 mm glass bottom plate for CLSM. Polymers were mixed with 2 μg of EGFP at a molar ratio of 20:1polymer to protein and allowed to complex for 30 minutes during which cells were aspirated and covered in fresh complete media. PTDM–protein complexes were applied drop-wise into each well. After 4 hours of treatment, cells were aspirated and lifted with 0.1% trypsin, then treated with complete media to bind excess trypsin. Cells were then washed 3 times with 20 U/mL heparin in PBS before being suspended in 2% FBS FACS buffer and stained with 7-aminoactinomycin D (7-AAD). Similar to the Jurakts, EGFP internalization and viability were assessed by flow cytometry under the same conditions.

3.2.3.3. Confocal Laser Scanning Microscopy

HeLa cells were seeded at 10^6 cells/ 2 mL of α-MEM with 10% FBS on 35 mm glass bottom plates and 10^5 cells/ 1 mL on 12-well plates 48 hours prior to treatment and cultured at 37˚C and 5% CO_2. Polymer was complexed with 2 μg of protein at a ratio of 20:1 polymer to protein for 30 minutes, during which the cells were aspirated and covered in fresh complete media. Cells were treated for 4 hours with the polymer protein complexes in a total volume of 1 mL α-MEM with 10% FBS. Before imaging, cells were washed three times with cold media and covered in 1 mL fresh cold α-MEM with 10% FBS. Cells were imaged using a FV300 CSLM Olympus IX81 microscope at 60X.

3.3. Results and Discussion

3.3.1. PTDM Design

The presence of guanidinium groups and hydrophobic moieties in PTDs and PTDMs has previously been reported as crucial for protein delivery.[194] To investigate the role of hydrophobicity and charge density, a series of monomers with varying hydrophobic and cationic content was synthesized (Figure 0.1). The hydrophobic magnitude of monomers in Figure 0.1B was assessed using reverse phase HPLC. The di-methyl (**dMe**) monomer had the lowest retention time (13.8 minutes), whereas methyl-phenyl (**MePh**), with an added benzene ring, had an intermediate retention time (27.5 minutes) and the di-phenyl monomer (**dPh**) had the longest retention time (35.9 minutes) (Error! Reference s ource not found.). These retention times indicate that the addition of phenyl groups to the monomer increases hydrophobic content and is thus translatable to the hydrophobic content of the polymers. Two guanidine containing monomers, methyl-guanidine (**MeG**) and di-

guanidine (**dG**), were also designed in order to investigate the role of cationic density within the positively charged block of the polymers.

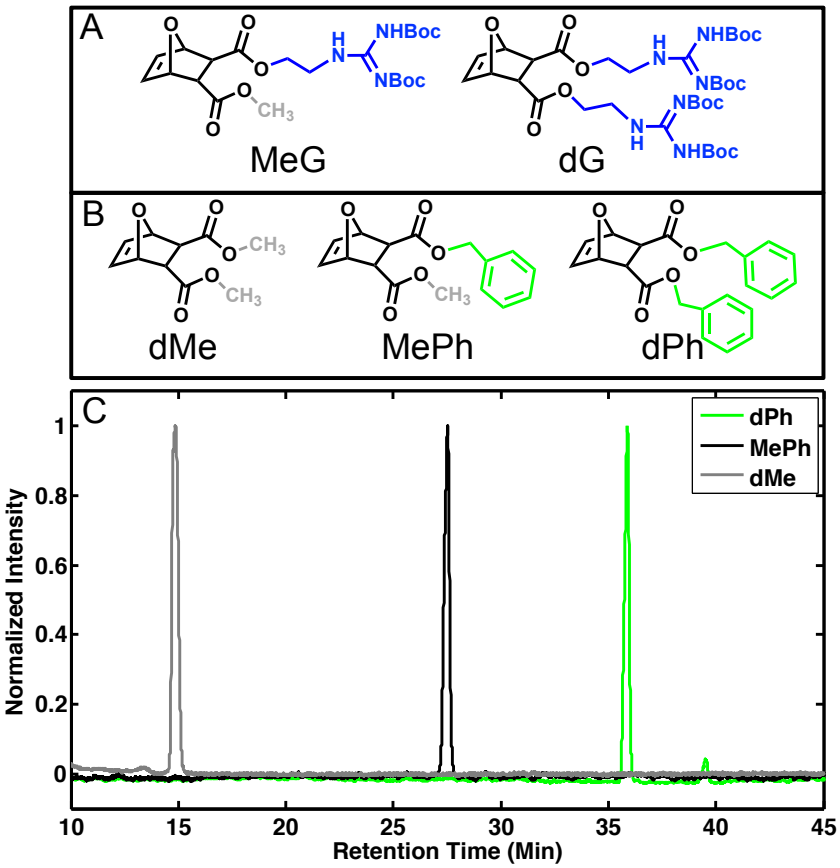

Figure 0.1. Oxanorbornene monomers used in this study. A) Guanidine containing monomers methyl guanidine (MeG) and di-guanidine (dG), with blue representing the cationic substituent and grey for the added methyl. B) Hydrophobic monomers di-methyl (dMe), Methyl-phenyl (MePh), and di-phenyl (dPh), with green representing the most hydrophobic components. C) Reverse-phase HPLC chromatographs for dMe, MePh, and dPh monomers elucidating relative hydrophobicity.

These difunctional monomers were polymerized by ROMP to yield low dispersity (Đ) oxanorbornene block copolymers. GPC traces showed a complete shift in the final diblock toward a higher molecular weight compared to the first block, illustrating controlled polymerization for efficient chain extension. All polymers had narrow Đ values (≤ 1.1) as determined by GPC, and a phenyl to guanidine ratio consistent with expectations, as determined by ^{1}H NMR spectroscopy.

A series of four block copolymers was created comprised of a first block with ten phenyl substituents and a second block with ten guanidine substituents. Within these samples, however, the density of these functional groups is varied using the smallest methyl substituent to add space between hydrophobic or cationic groups. These are depicted in Figure 0.2 as **dPh$_5$-*b*-dG$_5$**, **MePh$_{10}$-*b*-dG$_5$**, **dPh$_5$-*b*-MeG$_{10}$**, and **MePh$_{10}$-*b*-MeG$_{10}$**. This set of polymers was designed to explore the effect of varying charge and hydrophobic density along the polymer backbone on the ability of the PTDMs to deliver protein into HeLa, hTERT MSC, and Jurkat T cells.

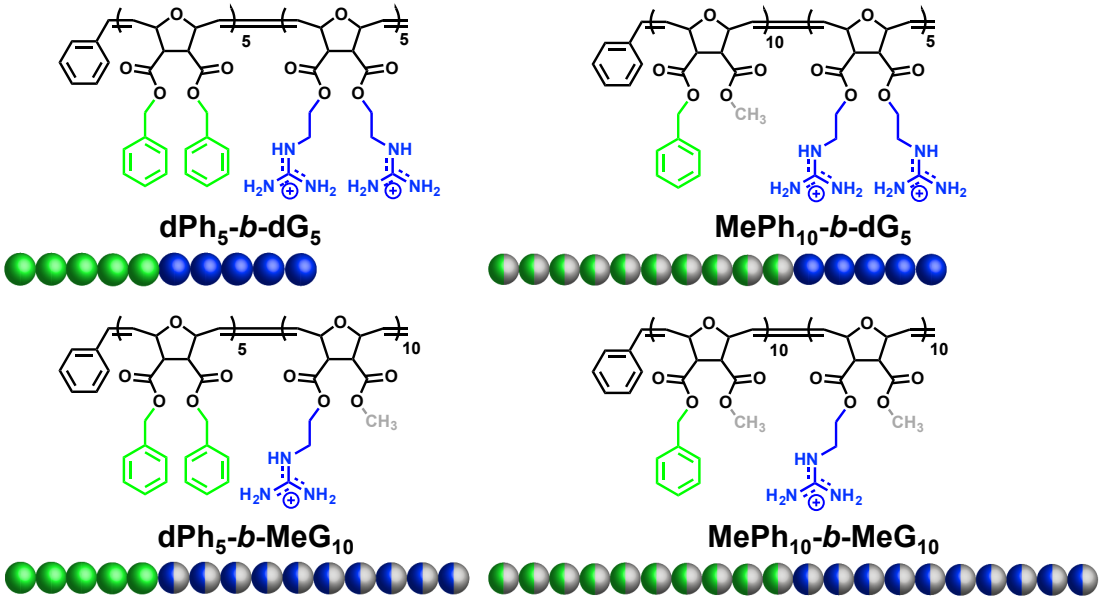

Figure 0.2. Structures and cartoons of a polymer series with varying cationic and hydrophobic density. Each polymer contains 10 phenyl groups represented in green and 10 guanidinium groups represented in blue. The density of the hydrophobic and cationic groups is varied using a methyl substituent (grey).

To further investigate the effect of hydrophobic moieties and backbone contribution on protein delivery, the series was expanded to include another set of polymers that hold the high guanidinium density (**dG$_5$**) constant but vary hydrophobic density (either **dPh**, **MePh**, or **dMe**) and length (5 or 10) to compliment the initial polymer set. For example, **dPh$_{10}$-*b*-dG$_5$** has high hydrophobic density (**dPh**) with a length of ten to match the

backbone length of the longest hydrophobic block (**MePh$_{10}$-*b*-dG$_5$**); **MePh$_5$-*b*-dG$_5$** was added to distinguish between added backbone length and decreased hydrophobic density (juxtapose **MePh$_{10}$-*b*-dG$_5$** and **dPh$_{10}$-*b*-dG$_5$**); lastly, **dMe$_5$-*b*-dG$_5$** and **dMe$_{10}$-*b*-dG$_5$** were included as controls to mimic the length of the backbone added by the hydrophobic blocks, while minimizing the hydrophobicity of the substituents. This second series of other polymers, displayed in Figure 0.3, was specifically designed to decouple hydrophobic block length from hydrophobic content with respect to protein delivery.

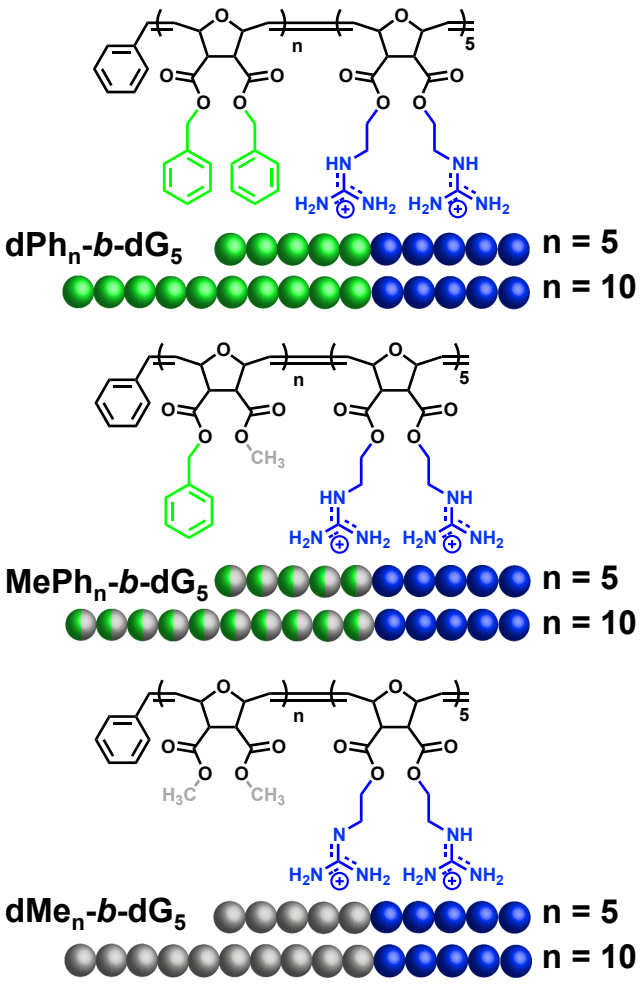

Figure 0.3. Structures and cartoons of the second polymer series with varying hydrophobic density and length. dPh$_5$-b-dG$_5$ and MePh$_{10}$-b-dG$_5$ are repeated from Figure 0.2 for ease of comparison. Hydrophobic phenyl substituents are represented in green, cationic moieties in blue, and methyl groups in grey.

3.3.2. Dynamic Light Scattering

Dynamic light scattering was performed on **dPh$_{10}$-*b*-dG$_5$**, **MePh$_{10}$-*b*-dG$_5$**, and **dMe$_{10}$-*b*-dG$_5$** to determine whether these molecules self-assemble in an aqueous environment Figure 0.4. These three polymers were chosen to compare the maximum hydrophobic block lengths with varying phenyl group density. While this is not a direct indication of their ability to interact with cargo or transverse the membrane, it is important to understand whether they present a "hydrophobic core" in which the protein might reside or act as individual, solvated chains. **dMe$_{10}$-*b*-dG$_5$** had an R_h of 33 nm, **MePh$_{10}$-*b*-dG$_5$** had an R_h value of 67 nm, and the relaxation curves (Figure 0.4) for **dPh$_{10}$-*b*-dG$_5$** indicated a polydisperse R_h fit of 29 nm showing that all three block copolymers self-assemble in aqueous solution. Given that the overall sizes are similar despite the variation in hydrophobic side chain suggests that the overall block architecture is more important to driving assembly than the side chain composition. Both polymers containing phenyl side chains had broader distributions, so it is possible that the side chains have some influence on the nanoparticles internal organization. Nevertheless, from these findings it can be hypothesized that the self-assembled aggregates provide a hydrophobic domain that allows the polymers to complex their cargo while the role of electrostatic interactions remains unclear given the phosphate buffer solution in which they are formed contains around 150 mM of salt.

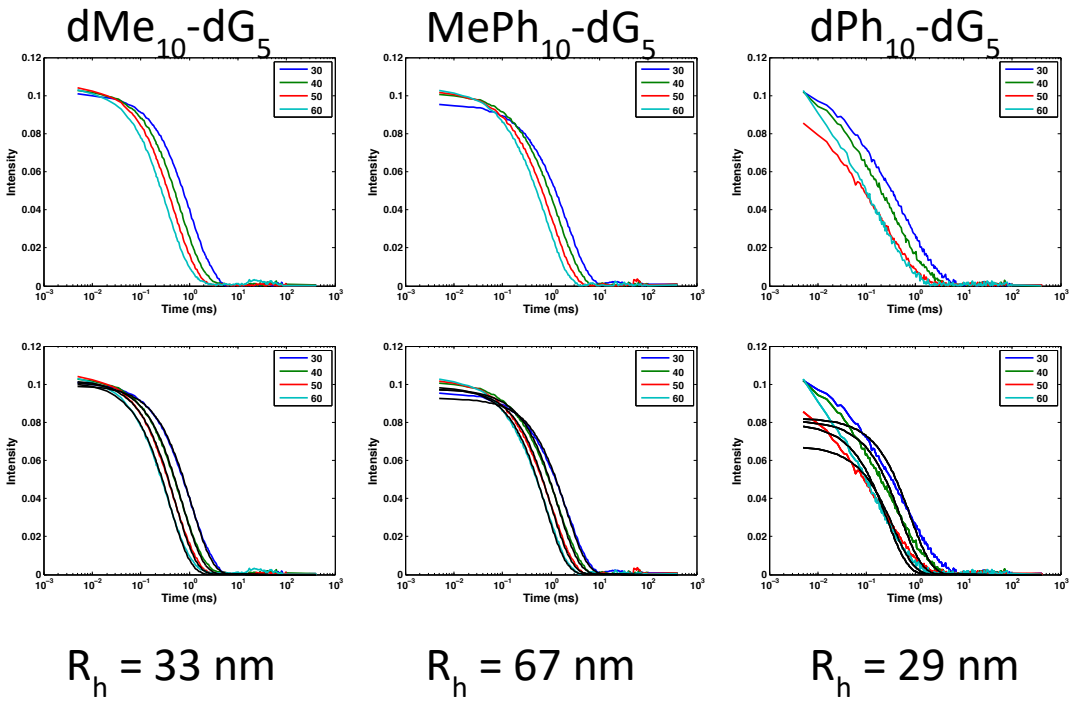

Figure 0.4. Dynamic light scattering curves (top) for dMe10-dG5, MePh10-dG5, and dPh10-dG5 overlayed with their CONTIN fits (bottom) used to predict the radius of hydration. Measurements were taken at 30˚, 40˚, 50˚, and 60˚ and used together for the prediction.

3.3.3. Protein Delivery

The ability of the polymers to facilitate the internalization of EGFP into cells was investigated in Jurkat T cells, HeLa cells, and hTERT MSCs. To assess protein delivery and viability, cells were analyzed using flow cytometry. In addition, confocal microscopy was used to image uptake into HeLa cells for the first series of polymers (Figure 0.2). Trends were relatively consistent across the three cell lines with respect to their percent uptake, median fluorescence intensity (MFI), and viability profiles. While all polymers tested were able to deliver consistently into greater than 50% of the cell populations (SI), the amount of protein delivered, determined by MFI, varied based on the polymer and, to a limited extent, cell type. Cell viability was above 95% in both HeLa and Jurkats, but

slightly decreased to just above 80% for **dPh$_5$-*b*-dG$_5$** and **MePh$_{10}$-*b*-dG$_5$** in the hTERT MSCs as seen in Figure 0.5.

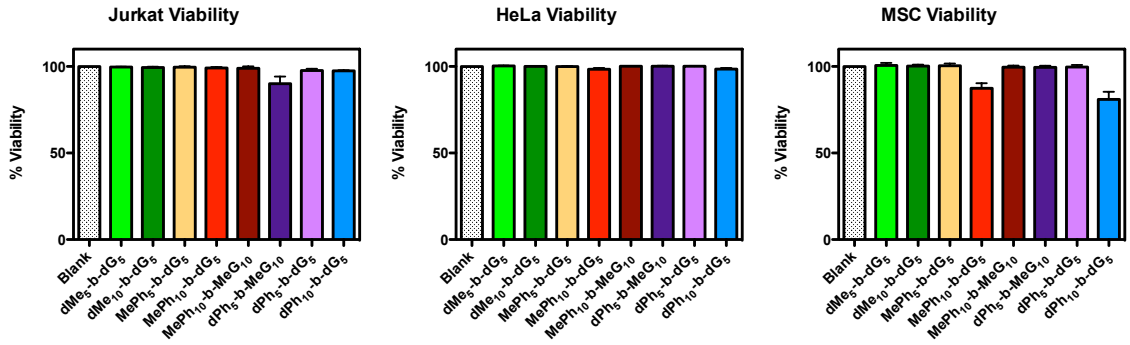

Figure 0.5. Cellular viability after cells were treated with 2 µg of protein at a 20:1 polymer to protein molar ratio for 4 hours, as determined by 7AAD staining compared with an untreated sample. Viability is above 90% in all cases, except with the MePh$_{10}$-dG$_5$ and dPh$_{10}$-dG$_5$ in the hTERT MSCs which are higher than 85%.

The MFI (Figure 0.6) in all cell types, as established by flow cytometry, showed that **MePh$_{10}$-*b*-dG$_5$**, containing the high cationic density **dG** monomer, yielded greater internalization than its counterpart, **MePh$_{10}$-*b*-MeG$_{10}$**, with the **MeG** monomer. This indicates that increasing the cationic density of the block copolymer improves protein internalization, corroborating the suggestion that high guanidine density is important for membrane interactions and therefore delivery.[187] It should be noted that while there was no statistical difference between delivery using **dPh$_5$-*b*-dG$_5$** and **dPh$_5$-*b*-MeG$_{10}$**, the fluorescent shift appears higher for the more cationically dense polymer (**dPh$_5$-*b*-dG$_5$**) in Jurkats, suggesting that similar correlations could be drawn from this more sensitive cell line. These findings were additionally confirmed by images taken with CLSM of HeLa cells treated with the polymer-protein complexes, Figure 0.7, which revealed both punctate and diffuse fluorescence within the cells.

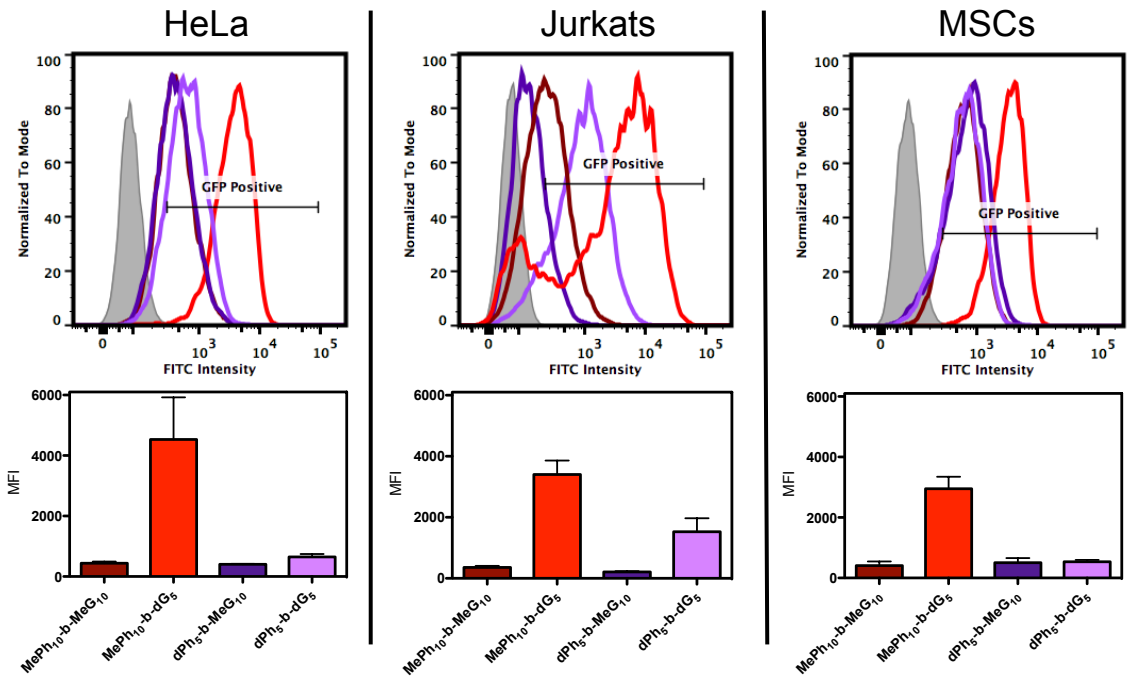

Figure 0.6. Representative histograms (top) compared to a blank (grey) and the corresponding median fluorescence intensity (bottom) for EGFP delivery with $MePh_{10}$-b-MeG_{10}, $MePh_{10}$-b-dG_5, dPh_5-b-MeG_{10}, and dPh_5-b-dG_5 into HeLa, Jurkat T cells, and hTERT MSCs. Cells were treated with 2 µg of protein at a 20:1 polymer to protein molar ratio for 4 hours, then washed with heparin to remove membrane bound proteins. A shift to the right from the grey blank in the histograms indicates higher fluorescence and was used to establish the median fluorescence intensity (MFI) as well as the percent uptake.

While all four polymers yielded a complete shift in the fluorescence population of the cells, the MFI was 10X higher when using **$MePh_{10}$-*b*-dG_5** in all three cell types. Surprisingly, increasing hydrophobic density did not improve the ability of the polymers to deliver protein into any of the cell types, as seen by comparing **dPh_5-*b*-dG_5** with **$MePh_{10}$-*b*-dG_5**. With **$MePh_{10}$-*b*-dG_5** able to deliver the most protein (MFI ranging between 3000 to 4000) into the highest percentage of cells (around 95% depending on the cell type), high cationic density coupled with a lower density hydrophobic block appeared to optimize protein internalization. However, these comparisons alone do not fully decouple hydrophobic density of the monomer functional groups from potential hydrophobic effects related to the length. To explore this specific relationship, the series

was expanded to include **dPh$_{10}$-*b*-dG$_5$**, **MePh$_5$-*b*-dG$_5$**, **dMe$_5$-*b*-dG$_5$**, and **dMe$_{10}$-*b*-dG$_5$**, as shown in Figure 0.3.

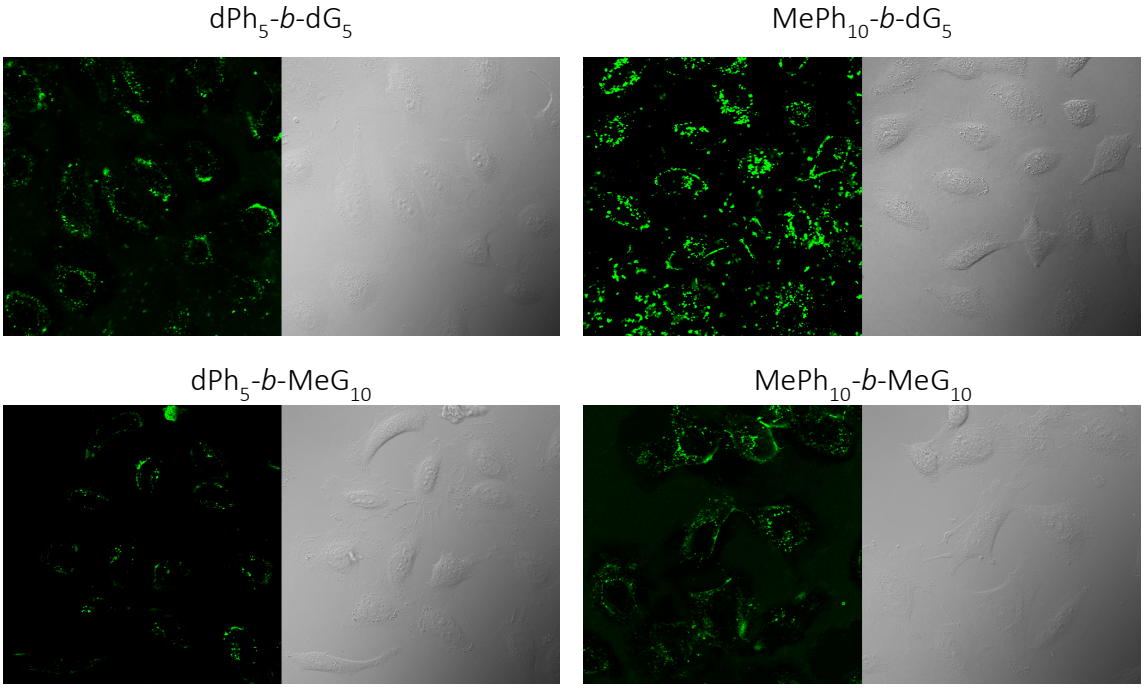

Figure 0.7. CLSM images of EGFP delivery into HeLa cells by MePh$_{10}$-b-MeG$_{10}$, MePh$_{10}$-b-dG$_5$, dPh$_5$-b-MeG$_{10}$, and dPh$_5$-b-dG$_5$. Cells were treated with 2 µg of protein at a 20:1 polymer to protein ratio for 4 hours, and then washed 3 times to remove excess protein.

These polymers all contain a cationic **dG** block length of 5, since high cationic density appears to be more optimal for protein delivery. Higher internalization was seen when the **dPh** block length was increased from 5 to 10 (**dPh$_{10}$-*b*-dG$_5$**) yielding a higher MFI and effecting a higher percentage of the cell population in all cell types. Decreasing the **MePh** block length from 10 to 5 (**MePh$_5$-*b*-dG5**) reduced delivery and the percentage of cells that received protein. More specifically, in Jurkats but not HeLa or the MSCs, there is an added advantage of using **dPh$_{10}$-*b*-dG$_5$** as it results in almost two fold higher MFI than **MePh$_{10}$-*b*-dG$_5$**. This difference highlights the tunability of this polymer platform to address specific cell types. Any additional hydrophobicity introduced by increasing the length of the polymer was investigated by replacing the phenyl substituents with methyl

groups (**dMe$_5$-*b*-dG$_5$** and **dMe$_{10}$-*b*-dG$_5$**). These polymers showed moderate protein delivery to a high number of cells, but the amount of protein delivered was far less than their phenyl containing counterparts (Figure 0.8). This indicates that, in addition to increased block length, the presence of a threshold hydrophobicity is important for efficient cellular internalization of this cargo.

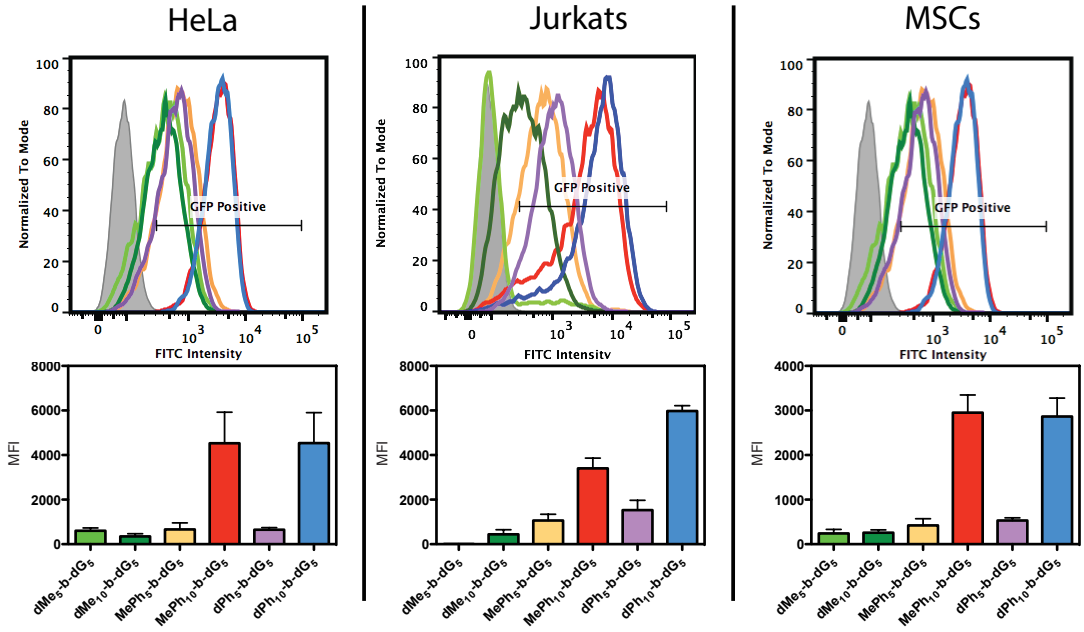

Figure 0.8. Representative histograms and the corresponding median fluorescence intensity for EGFP delivery with dMe$_5$-b-dG$_5$, dMe$_{10}$-b-dG$_5$, MePh$_5$-b-dG$_5$, MePh$_{10}$-b-dG$_5$, dPh$_5$-b-dG$_5$, and dPh$_{10}$-b-dG$_5$ into HeLa, Jurkat T cells, and hTERT MSCs. Cells were treated with 2 µg of protein at a 20:1 polymer to protein molar ratio for 4 hours, then washed with heparin to remove membrane bound proteins. A shift to the right from the grey blank in the histograms indicates higher fluorescence and was used to establish the median fluorescence intensity (MFI) as well as the percent uptake.

The ability to deliver proteins is substantially amplified when the hydrophobic block length is increased for the two phenyl-containing monomers (**MePh**, **dPh**), regardless of cell type. Both adherent cell types showed insignificant differences in MFI between **MePh$_{10}$-*b*-dG$_5$** and **dPh$_{10}$-*b*-dG$_5$**, while Jurkats were sensitive to the hydrophobic substituents with **dPh$_{10}$-*b*-dG$_5$** outperforming **MePh$_{10}$-*b*-dG$_5$**. Further investigation with

other cell types, both adherent and suspension, might provide insight into this difference. Additionally, other polymer series with different hydrophobic substituents may help determine if the aromaticity of the phenyl group is indeed crucial, or cell type dependent. Lastly, optimization with different cargos would allow for further development and specificity of this polymer platform for increased internalization of proteins and antibodies into hard to transfect cell types.

3.4. Conclusion

Oxanorbornene block copolymers with varying cationic and hydrophobic density but the same charge and hydrophobic content were synthesized and characterized. While all of the PTDMs displayed the ability to deliver protein into HeLa, Jurkats, and hTERT MSCs, increased cationic density proved to have a slight edge over those with a methyl substituent on each guanidinium-based monomer. A second series of polymers highlighted the importance of hydrophobic length over density, although additional hydrophobicity from increasing the polymer backbone length does not exceed the hydrophobic threshold that is required for protein internalization. Increasing the length of the hydrophobic blocks may introduce better PTDM–protein interactions, facilitating delivery across the membrane. Further studies using different cargo types such as intracellularly active proteins would highlight the capabilities of these block copolymers.

CHAPTER 4

SERUM SENSITIVE PROTEIN DELIVERY BY POLYMERIC PEPTIDE MIMICS

4.1. Introduction

The field of transfection has been dominated by the delivery of DNA for constitutive expression within the cell. The delivery of proteins into the cytosol can be exploited to produce highly specific intracellular interactions with spatial and temporal control.[6] Results from protein transfection can be extremely fast in comparison with traditional gene expression as it does not require transcription and translation.[226] The temporal control allows for investigation of transient effects of proteins, while avoiding over expression or random insertion of DNA into the targeted genome.[8] Protein and antibody delivery into the cytosol provide a platform to probe intracellular pathways involved in protein expression, transcriptional regulation, cell cycle, as well as many others.[26]

To date, the concept of protein delivery has been predominantly addressed by viral transfection, electroporation, and liposomal carriers.[6] While relatively effective, these techniques have severe limitations such as high toxicity and low efficiency that have been addressed by the development of a category of protein delivery vehicles based on cationic polymeric systems.[7,8,114,227] While several polymer systems are currently commercially available, often they are limited in their cargo variety, as well as the type of cell they are able to deliver into. Additionally, almost all delivery platforms require serum free conditions, which can be detrimental to the viability of the cells. Herein, we compare a variety of commercially available amphiphilic polymers and peptides in their ability to deliver GFP into HeLa, HUVEC, hTERT mesenchymal stem cells, and Jurkat T cells in

both serum free and complete media. While most of the reagents are proprietary, the following are descriptions of each of the carriers from their respective manufacturers.

4.1.1. Pep-1

Pep-1 was first reported by Morris et. al. to deliver proteins intracellularly using non-covalent interactions with the macromolecule of interest.[119] Since then Pep-1 and its derivatives have been patented and are now marketed by Active Motif® under the name Chariot™. Chariot™ claims delivery efficiency between 60-95% in less than two hours after delivery, at which time live cells can be assayed to determine the effects of the introduced material, without the need for fixing. According to Morris et. al. and Active Motif®, the peptide stabilizes the protein, reducing degradation and preserving its natural characteristics during delivery.[118,119,161] After delivery, the complex dissociates, leaving the macromolecule biologically active and free to proceed to its target organelle. Previous reports indicate delivery occurs in the presence or absence of serum and is independent of the endosomal pathway, which can modify macromolecules during internalization.[228] Additionally, Chariot™ boasts low toxicity to the cells being transfected.

4.1.2. PULSin

PULSin™ is a cationic amphiphilic reagent designed by Polyplus Transfection® for the delivery of peptides, antibodies and proteins into cells. The proprietary formulation claims efficient delivery of anionic proteins and antibodies into a large variety of eukaryotic cell lines and primary cells. PULSin™ is most efficient when able to interact with the protein by electrostatic and/or lipophilic interactions. According to Polyplus Transfection®, complexes are internalized via anionic cell-adhesion receptors and are

released into the cytoplasm where they disassemble. The process is non-toxic and delivers functional proteins, without the requirement of fixation.

4.1.3. ProteoJuice

ProteoJuice™ is a reagent produced by Novagen® owned by MerckMillipore® for the introduction of intact functional protein into mammalian cells. ProteoJuice™ forms non-covalent interactions with protein and has endosome protective properties ensuring delivery of intact protein within the cell. ProteoJuice™ is compatible with delivery of peptides and small proteins, large proteins, and even multimeric protein complexes with minimal toxicity and broad cell specificity. Live cells can be examined less than two hours after delivery to determine the effects of the introduced material without the need for cell fixation.

4.1.4. Xfect

The Xfect™ Protein Transfection Reagent uses a cell-penetrating peptide developed at Clontech® to bind and transport active proteins directly into a wide variety of mammalian cell types, including hard-to-transfect human suspension cell lines and mouse embryonic stem cells. Xfect™ is a modified peptide with cell-penetrating activity whose amino acid composition enables it to interact with a protein cargo and transport this protein across a cell membrane barrier within 2 hours.

4.1.5. Protein Transduction Domain Mimics

The amphiphilic polymeric protein transduction domain mimic (PTDM) **$MePh_{10}$-*b*-dG_5** was designed to mimic cell penetrating peptides incorporating a dense block of guanidine, known for its ability to permeate cell membranes, attached to a hydrophobic block, which has been shown to facilitate cargo delivery.[134,135,229,230] Here, the

nomenclature **MePh** refers to a block that contains monomers that have methyl and phenyl substituents, and **dG** is constituted of two guanidine groups per monomer imparting dense cationic charge. The Tew group has previously shown proof of concept for cellular uptake of similar PTDMs using a fluorescent label and subsequent delivery of proteins, peptides, and antibodies into Jurkat T cells as well as primary cells.[115,134,136,187,191,229–232] The amphiphilic nature of this PTDM allows it to form a non-covalent complex with the desired cargo and facilitate its transport across the cell membrane in both complete media and serum free conditions with low cytotoxicity. Internalization of the cargo has been tested as early as 4 hours after delivery and protein function has been recorded out to 72 hours.

4.2. Materials and Methods

A total of five cationic polymer delivery vehicles were tested for their ability to deliver GFP into a variety of cell types. Specifically, the commercially available Pep-1, also known as Chariot™, ProteoJuice™, PULSin™, and Xfect™ were compared with our amphiphilic polymeric peptide mimic, herein referred to as the protein transduction domain mimic (PTDM), in both complete and serum free conditions. All purchased delivery reagents claim non-covalent interactions with their cargo and broad cell specificity.

A variety of human cell lines were chosen to demonstrate translation across cell types: HeLa, HUVEC, Jurkat, and hTERT mesenchymal stem cells (MSCs). HeLa cells are the oldest and most commonly used adherent cell line and are used in many research fields due to their stability and relative ease of transfection. HUVECs are derived from the endothelium of veins from a human umbilical cord and have different surface properties than many other cell lines. Jurkat T cells are a suspension cell line of T cells that have

proven difficult for many transfection reagents. Lastly, we used MSCs as a proof of concept cell type whose differentiation could be affected by protein cargo delivery.

To assess the ability of protein delivery, GFP was chosen as a cargo as it is self-reporting and readily accessible to most laboratories. The amount of protein delivered was held constant at 2 μg so that the different reagents could be compared to one another. Uptake was assessed by flow cytometry after treatment with the complexes and subsequent washing of the cell surface with trypsin followed by three heparin washes (20 U/mL) to remove any complexes stuck to the cell surface.

The commercial reagents all required some optimization regarding the ratio of reagent to protein cargo, incubation time, and cell density to improve their ability to deliver specific proteins. Delivery conditions were optimized for each of the reagents using HeLa and Jurkat T cells and translated across the other cell types. All adherent cells were plated 24 hours prior to transfection at respective cell densities to achieve 70-90% confluency at the beginning of the experiment.

Even though some of the reagents claim the ability to deliver in complete media, most suggest removal of any exogenous protein during the actual transduction. Several suggest washing the cells up to three times with PBS to remove the presence of serum. To accommodate this, delivery was performed on cells that had been washed two times with PBS and then suspended with serum free media. Optimization regarding serum free conditions revealed higher viability (using 7-AAD) if cells were treated for 2 hours and then supplemented with complete media for an additional 2 hours. A comparison of the reagents was also made in complete media (10% FBS) to show the effect of the presence of serum on uptake.

4.3. Results and Discussion

As measured by a shift in cell fluorescence in relation to the untreated control (% Positive), all of the commercial reagents except Chariot™ were able to deliver GFP into all four cell types effecting 80% or less of the cells as shown in Figure 0.1. As expected, a reduction in percent positive cells was observed when the complex delivery was done in the presence of complete media. In contrast, the median fluorescence intensity (MFI), which is directly proportional to the amount of protein delivered was exceptionally low for all the commercial carriers in all cell types indicating that while they were able to target many cells, they were not able to deliver large amounts of protein into the cells.

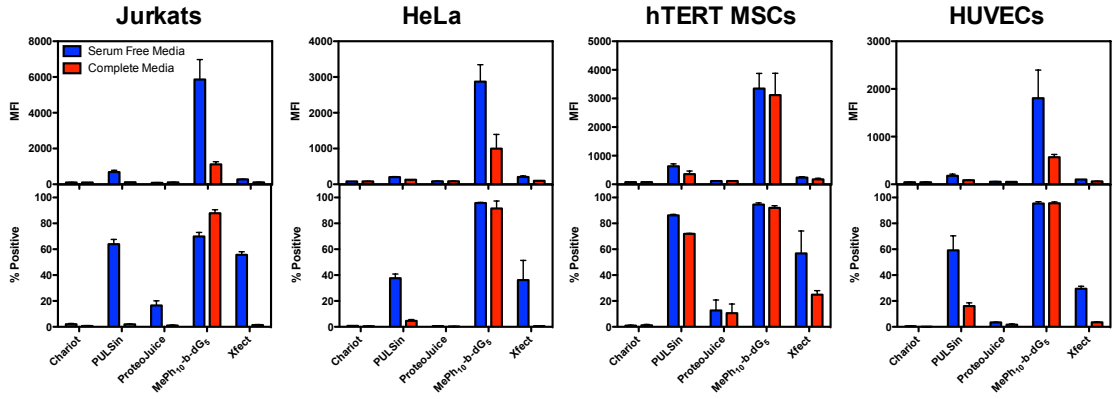

Figure 0.1. Delivery efficiency of 2 µg GFP into Jurkats, HeLa, hTERT mesenchymal stem cells, and human umbilical vein endothelial cells after 4 hours of treatment in serum free conditions or complete media with amphiphilic polymers designed for non-covalent delivery. The top row shows the median fluorescence intensity, signifying the amount of protein that was delivered into the cells, while the bottom is the percentage of cells that were positive for the fluorescent cargo. Data is displayed as the mean and SEM of three replicates.

Chariot™ showed no delivery of GFP into any of the cell types in either serum free or complete media. Extra effort was spent optimizing for this carrier with GFP, but regardless of conditions, it never showed substantial uptake or increase in MFI. This could

be related to the nature of the cargo and its subsequent interactions with the peptide, since the manufacture claims it can deliver β-galactosidase efficiently into a variety of cell types.

Moderate delivery was achieved using PULSin™, especially in serum free conditions delivering into 40-80% of the cells. The positive shift was muted in the presence of serum, with a smaller positive shift shown in HUVEC and MSCs. While there was a small shift in MFI from the blank in all cell types for PULSin, it appears that the relative shift was low when compared with the PTDM. Serum free conditions appeared to facilitate delivery, suggesting that PULSin might not bind to the GFP very strongly and that it can easily swap out serum proteins for the fluorescent cargo. Alternatively, the serum proteins may help inhibit interactions with the cell membrane.

ProteoJuice™ was largely ineffective in the HeLa and HUVEC cell types but showed around 20% delivery into Jurkats and MSCs. Uptake was not reflected in the MFI, where ProteoJuice appears to only deliver a small amount of GFP into any of the cell types. Unfortunately, the cell viability in Jurkats was greatly reduced in serum free conditions for this reagent (Figure 0.2).

Xfect™ performs well in serum free conditions, delivering in up to 60% of Jurkats, though the MFI of those cells remains low indicating low amounts of protein are delivered into the GFP positive cells across all cell types. Only in MSCs does Xfect™ show any delivery in complete media.

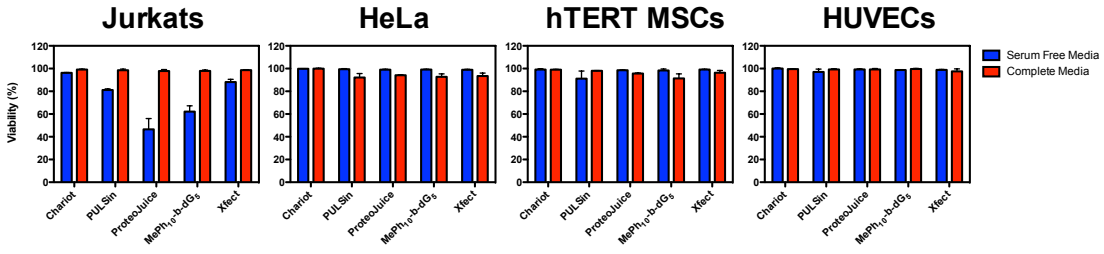

Figure 0.2. Viability as determined by 7-AAD of the cells treated with the protein-carrier complexes in both serum free (blue) and complete media (red). Samples were normalized against the untreated control and the mean ± SEM is shown for three separate experiments.

Most notably, the PTDM used here could deliver into a high percentage of all cell types in both serum free and serum containing conditions and had a large shift in MFI, indicating that most of the cells were receiving a large portion of protein. As seen with the other transfection reagents, the presence of serum slightly hampers the delivery of GFP. A decrease in viability was seen in Jurkats in the case of delivery with the PTDM in serum free conditions, but the other cell types seemed unaffected. In all cases the PTDM in complete media out performs the optimized conditions of the other delivery reagents in all cell types (serum free conditions).

4.4. Conclusion

While many products are being developed for protein delivery, all the commercially available options within the class of amphiphilic polymers require optimization, performing only in serum free conditions, and do not deliver a large payload into the cells of interest. Here, we demonstrate the use of a polymeric peptide mimic (PTDM) that is capable of non-covalent protein delivery of GFP into a variety of cell types in complete media, outperforming its commercially available counterparts within the same class of amphiphilic polymers. In all cell types, the PTDM was able to deliver significantly higher amounts of protein into over 80% of cells both in serum free and serum containing

conditions. Future work on understanding how amphiphilic polymers interact with their cargo protein, as well as protein in the media will enhance development of protein delivery into cells.

CHAPTER 5

PROTEIN TRANSDUCTION DOMAIN MIMICS FACILITATE RAPID ANTIGEN DELIVERY INTO MONOCYTES

5.1. Introduction

Vaccines are currently one of the most effective means of preventing diseases and are actively being sought after to train the immune system against innately harder to treat diseases such as cancer and HIV as more of a therapeutic approach.[233] For protein based vaccines, delivering the antigen into the cytosol has considerable challenges due to the impermeability of the cell membrane.[234] A diversity of approaches has been explored for delivering antigens to optimally stimulate a T cells and mount an adaptive immune response.[235–237]

A sustained T cell response is driven by activation by an antigen presenting cell (APC), the bridge between the innate and adaptive immune system. Professional APCs, such as macrophages, B cells, and dendritic cells (DCs), promote the activation and proliferation of T cells against their major histocompatibility complexes (MHCs) displaying a specific antigen.[238] When a circulating activated CD8+ T cell recognizes material presented in an MHC class I that is foreign, it induces apoptosis in the host cell. The distinction between the T cells is important because CD4+ T cells, also known as helper T cells, promote an inflammatory environment that encourages the proliferation of B cells and subsequent antibody production against the foreign material. CD8+ T cells, also known as cytotoxic T lymphocytes (CTLs), function to destroy infected or deformed cells within the body.

Two types of MHCs exist; class I, located on all cell types, interacts with CD8+ T cells, while class II, only present on professional antigen presenting cells, is associated

with CD4+ T cells. The role of the MHC is to present both foreign and endogenous peptides to the immune system and, in the case of APCs, to train T cells against foreign material. In APCs, antigen presentation happens via two processes; material that is taken up through endosomes is degraded by proteases and fuses with endosomes produced by the ER that contain MHC class II, while exogenous material in the cytosol is degraded by proteasomes and shuttled to the ER where it is loaded on MHC class I.[238] In either case, once the peptide is loaded onto the MHC, the complex is then transported to the cell surface, where it can be accessed by T cell receptors. A schematic of both processes is presented in Figure 0.1.

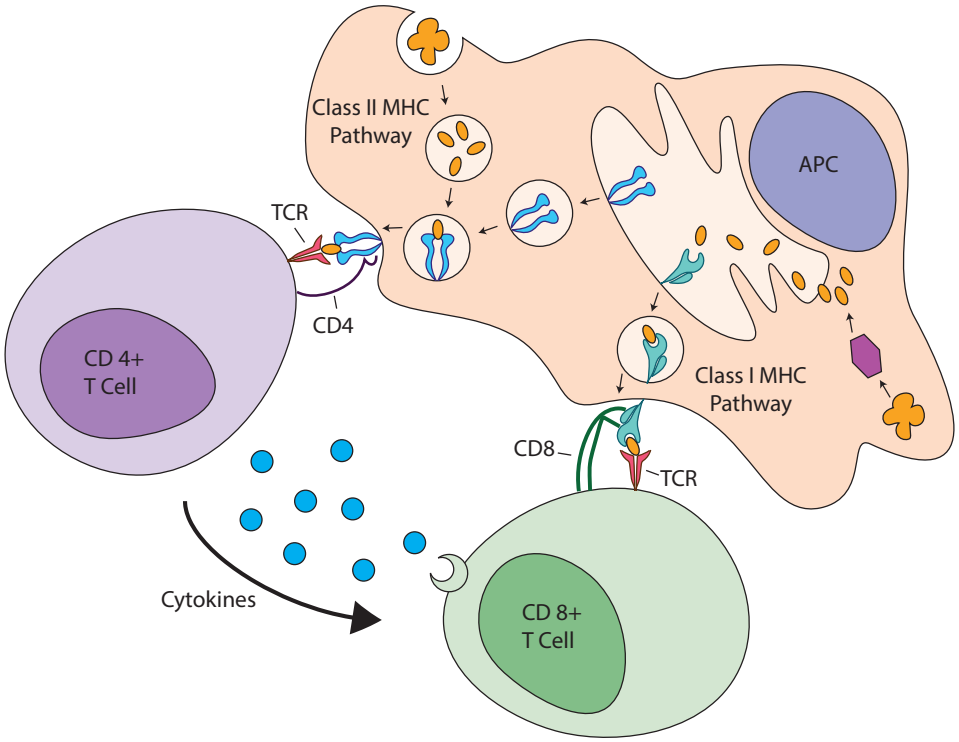

Figure 0.1. Processing and presentation of exogenous proteins by antigen presenting cells. If the protein is present in the cytosol of the APC, it is processed by a proteasome and trafficked to the ER where it is loaded through the MHC class I pathway to prime CD8+ T cells. Endosomal uptake of antigen is processed through the class II MHC pathway where the protein is degraded within the endosome, which fuses with vesicles with the MHC class II and presented to prime CD4+ T cells. Along with presentation secondary co-stimulation from the CD4 or CD8 with CD80 and CD86 along with cytokine production is required for activation of both types of T cells.

Besides antigen recognition by the T cell receptor, T cells require co-stimulation and cytokine stimulation to be activated and begin proliferating.[239] APCs upregulate the expression of costimulatory molecules, such as CD40, CD80, and CD86, and the secretion of cytokines, like INF-γ, IL-1β, TNF-α, and IL-12p70, when they are triggered by danger signals such as agonist like toll-like receptors (TLRs).[240]

Almost all vaccines are based on exogenous antigens being endocytosed, processed, and presented through the major histocompatibility complex (MHC) class II. The antigen loaded MHC II then interacts, along with co-stimulatory molecules, with naïve CD4+ T cells which then become activated and begin to divide, promoting an immune response against the specific antigen.

Activation of CD8+ T cells is slightly more complicated because it requires the antigen presenting cell to have the foreign material available in the cytosol. While possible, this event is rare due to the integrity of the cell membrane and the low number of APCs compared with other cell types in the case of viral infection. If the foreign material is present in the cytosol, the APC displays the antigen on the MHC I and, along with costimulatory molecules (CD86, CD80, and CD40), stimulates CD8+ T cells specific to that antigen to divide and become activated.

In addition to the two classical loading mechanisms, some APCs are able to shuttle antigen from endosomes (normally destined for loading on MHC class II molecules) into the MHC class I pathway.[241] This process is known as cross-presentation and it facilitates a CTL response, but is only efficiently performed by dendritic cells (DCs). Along with their ubiquitous presence throughout the body and their ability to efficiently activate naïve T cells, DCs are a key target for therapeutic vaccines. In an effort to increase DC numbers

and immune activation, several targeting strategies have been employed to increase uptake in monocytes, a DC precursor.[242–246] Since monocytes require differentiation into DCs, one strategy that has been explored is the co-formulation of the antigen with endosomal TLR agonists.[244,247]

Designing an effective MHC I vaccine is the grail of immunotherapy because it would allow for the training and expansion of CTLs against a very specific epitope. Recent advances in understanding antigen presentation by the innate immune cells and their interaction with the adaptive immune system have facilitated a rational approach for design and development of vaccine delivery systems. The key elements of an effective vaccine are the antigen, or the motif to mount an immune response against, an agonist to stimulate the innate immune system, and a delivery system to facilitate the uptake of the cargos into the cytosol of APCs for presentation on MHC class I.[139]

Nanocarriers are well suited for vaccines because they provide encapsulation of the antigen and agonist, as well as allow for delivery into the cytosol of APCs for priming of CTLs. Recently, there has been a substantial increase in publications around immunization based on synthetic carriers, advancing our understanding of important design criteria to elicit a robust immune response with minimal toxicity.[139] Many of these nanocarriers are able exhibit a strong immune response both *in vitro* and *in vivo*, demonstrating their ability to prime CTLs against a specific antigen.[89,90,234,248,249]

In addition to a variety of lipid and synthetic carriers, cell penetrating peptides (CPPs) have been studied for intracellular delivery in vaccine delivery systems.[233,250] Previous reports use either chemical conjugation or a fusion construct with different types of antigen cargos, including protein, peptides, DNA, and siRNA.[158,251,252] Apart from

facilitating intracellular delivery, several examples of CPPs have been reported to prime antigen-specific CTLs.[252–258] CPPs are attractive because they offer an all-inclusive delivery platform that has shown enhanced immune stimulation, though there are still many barriers to overcome in this field.[233]

Although straightforward, CPPs often require conjugation to their cargo. Previously, we have shown non-covalent delivery of functional cargos into the cytosol and nucleus of T cells using synthetic CPPs, also termed protein transduction domain mimics (PTDMs).[134,259] In addition to T cells, we have shown uptake into a variety of other cell types (unpublished), suggesting that the PTDM might provide a facile solution to delivering antigen into the cytosol of APCs. Herein, we describe the optimization of delivering the model antigen SIINFEKL into monocytes in whole blood, as well as immature dendritic cells *in vitro* for presentation on the MHC class I using an amphiphilic block copolymer. Additionally, the differentiation of the monocytes and production of inflammatory cytokines was explored when the antigen was delivered with the endosomal TLR9 agonist CpG. Understanding the efficacy of these PTD mimics provides an important foundation for future applications of PTD technology in the field of peptide-based vaccines towards intracellular pathogens and immunomodulation of disease.

5.2. Materials and Methods

5.2.1. PTDM Synthesis and Characterization

Monomers and polymers were synthesized according to previously established procedures as reported in 2.2.3.[229,260] Briefly, to create the monomer, the *exo* Diels-Alder adduct of maleic anhydride and furan was ring-opened with the desired alcohol to introduce the first substituent. A second alcohol was then added using EDC coupling. The desired polymers were obtained by ring-opening metathesis polymerization using Grubb's third

generation catalyst in dichloromethane and end terminated with either ethyl vinyl ether or an activated ester, which was then reacted with FITC. After polymerization, the Boc groups protecting the guanidinium groups were removed with a 1:1 solution of trifluoroacetic acid and dichloromethane. The final products were purified by dialysis against RO water and recovered by lyophilization.

5.2.2. Cell Preparation

5.2.2.1. Whole Blood

Whole human blood was obtained from healthy volunteers under signed consent in BD Vacutainers containing hirudin. In all cases, blood was used within 10 minutes of the tapping from the donor. The blood was distributed into Eppendorf tubes containing preassembled polymer preparations in RPMI 1640 with no supplements and incubated up to 1 hour at 37˚C on rotation (60 RPM). In general, 400 µL of blood was combined with 100 µL of polymer complex prepared in RPMI 1640 for a final volume of 500 µL.

In the case of plasma free whole blood delivery, whole blood was centrifuged at 200 g immediately upon receipt, plasma was removed, and cells were washed with RPMI 1640 three times before suspension to the original volume with RPMI 1640. The washed blood was then allocated to the polymer preparations and incubated on rotation (60 RPM) for 1 hour at 37˚C.

5.2.2.2. Cell Lines

Jurkat T cells (clone E6-1, ATCC TIB-152) and THP-1 cells (ATCC TIB-202), were grown in RPMI 1640 supplemented with 10% (v/v) FBS, L-glutamine, Non Essential Amino Acids (NEAA), Na-pyruvate, HEPES, 100 U/mL penicillin, and 100 U/mL streptomycin at 37˚C, 5% CO_2 and were passaged 24 hours before treatment. Polymers were mixed with cargo and allowed to complex for 30 minutes. Jurkats were harvested and

suspended in fresh complete media and placed into a 12 well plate at $4X10^5$ cells/mL. Polymer-cargo complexes were applied drop-wise to each well. Cells were treated for 4 hours, then washed 3 times with 20 U/mL heparin in PBS before being suspended in 0.2% BSA in PBS FACS buffer and stained with 7-AAD for analysis by flow cytometry.

To establish immature dendritic cells, previously established protocols were used.[261] Briefly, THP-1s were incubated with 100 ng/mL IL-4 and 100 ng/mL GM-CSF for 5 days, with the media and cytokines being replaced every 2 days. Differentiation was confirmed by increased expression in CD11c and HLA-DR as well as a morphological change.

5.2.2.3. Bone Marrow Derived Dendritic Cells

Immature dendritic cells were differentiated from murine bone marrow according to established protocols.[262] Discarded legs from C57BL/6 mice were graciously donated by the Pobezinsky lab. Bones were cleaned with ethanol and cells were harvested using a 28-gauge syringe. RBCs were lysed using BioLegend® lysis buffer and cells were plated at a density of $2X10^5$ cells/mL in complete RPMI (listed under cell lines) with the addition of 20 ng/mL recombinant mouse GM-CSF. Cells were cultured for 6 days with the addition of 10 mL fresh media and cytokines on day 3. Non-adherent and loosely adherent cells were harvested on day 6 and cells were pelleted, counted, and plated at a density of $2X10^6$ cells/mL.

5.2.3. Flow Cytometry

After incubation, cells were pelleted at 200 g for 5 minutes and the supernatant was removed. Red blood cells were lysed in using BD Pharm lysis buffer and subsequently washed with 1% FBS in PBS twice before staining with antibodies. Unspecific binding

was blocked for 10 minutes using human or mouse IgG respectively. Antibody surface staining was performed using antibodies for Human CD14-APC, CD40-PE, CD80-AF488, CD86-BV711, CD209-APC, HLA-DR-APC-Cy7, or Mouse CD11c-AF488, CD86-AF647, HLA-DR, H-2K^{b}-PE as indicated by manufacturer (BD® or BioLegend®).

Briefly, cells were transferred to a 96 well plate where the respective antibodies were added accordingly. Samples were incubated for 30 minutes on ice after which samples were washed 3 times with 1% FBS in PBS before analysis by flow cytometry.

Whole blood samples were collected on a BD® Accuri C6™ flow cytometer with two lasers (488 and 640nm) with three channels on the blue laser (533/30, 585/40, and 670 LP) and one channel on the red laser (675/25). For whole blood experiments, 100,000 single events were collected for each sample using a minimum FSC-H cutoff of 1,200,000.

THP-1 monocytes, immature dendritic cells, and bone marrow derived dendritic cells were analyzed using a BD LSR Fortessa 20X flow cytometer with five lasers and 18 channels. For both cell lines, 10,000 single events were collected for each sample, while for the bone marrow derived cells, a minimum of 50,000 single cell events were collected. Only cells negative for 7-AAD were assessed for either uptake or presentation of markers. Multi-color flow cytometric analysis spectral overlap was corrected by appropriate compensation and analyzed using FlowJo™ 10.2 by Tree Star®.

5.2.4. Cytokine Profiling

After one hour of incubation with treatment as reported under cell preparation and culture, cells were pelleted at 400 g for 2 minutes and supernatant was removed. Cells were washed 3 times with RPMI supplemented with 100 U/mL pen/strep, and plated into a 96 well round bottom plate where they were incubated at 37˚C and 5% CO_2 for 24 hours. After

incubation, cells were pelleted at 5000g and supernatant was transferred to a fresh 96 well plate and frozen at -80˚C until testing. Measurements of IL-6 were performed immediately after thawing frozen supernatant using ELISA, R&D Systems. Cytokine production was detected using the inflammatory cytometric bead array Legendplex™ from BioLegend® which included IL-1β, IFN-α, IFN-γ, TNF-α, MCP-1, IL-6, IL-8, IL-10, IL-12p70, IL-17A, IL-18, IL-23, and IL-33.

5.2.5. Statistical Analysis

All flow cytometry experiments were repeated in at least biological triplicate. Data sets were expressed as means ± SEM Statistical significance of differences was determined by one or two way ANOVA followed by a Bonferroni post hoc test. Differences were considered statistically significant for $p<0.05$. Statistical analysis was performed using Prism™ 5.0a by Graphpad® Software.

5.3. Results and Discussion

5.3.1. MePh10-b-dG5-FITC Treatment of Whole Blood

To understand the interaction of the PTDM with cells in whole blood, FITC labeled **$MePh_{10}$-*b*-dG_5** (Figure 0.2A) was added to freshly collected human whole blood for 1 hour at a final concentration of 2.8 μM. After lysis of red blood cells (RBCs) and staining with anti-CD14 and anti-CD15, polymer showed low association with granulocytes (CD15+) and lymphocytes (morphological gate) as seen in Figure 0.2C, while the MFI and uptake in monocytes (CD14+) was statistically higher than the blank and the other two cell populations. Viability, determined by staining with 7-AAD, was not statistically different from the blank with 95.8 ± 1.6 % live cells.

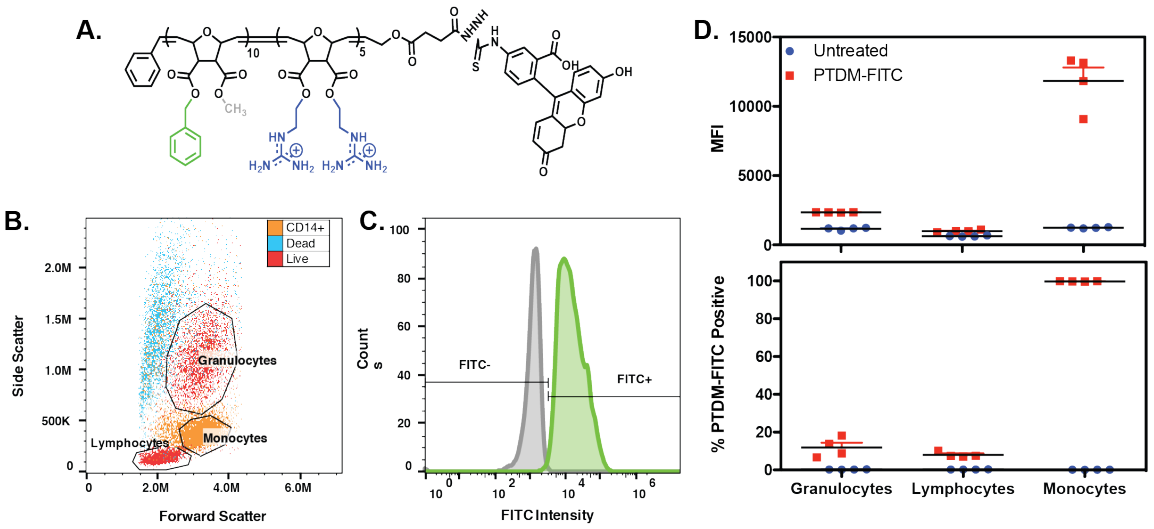

Figure 0.2. Delivery of 2.8 µM FITC labeled polymer (A) into whole blood for 1 hour. Cells were gated morphologically (B) and monocytes were confirmed with CD14 staining, while granulocytes were confirmed with CD15 staining within the respective morphological gate. Uptake within each of the morphological gates was determined by a shift in FITC intensity from the blank (C). The mean±SEM of the median fluorescence intensity (MFI) on the top and percent positive cells on the bottom of 4 separate donors is shown (D).

Specific uptake by the monocyte population is interesting but slightly unsuprising due to their phagocytotic nature. Since we have previously shown delivery into a variety of cell types, the logical next step was to deliver a cargo complexed with the polymer. SIINFEKL peptide, the MHC class I specific sequence of ovalbumin (OVA) was chosen as a model antigen.

5.3.2. Optimization of Delivery into Jurkat T Cells

In order to determine the most effective concentration of peptide and the subsequent ratio of peptide to polymer (**MePh$_{10}$-*b*-dG$_5$**), a survey of peptide concentrations (0.1, 0.5, 1, and 5 µM) crossed with protein to polymer ratios (1:5, 1:10, 1:15, and 1:20) was investigated in Jurkats. In this case, SIINFEKL was fluorescently labeled with FAM to showcase ability of cargo delivery. Peptide-polymer complexes were allowed to form for 30 minutes prior to addition to the cells in complete RPMI. Cells were treated for 4 hours,

after which they were washed three times with heparin to remove excess peptide adhered to the outside of the cell. Uptake and viability (7-AAD staining) was assessed using flow cytometry and is shown in Figure 0.3. The trend between peptide to polymer ratios was consistent across all peptide concentrations, with a ratio of 1:10 performing similarly to 1:20 indicating that higher ratios of polymer would not necessarily enhance delivery.

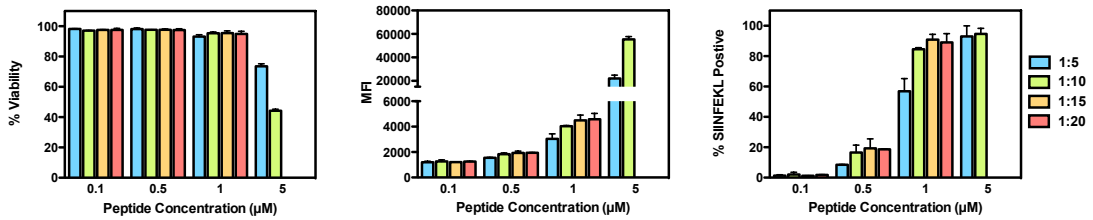

Figure 0.3. A concentration survey for the delivery of SIINFEKL into Jurkat T cells at varying ratios of peptide to polymer. Cells were treated with the complexes for 4 hours, washed three times with heparin, and analyzed by flow cytometry for their ability to deliver SIINFEKL. Viability (left) was determined using 7-AAD, MFI (middle) indicates the amount of peptide delivered to the cells, and % positive cells (right) indicates the population of cells that were delivered into. Experiments were repeated in triplicate and the mean and SEM are displayed.

5.3.3. Time Survey of Peptide Delivery into Whole Blood

The specificity of uptake of the polymer-antigen complex by monocytes was tested in whole blood. 1 μM FAM labeled SIIFNEKL was delivered into whole blood using **MePh$_{10}$-*b*-dG$_5$** at a ratio of 1:10, for 15, 30, 45, or 60 minutes to investigate the kinetics of uptake. MFI and uptake were not statistically different regardless of the incubation time. Additionally, complex uptake was compared with free SIINFEKL-FAM allowed to incubate with whole blood for 60 minutes. High association with the monocytes is seen within the first 15 minutes (Figure 0.4) compared with lymphocytes and granulocytes, consistent with the previous observations. The free peptide is not readily taken up in large amounts by any of the white blood cells.

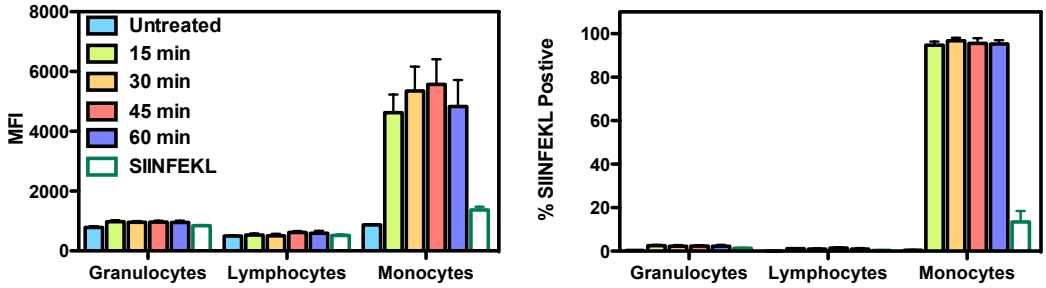

Figure 0.4. Delivery of fluorescently labeled SIINFEKL complexed with PTDM at a ratio of 1:10 into whole blood for 15, 30, 45, and 60 minutes. Whole blood was also treated with soluble SIINFEKL for 60 minutes as a comparison. Cell types were gated on morphologically then with CD14 and CD15 to determine true monocytes and macrophages, respectively. The mean and SEM of 4 separate donors is displayed for the MFI (left) and % positive (MFI) cells within the established gates.

Rapid specific uptake of the fluorescently labeled antigen in monocytes showcases the ability of the PTDM to significantly enhance uptake of the model cargo. The relatively low association and uptake seen with the free peptide suggests that some property of the polymer enhances association and uptake with monocytes. Since the PTDM has been shown to deliver into multiple cell types, increased concentrations were investigated for induced uptake in the granulocyte and lymphocyte populations.

5.3.4. Concentration Survey of Peptide Delivery into Whole Blood

FAM labeled SIINFEKL was delivered into whole blood using **MePh$_{10}$-*b*-dG$_5$** at a ratio of 1:10 at increasing concentrations of peptide (0.25, 0.5, 1, and 2 μM). The MFI and % positive cells are shown in Figure 0.5A, suggesting that 1 μM of peptide was optimal because almost 100% of the cells show uptake and the MFI is significantly distinguishable from the untreated sample. Increasing the concentration to 2 μM appears to yield a higher MFI, but also requires more polymer. High uptake was exhibited almost exclusively in the monocytes labeled with CD14 and not significantly in the lymphocytes and granulocytes, consistent with the previous observations.

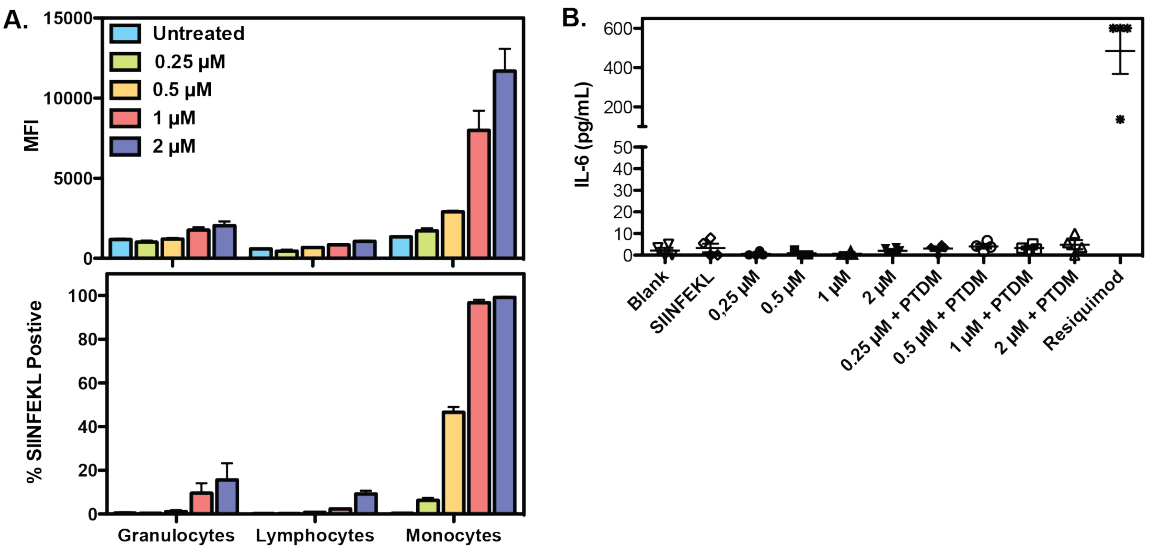

Figure 0.5. (A)Delivery of fluorescently labeled SIINFEKL complexed with PTDM at a ratio of 1:10 into whole blood at peptide concentrations of 0.25, 0.5, 1, and 2 µM of peptide. Cell types were gated on morphologically then with CD14 and CD15 to determine true monocytes and macrophages, respectively. (B) IL-6 production was determined for unlabeled SIINFEKL delivered under the same conditions 24 hours after treatment in comparison to the positive control Resiquimod, a TLR7 agonist. The mean± SEM of 4 separate donors is displayed.

Even at high concentrations, uptake is promoted in only the monocyte population, confirming that the polymer promotes specific interaction with these phagocytic cells. Although uptake is promoted, monocytes themselves do not serve a specific function in terms of promoting a specific immune response. Monocytes can differentiate into two types professional antigen presenting cells, macrophages and dendritic cells, upon stimulation and activation.[238] Usually, the differentiation into dendritic cells can be marked by a change in cell specific surface marker expression such as upregulation of MHC class I and DC-sign (CD209) as well as in inflammatory cytokine production.[261,263]

To further investigate the ability of the polymer-peptide complexes to cause an inflammatory cytokine environment, whole blood was treated with the same conditions as in the concentration survey (0.25, 0.5, 1, and 2 µM peptide at a 1:10 peptide to polymer ratio) and the production of IL-6 was probed 24 hours after the treatment (Figure 0.5B).

The whole blood was added to the polymer complexes for 1 hour on rotation, after which the plasma was removed and the cells were washed three times with non-supplemented RPMI. The cells were incubated at 37˚C for an additional 24 hours and the supernatant was collected to perform an IL-6 ELISA. No significant IL-6 production detected with any of the treatments, except the positive control Resiquimod, a TLR7 agonist. The results indicate the polymers alone and in complex with SIINFEKL do not produce pro-inflammatory signals in blood, even at high concentrations. Since the complexes show high uptake but are not inflammatory, they most likely do not cause the monocytes to differentiate. The differentiation and activation of the monocytes in whole blood can be induced by delivering an agonist in addition to the antigen.

5.3.5. SIINFEKL Delivery with Amphiphilic Peptides

Since high uptake in monocytes was demonstrated using **$MePh_{10}$-*b*-dG_5**, similar peptides were tested to compare their ability to non-covalently associate SIINFEKL and facilitate uptake in whole blood. Two peptides were chosen, R9 and Pep-1, for their cationic nature and previously shown ability to translocate cells to deliver biomolecular cargo.[35,119] As before, the peptides were complexed for 30 minutes in the presence of SIINFEKL. Since delivery in the presence of protein inhibits the ability of many carriers to deliver into cells, the plasma was removed from the blood by washing with RPMI three times and suspending the cells back to the original collected volume. The plasma free blood was then added to the complexes and put on rotation for 1 hour at 37˚C after which the RBCs were lysed and cells were stained with anti-CD14.

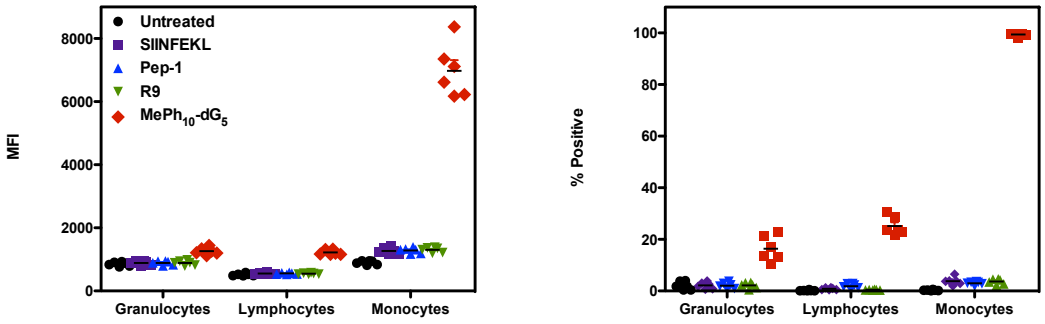

Figure 0.6. Delivery of fluorescently labeled SIINFEKL into whole blood using the well known cell penetrating peptides pep-1 and R9 in comparison with $MePh_{10}$-b-dG_5 after 1 hour incubation. Cell types were gated on morphologically then with CD14 and CD15 to determine true monocytes and macrophages, respectively. The mean and SEM of 6 separate donors is displayed for the MFI (left) and % positive (MFI) cells within the established gates.

Analysis by flow cytometry, shown in Figure 0.6, indicated negligible delivery when the SIINFEKL was introduced by itself or in the presence of the tested peptides. In contrast, the **$MePh_{10}$-*b*-dG_5** facilitated uptake in the monocytes, clarifying that plasma proteins are not directly responsible for the uptake of the polymer-antigen complex in terms of aggregation or opsonization.

5.3.6. Optimization of CpG and OVA Protein Ratio to Polymer

To introduce a controlled cytokine response, CpG, a TLR9 nucleotide agonist was chosen for co-delivery with the chosen agonist. Since the polymers studied here have never been tested for co-delivery, optimization was required to determine the optimal ratio of polymer to CpG and the protein OVA, as well as any requirements about complex formation. In this case, the whole protein was chosen over the peptide antigen due to the compatibility of fluorophores that were readily available for each of the cargos. Additionally, a second polymer, **dPh_{10}-*b*-dG_5**, was added to briefly determine if polymer architecture would affect association and uptake of the two different cargos.

The delivery of CpG-FITC and OVA-AF647 were optimized separately in Jurkats through determining the optimal N/P ratio for 100 nM CpG and protein/polymer ratio for 50 nM OVA. Cargos were complexed with two polymers (**$MePh_{10}$-*b*-dG_5** and **dPh_{10}-*b*-dG_5)** at increasing ratios for 30 minutes in PBS. N/P ratios of 1:1, 2:1, 4:1 and 8:1 (Figure 0.7A and B) and protein-polymer ratios of 1:5, 1:10, 1:20, and 1:40 (Figure 0.7C and D) were assessed for CpG and OVA, respectively. Complexes were added drop-wise to Jurkats and incubated at 37˚C for 4 hours after which they were washed with heparin to remove any residual cargo stuck to the outside of the membrane and uptake was assessed by flow cytometry. CpG-FITC delivery peaked at a ratio of 4:1 for both polymers, while OVA delivery was best at a ratio of 1:40 for the **$MePh_{10}$-*b*-dG_5** compared with 1:20 being sufficient for the **dPh_{10}-*b*-dG_5.**

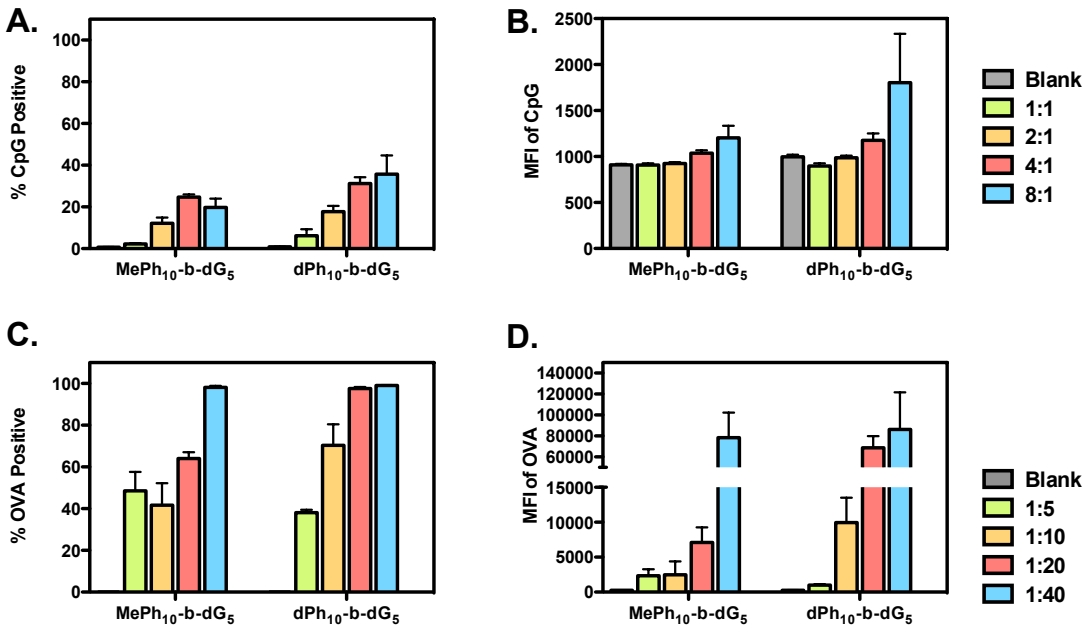

Figure 0.7. Optimization for delivery of CpG-FITC and Ovalbumin (OVA-AF647) in Jurkat T cells to determine the optimal ratio of cargo to polymer. Two polymers were assessed for their ability to deliver both cargos. Polymers were complexed with 100 nM CpG at N:P ratios of 1:1, 2:1, 4:1, and 8:1 for 30 minutes and then applied to cells in complete media for 4 hours. The percentage of cells positive for CpG (A) and MFI (B) were determined by flow cytometry. 50 nM OVA was complexed with the polymers at ratios of 1:5, 1:10, 1:20, and 1:40 prior to 4 hours of delivery. Similarly, percent positive (C) and the MFI (D) were assessed via flow cytometry. The mean and SEM are displayed for three independent experiments.

The ability of the polymers to deliver the CpG and OVA into the same cell was tested for the necessity to complex the cargos with the polymers separately (postmix) or together with the polymer at the same time (premix). In the case of postmix, the cargos were mixed with either **MePh$_{10}$-*b*-dG$_5$** or **dPh$_{10}$-*b*-dG$_5$** and allowed to complex before simultaneous addition of the antigen complex and agonist complex to the cells, while in the premix version, all three substituents were added and allowed to complex together before addition to the cells. The fluorescence intensity of both cargos was assessed by flow cytometry after 4 hours incubation and subsequent heparin washing (Figure 0.8).

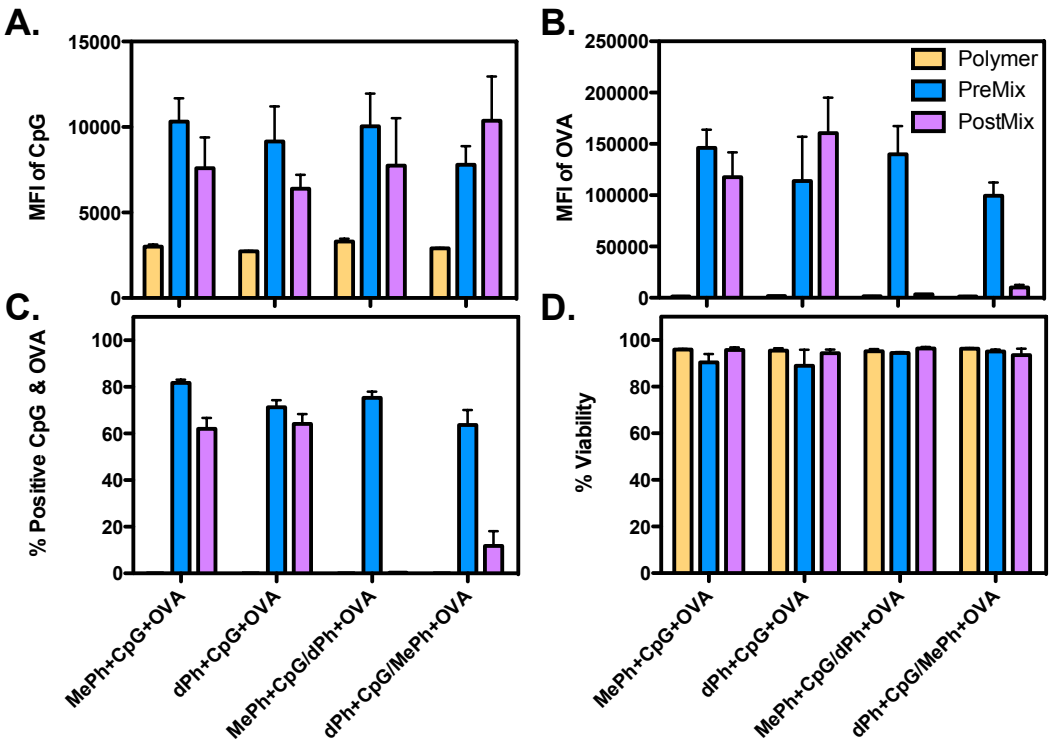

Figure 0.8. Optimization of co-delivery of 100 nM CpG-FITC and 50 µM OVA-AF647 into Jurkat T cells. $MePh_{10}$-b-dG_5 **or** dPh_{10}-b-dG_5 **was complexed with CpG and OVA either individually (postmix) or all together (premix) for 30 minutes before treatment of cells in complete media. The MFI for CpG (A) and OVA (C) were assessed individually on the population as a whole. The percentage of cells positive for both cargo types (B) was assessed along with Viability (D) using 7-AAD after 4 hours by flow cytometry. The mean and SEM are shown for 3 independent experiments.**

For the single polymer samples (MePh+CpG+OVA and dPh+CpG+OVA), no statistical difference was seen between the set that was mixed individually (PTDM with OVA separate from PTDM with CpG) and those that were mixed together (PTDM with OVA and CPG). Additionally, both polymers appeared to deliver with the same efficacy. When both polymers were used together to complex cargo, the premix strategy was far superior. Consequently, premixing everything together was adopted and only **$MePh_{10}$-*b*-dG_5** was continued with for all subsequent co-delivery experiments.

5.3.7. Co-Delivery of CpG and OVA in Whole Blood

After optimization, the polymer-antigen-agonist complex was delivered into whole blood to see if the addition of the agonist effected the association with monocytes and if the complex promoted differentiation or activation. CpG and OVA were premixed with the polymers at the previously determined ratios of N/P = 4:1 for the CpG and 1:20 or 1:40 for the respective polymers with increasing concentrations of CpG. Whole blood was treated with the various complexes for 60 minutes to investigate uptake. Based on MFI, Figure 0.9, the polymers cause significantly higher uptake in the morphological granulocytes and monocytes gates at the higher concentrations. It was apparent with the loss of cells within the typical monocyte morphological gate that the assay was inconclusive. The cells positive for both OVA and CpG lie within the lower side of the granulocyte population. Further evidence to support the idea of monocyte differentiation into macrophages, and the subsequent shift up in side scatter is required. To follow up, delivery into a single culture of monocytes was investigated.

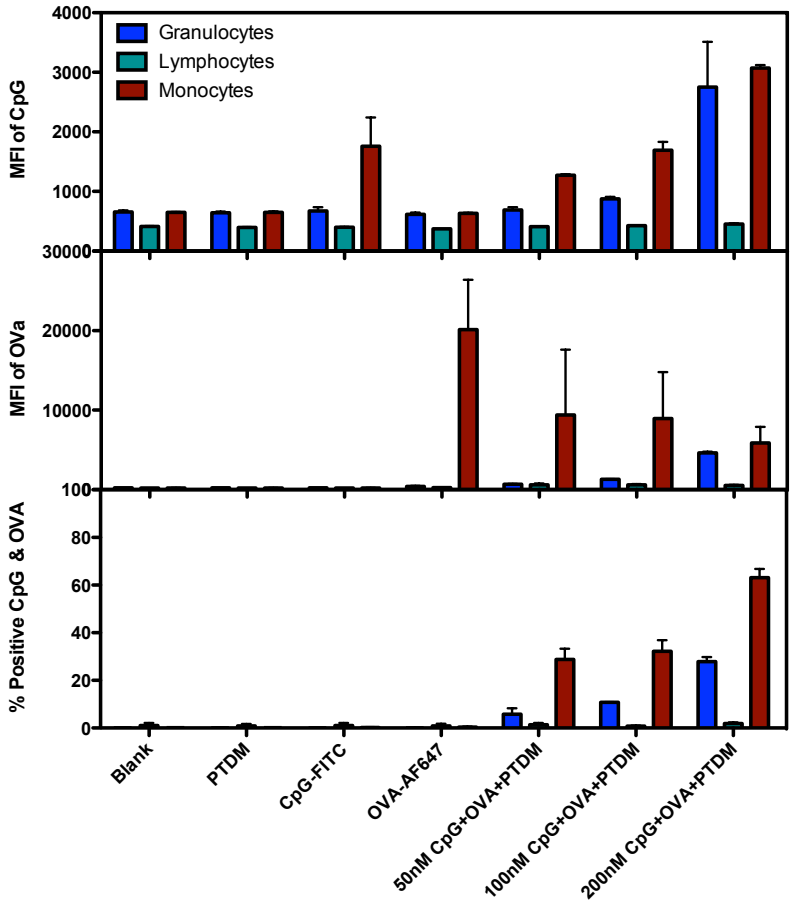

Figure 0.9. Co-delivery of CpG-FITC and OVA-AF647 complexed with $MePh_{10}$-b-dG_5 into whole blood. Increasing concentrations of CpG were used (50, 100, and 200 nM) along with 50 nM OVA protein. Uptake into the morphological granulocyte, lymphocyte, and monocyte gates are shown as a function of CpG MFI (top), OVA MFI (middle), and percentage of cells positive for both cargos (bottom).

To quickly check for upregulation of differentiation marker DC-sign, the complex was compared with treatment of whole blood with IL-4 and GM-CSF, cytokines that can be used to induce differentiation into dendritic cells. After 1 hour of treatment, followed by washing and a 24 hour incubation, the cells treated with the polymer-antigen-agonist complex showed a slight increase in upregulation of DC-sign, as seen in Figure 0.10, but the increase was not substantial in relation to the cytokine treated cells. It is possible that

at a longer time point higher upregulation of this marker would occur. Alternatively, the amount of CpG added might be too low to cause significant upregulation of DC-sign.

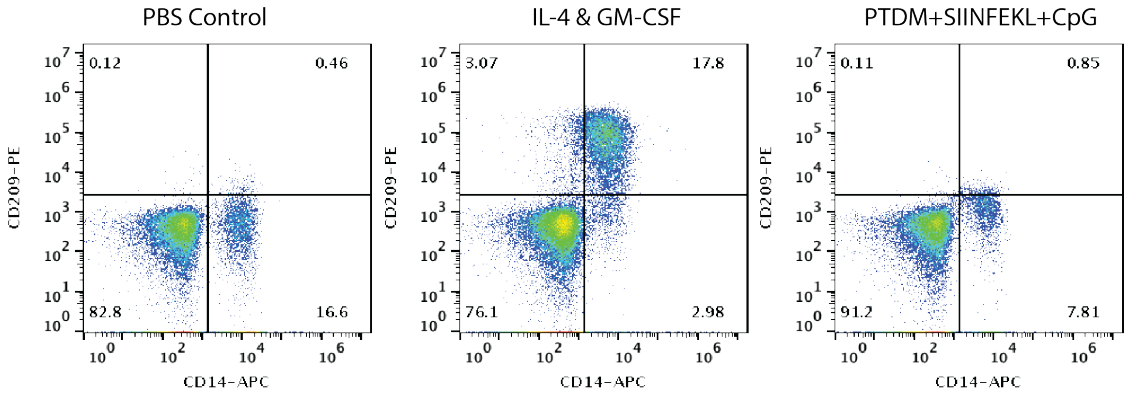

Figure 0.10. Co-delivery of SIINFEKL and CpG with $MePh_{10}$-b-dG_5 compared with cytokine treatment to differentiate monocytes into dendritic cells. Whole blood was treated for 1 hour, then washed and incubated for an additional 24 hours to look at the upregulation of DC-sign (CD209) within the monocyte (CD14) population. The PBS negative control (left) and cytokine positive control (middle) compared with the polymer-antigen-agonist complexes.

5.3.8. Delivery into THP-1 Monocytes

A multi-analyte inflammatory cytokine panel was used to understand the immune response for the addition of CpG into the complexes. Supernatants from whole blood at 24 hours after a 60 minute treatment with the polymer-SIINFEKL-CpG complexes were tested using a standardized inflammation panel including IL-1β, IFN-α, IFN-γ, TNF-α, MCP-1, IL-6, IL-8, IL-10, IL-12p70, IL-17A, IL-18, IL-23, and IL-33. A statistical summary of cytokine production is summarized in Table 0.1. When CpG was delivered by itself, it caused an increase in IL-1β, IFN-α IFN-γ, TNF-α, IL-6, MCP-1, and IL-12p70, which are all indicative of a pro-inflammatory response directed by the differentiation and activation of professional antigen presenting cells. In general, cytokine response with the addition of SIINFEKL did not change this profile suggesting that the two cargos can be delivered together to perform their individual functions. Additionally, the production of IL-12p70 is

especially interesting because it indicates the active heterodimer is being produced by APCs to stimulate T cells. In combination with INF-γ and TNF-α, IL-12p70 enhances the cytotoxic activity of CTLs suggesting that the delivery of CpG and SIINFEKL with the PTDM may facilitate an enhanced immune response.

Table 0.1. Inflammatory cytokine panel for the co-delivery of SIINFEKL and CpG using $MePh_{10}$-b-dG_5 into whole blood. Supernatant was collected 24 hours after treatment and analyzed using a cytometric bead array. Statistical difference was determined from the untreated sample from 3 independent donors (*p<0.05, **p<0.005, ***p<0.0005)

	IL-1B	IFN-a	IFN-g	TNF-a	MCP-1	IL-6	IL-8	IL-10	IL-12p70	IL-17A	IL-23	IL-33
SIINFEKL	ns	ns	ns	ns	ns	ns	ns	ns	ns	ns	ns	ns
CpG	ns	ns	ns	ns	***	***	ns	ns	ns	ns	ns	ns
GpC	ns	ns	ns	ns	ns	ns	ns	ns	ns	ns	ns	ns
SIINFEKL+CpG	ns	ns	ns	ns	***	***	ns	ns	ns	ns	ns	ns
PTDM	ns	ns	ns	ns	ns	ns	ns	ns	ns	ns	ns	ns
PTDM+SIINFEKL	ns	ns	ns	ns	ns	ns	ns	ns	ns	ns	ns	ns
PTDM+CpG	**	***	ns	**	***	**	ns	ns	***	ns	ns	ns
PTDM+SIINFEKL+CpG	ns	***	ns	ns	***	**	ns	ns	***	ns	ns	*
IL-4 + GM-CSF	ns	ns	ns	ns	***	ns	***	ns	ns	ns	ns	ns
DMSO	ns	ns	ns	ns	ns	ns	ns	ns	ns	ns	ns	ns

5.3.8.1. Cytokine Response to Co-Delivery of SIINFEKL and CpG

FAM labeled SIINFEKL or OVA labeled with FITC were delivered respectively using **$MePh_{10}$-*b*-dG_5** into THP-1s, a human monocyte cell line. 1 μM of each cargo was complexed respectively with the polymer at a 1:10 protein/peptide to polymer ratio for 30 minutes before application to cells in complete media. The lowered ratio used in this experiment was an attempt to lower the amount of polymer required and therefore mitigate cytotoxicity. Cells were treated for 4 hours, then washed 3 times with 20 U/mL heparin prior to analysis by flow cytometry. The **$MePh_{10}$-*b*-dG_5** facilitated delivery of both cargos into the THP-1 monocytes, shown in Figure 0.1A and B, confirming its ability to deliver into this cell type. Viability, determined by 7-AAD staining, remained similar to untreated cells above 95% in relation to the untreated blank.

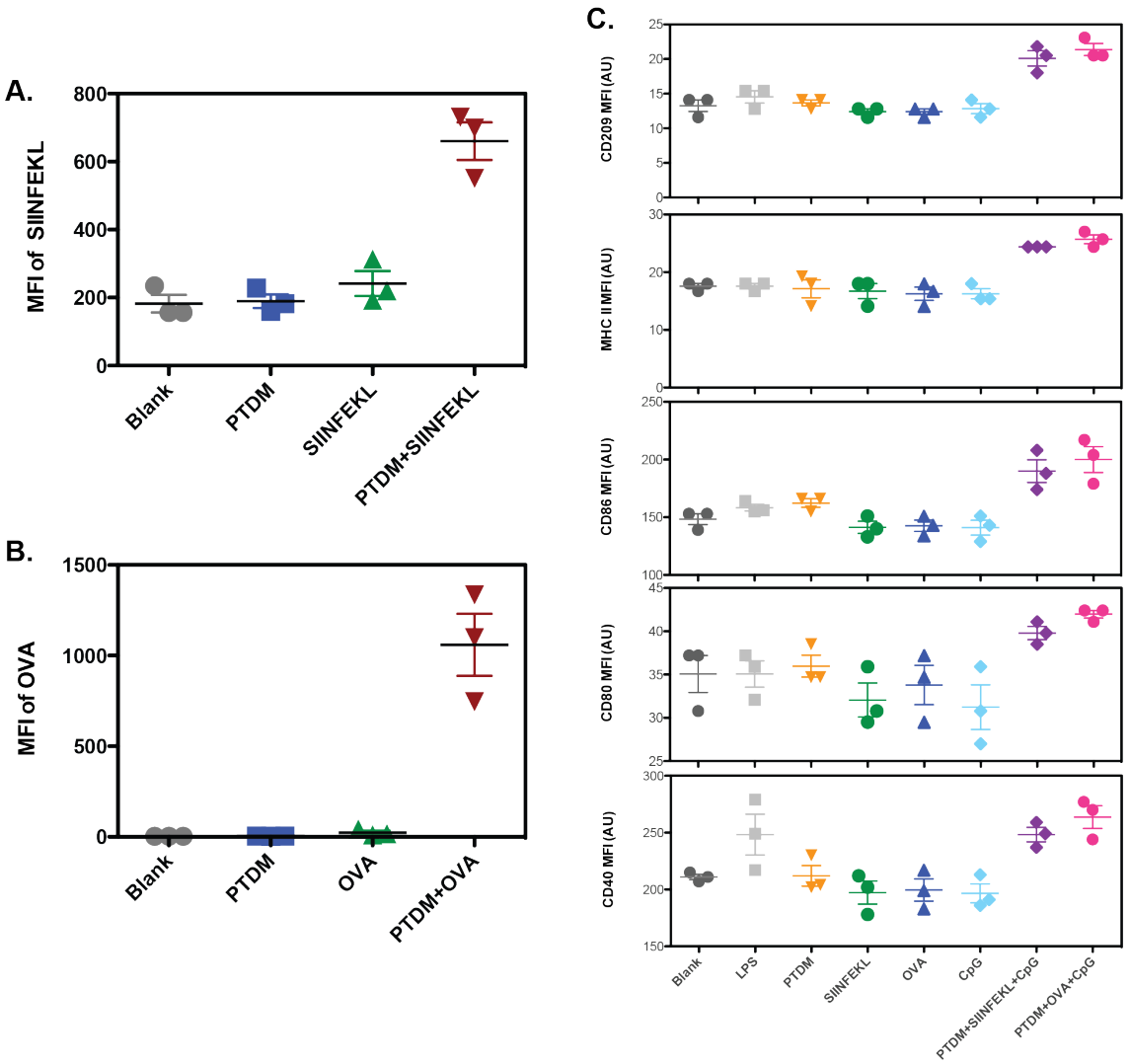

Figure 0.11. Delivery of SIINFEKL-FAM (A) and OVA-AF647 (B) into THP-1 cells using $MePh_{10}$-b-dG_5. Cells were treated for 4 hours, then washed 3 times with heparin (20 U/mL) and assessed for uptake of the cargos by flow cytometry. Upregulation of activation surface markers (C) on THP-1s 24 hours after delivery of polymer-antigen-agonist complexes. Cells were treated for 4 hours, then washed one time with media and allowed to incubate for 20 more hours. LPS was used as a positive control. Cells were stained with antibodies for DC-sign (CD209), HLA-DR (MHC II), CD86, CD80, and CD40. The mean ± SEM are shown from 3 independent experiments.

To investigate the differentiation and activation of the monocytes by a polymer-antigen-agonist complex, the 10 μM **$MePh_{10}$-*b*-dG_5** was complexed with 1 μM unlabeled SIINFEKL or OVA along with 1 μM CpG, a TLR9 agonist, for 30 minutes and cells were treated for four hours. The cells were centrifuged and washed one time with PBS before

being suspended in complete media for an additional 20 hours, after which the supernatant was collected for ELISA and the cells were stained with antibodies for CD11c (a DC marker), CD40, CD80, CD86, and MHC class II (HLA-DR). Minor upregulation of the CD40, CD80, and CD86 could be seen in samples treated with the polymer-antigen-agonist complex (Figure 0.11C).

Although a multi-analyte cytometric bead array was used to determine cytokine production during the 20 hour incubation after treatment, no statistical increase was seen in any of the analytes, not even when treated with LPS, the positive control. These results may be due to too low cytokine concentration in all of the samples, requiring the experiment to be done in a higher density of cells with a lower volume, over a variety of time points. It is also possible that the monocytes were not stimulated enough by the concentrations of polymer-antigen-agonist and that higher concentrations of the complexes would lead to more definitive results.

5.3.9. Delivery into Immature Dendritic Cells

Delivery into immature dendritic cells (iDCs) was also investigated in partially differentiated antigen presenting cells. iDCs were stimulated for 6 days to cause upregulation of MHC class II (HLA-DR) and DC-sign, indicating their ability to be primed for T cell stimulation. Similar to the THP-1s, 1 μM fluorescently labeled SIINFEKL or OVA complexed with **MePh$_{10}$-*b*-dG$_5$** at a ratio of 1:10 were delivered into the iDCs derived from THP-1s (Figure 0.12A and B), showing significant uptake of the peptide compared with the free soluble counterpart. More variation of OVA protein uptake was seen than with the Thp1s, possibly due to inconsistent differentiation between the three

trials. The high SIINFEKL uptake in these cells indicate that the PTDM facilitates the delivery of antigen into iDCs.

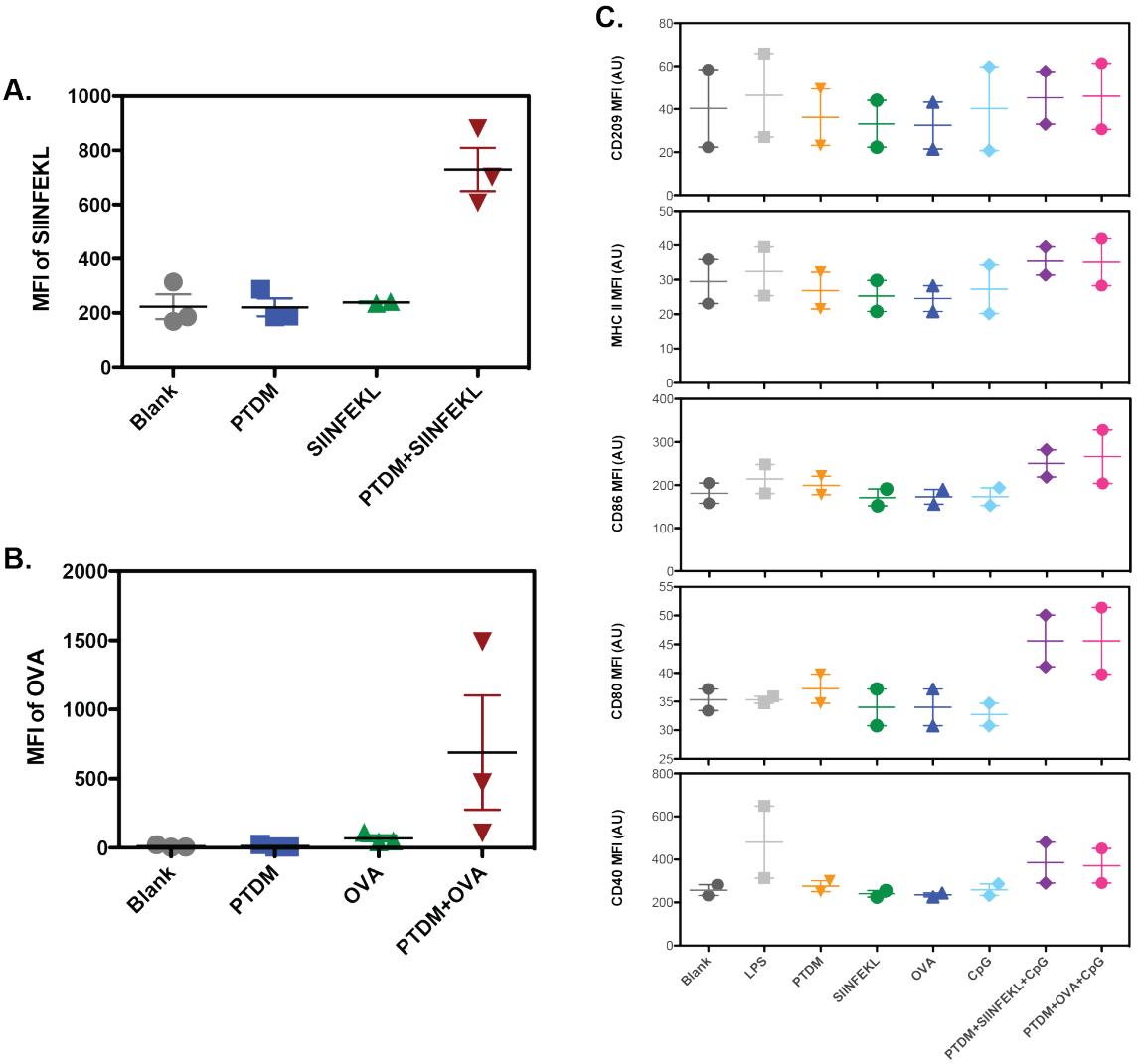

Figure 0.12. Delivery of SIINFEKL-FAM (A) and OVA-AF647 (B) using $MePh_{10}$-b-dG_5 **into immature dendritic cells derived from the THP-1 cell line. Cells were treated for 4 hours, then washed 3 times with heparin (20 U/mL) and assessed for uptake of the cargos by flow cytometry. The mean and SEM are shown as a result of 3 independent experiments. Upregulation of activation surface markers (C) on iDCs 24 hours after delivery of polymer-antigen-agonist complexes. Cells were treated for 4 hours, then washed one time with media and allowed to incubate for 20 more hours. LPS was used as a positive control. Cells were stained with antibodies for DC-sign, MHC II, CD86, CD80, and CD40.**

Co-delivery of the antigen and agonist was performed to probe upregulation of co-stimulatory molecules, as well as production of inflammatory cytokines. Surface marker

staining, Figure 0.12C, revealed a slight upregulation of CD80, CD86, and CD40 in the samples that received the polymer-antigen-agonist complex. Although the upregulation was not substantial, it is possible that higher concentrations of CpG or for longer are required to produce significant upregulation of surface markers and production of inflammatory cytokines.

5.3.10. Delivery into Bone Marrow Derive Dendritic Cells

Perhaps the most conventional and telling way to scrutinize whether the PTDM-antigen-agonist complex will enhance vaccination through delivery of a specific peptide is to probe immature dendritic cells that would subsequently be able to stimulate T cells. In this case, complexes are delivered into mouse bone marrow derived dendritic cells (BMDCs) that would internally process the antigen via the MHC class I and class II pathways and present the antigen along with respective costimulatory molecules. Since we have chosen a peptide that is specifically presented in MHC class I, we can probe for the display, as well as the upregulation of CD86, a costimulatory molecule.

To test SIINFEKL delivery and presentation for T cell activation, bone marrow derived dendritic cells were differentiated from C57BL/6 mouse bone marrow for 6 days in the presence of 20 ng/mL mouse GM-CSF. After 6 days, cells were harvested and treated with 1 μM fluorescently labeled SIINFEKL or OVA both free and in complex with **MePh$_{10}$-*b*-dG$_5$** ratio of 1:10 for 4 hours. Substantial uptake was seen in the presence of polymers while significantly less uptake was seen for the free antigen in both cases (Figure 0.13A and B).

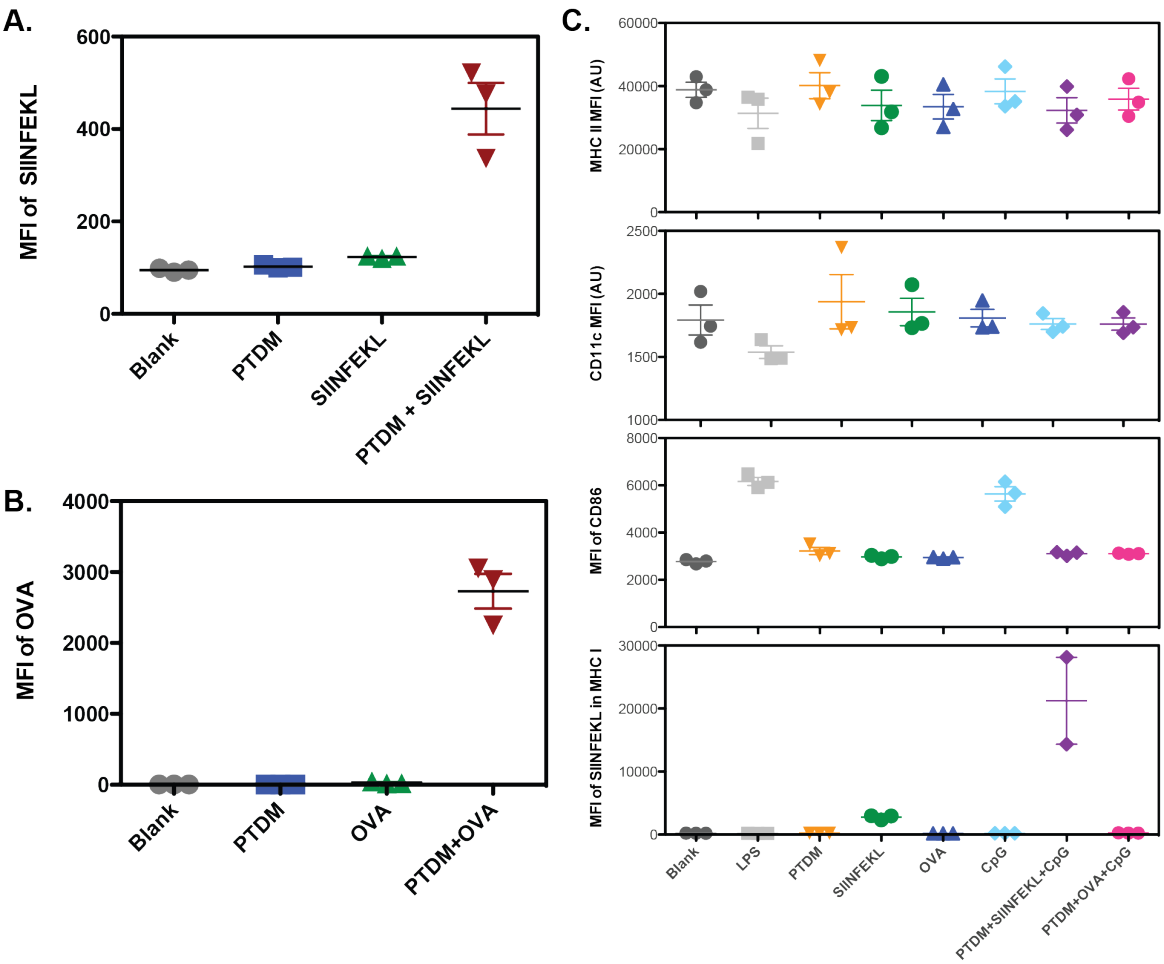

Figure 0.13. Delivery of SIINFEKL-FAM (A) and OVA-AF647 (B) using $MePh_{10}$-b-dG_5 **into immature dendritic cells derived from C57BL/6 mouse bone marrow. Cells were treated for 4 hours, then washed 3 times with heparin (20 U/mL) and assessed for uptake of the cargos by flow cytometry. Upregulation of activation markers (C) on BMDCs 24 hours after delivery of polymer-antigen-agonist complexes. Cells were treated for 4 hours, then washed one time with media and allowed to incubate for 20 more hours. LPS was used as a positive control. Cells were stained with antibodies for MHC II, CD11c, CD86, and H-2K^b (presentation of SIINFEKL in MHC class I). The mean and SEM are shown for BMDCs derived from 3 mice.**

In addition to delivery of fluorescently labeled cargo, both OVA and SIINFEKL were delivered in combination with 1 μM CpG to investigate presentation of SIINFEKL in the MHC class I along with upregulation of CD86 and the production of inflammatory cytokines indicating the ability of these DCs to activate T cells. After differentiation, cells were treated for 4 hours with the polymer-antigen-agonist complexes, after which cells were washed 1 time with PBS and suspended in fresh media for 20 hours. To determine

upregulation, cells were stained with antibodies for CD11c and MHC class II to indicate DCs, as well as CD86, and H-2K^b and results are shown in Figure 0.13C.

Since SIINFEKL can be extracellularly loaded into the MHC class I by diffusion,[238] some display was expected just by adding the soluble peptide to the cells. The presentation of SIINFEKL on the MHC class I was observed to be significantly higher for samples treated with polymer-SIINFEKL-CpG compared with just soluble SIINFEKL alone or when the polymer is used to deliver only the peptide. The high level of the antigen in the MHC class I confirms that the complexes deliver and facilitate presentation for T cell stimulation. Unexpectedly, the costimulatory molecule CD86 was not significantly upregulated in any of the polymer treated samples, though the time point or concentration of chosen agonist may directly affect display of this marker.

Additionally, samples treated with polymer-OVA-CpG did not result in any display of SIINFEKL on the MHC class I as determined by staining with the H-2K^b. Lack of display for OVA treated samples may be due to slow and inconsistent processing of the OVA protein intracellularly. Higher presentation may be observed at a different time point or at higher concentrations of OVA. While delivering a complete protein is conceptually interesting, the ability to deliver a specific sequence or set of sequences allows more control over what the specific immune response will be against.

5.4. Conclusion

In summary, we have shown specific delivery of SIINFEKL into monocytes in whole blood is a rapid process, happening in under 15 minutes without concentration dependence. The complex of the polymer with antigen does not appear to be immunogenic even at increased concentrations lending the ability to tune the immunogenicity using the

TLR9 agonist CpG. Additionally, the PTDM described here is superior to directing monocyte uptake of the non-covalently complexed cargo when compared with amphiphilic peptide counterparts.

When the SIINFEKL was delivered in combination with CpG in whole blood, a pro dendritic cell cytokine environment was observed suggesting the differentiation of the monocytes into professional APCs. The differentiation was not easily substantiated in the mixed cell culture, so THP-1s were cultured with the polymer-antigen-agonist complexes to investigate maturation of the monocytes. Although no inflammatory cytokines were produced from the monocyte culture, there was a slight upregulation of CD40, CD80, and CD86 suggesting that further time points as well as concentrations may elucidate whether the monocytes differentiate. Similar results were seen in immature dendritic cells differentiated from the THP-1s showing that uptake is possible in both cell types.

Delivery of both peptide and protein antigen into BMDCs showed high uptake. High levels of presentation of the SIINFEKL in the MHC class I was observed in samples treated with the polymer-SIINFEKL-CpG complexes indicating increased presentation. Although no co-stimulatory molecules were detected, further investigation into the concentration and timing of the complexes remains to be explored.

The enhanced display of SIINFEKL in MHC class I is a promising step toward using PTDMs to stimulate a specific immune response using antigen presenting cells. This study opens the door for further investigation of using amphiphilic polymers to promote antigen and agonist delivery into antigen presenting cells for training and eliciting a specified activation and response from CTLs. Future exploration is focused on the expansion of T cells against the antigen and agonist treated BMDCs as well as

understanding how concentration of the antigen and agonist are reflected in their ability to promote a sustained T cell response.

PERSPECTIVES AND FUTURE WORK

The exploration of how PTDM structure affects the internalization of cargo is just at its beginning. Herein, we have motivated how small changes in length and hydrophobicity can greatly influence the ability of protein delivery using non-covalent interactions. Current work understanding how the polymers interact with their cargos is underway and future exploration regarding how the structure of the polymer influences self-assembly both in the presence and absence of serum would benefit the design of the polymer system. The assembly properties may influence interaction with the cell membrane, changing the ability of the polymers to permeate into the cytosol with their cargo. To accomplish this, further experiments using light scattering should be combined with ion exchange chromatography and cryo-TEM to fully understand self-assembly and assembly with cargos.

In addition to fluorescence, proteins that have functional biological activity would further bolster claims of cytosolic delivery. To date, Cre recombinase is the only enzymatic protein that has been shown to have function in the cell.[134] While it is encouraging that delivered proteins retain their function, since we do not totally understand the polymer protein interaction, it is hard to know if the PTDMs affect the function of the protein. To explore this, a survey of enzymes should be delivered to correlate binding affinity with protein function. Not only would a survey prove that the PTDMs are compatible with a variety of proteins, it would also facilitate understanding of protein-polymer dynamics.

The CRISPR/Cas9 system is of particular interest because it would allow for gene editing. Delivery of the ribonuclear protein in conjunction with the cRNA would enable a simple, fast way to edit genomes of cells. Exploration of this protein cargo is already underway with several research groups, suggesting that it can be achieved using the right

protein carrier. Labeled versions of the protein and cRNA can be used to assess delivery conditions, as well as what architecture polymer best delivers the cargo into cell. Enzymatic activity can be easily tested using an T7E1 assay to determine gene knockout efficiency. Alternatively, several designer cell lines exist that allow for knock out or knock in of fluorescent genes. The ability to knock out a gene using the CRISPR/Cas9 system would prove preserved enzyme functionality, as well as support the ability of the cargo to reach the nucleus via delivery into the cytosol.

With a better understanding of how polymer structure can be tailored to different types of cargo, PTDMs can be used in various capacities to probe molecular pathways in immune cells through the delivery of proteins and antibodies. In terms of vaccines, we have established the ability to deliver both an antigen and an agonist into both monocytes as well as immature dendritic cells and see enhanced display of the antigen in the MHC class I at a prolonged time point. The correct timing and concentrations of agonist to boost costimulatory molecules and cytokines remains largely unexplored. Evaluation of the effect of antigen and agonist concentrations on surface marker and cytokine expression over a series of time points would provide insight into how much of these cargos are required to facilitate an immune response. APCs derived from mouse bone marrow serve as the best *ex vivo* example since comparable cell lines cannot express some of the classical cytokines or markers.

Further optimization in terms of antigen presentation on APCs and T cell priming would elucidate the ability of the PTDMs to help mount a specific T cell response against the chosen antigen. Specifically, T cell proliferation against the delivered antigen, as well as cytotoxicity of those trained T cells would provide evidence of enhanced vaccines. To

achieve this, DCs differentiated from C57BL/6 bone marrow should be treated with optimized antigen-agonist-polymer complexes as determined by production of high cytokine levels of TNF-α and IFN-γ along with upregulation of CD80 and CD86. After the DCs are pulsed with the complex, $CD8^+$ T cells isolated from OT1 mice with the same C57BL/6 background and stained with CFSE should be co-cultured with the DCs to investigate their ability to prime T cells. Expansion of this specific transgenic OT1 $CD8^+$ T cell against the agonist OVA, will substantiate the ability of the polymers to deliver functional antigen and prime an immune response.

Primed $CD8^+$ T cells can be further tested for their cytotoxic functionality against cells that display the delivered antigen. Several cell lines can be purchased that display the OVA on their surface providing a model for how well the T cells are primed *ex vivo*. OT1 $CD8^+$ T cells that have been expanded against the DCs treated with the antigen-agonist-polymer complexes could be co-cultured with a mouse cell line expressing OVA that has either been stained or loaded with chromium. As the $CD8^+$ T cells function as cytotoxic killer cells against their target, chromium or dye will be released into the media and can be measured either by radio isotopes or by flow cytometry respectively. High levels of cell death will indicate that the T cells have been sufficiently primed against the OVA target and are capable of providing an effective immune response against cell displaying the target antigen.

Additionally, delivering other types of antigens and adjuvants by PTDMs into APCs could be explored to ensure that they system translates to other cargos. Examples of antigens that have readily available transgenic $CD8^+$ T cell receptor models include gp100 and MUC1. Along with new antigens, several other adjuvants are being developed for

clinical applications including TLR7 agonists and cytosolic danger signals that will stimulate the STING pathway. New agonists, or a mixture of agonists may improve the inflammatory response against the desired antigen and could easily be incorporated into future work at any stage. Lastly, cytosolic signals to promote tolerance could also be delivered into APCs to, causing otherwise active T cells to become senescent in the case of autoimmunity.

The ultimate test of T cell priming would be to put the expanded T cells and DCs back into an animal model with a tumor expressing the delivered antigen. If there were stabilization or reduction in tumor size, it would confirm the robustness of the DC vaccine. There are still many things to be optimized before these experiments could be achieved. Further resources would be required in the form of collaboration to support animal studies. Specifically, a group interested in the interface of oncology and immunity would provide the support required to carry out such extensions of these PTDM delivery systems.

Overall, the PTDMs discussed here have demonstrated delivery of functional cargo into a variety of cell types. Synthetically, the scaffold allows for tuning of molecular architecture for probing structure activity relationships in terms of both membrane and protein interactions. Additionally, functional protein delivery remains a largely uncharted territory, rich with application regarding fundamental understanding of molecular pathways. PTDMs provide many opportunities for future research at the materials immunology nexus.

BIBLIOGRAPHY

1. Manning, M. C., Patel, K. & Borchardt, R. T. Stability of Protein Pharmaceuticals. *Pharmaceutical Research* **6,** 903–918 (1989).

2. Kim, T. K. & Eberwine, J. H. Mammalian cell transfection: The present and the future. *Anal. Bioanal. Chem.* **397,** 3173–3178 (2010).

3. Zuris, J. A. *et al.* Cationic lipid-mediated delivery of proteins enables efficient protein-based genome editing in vitro and in vivo. *Nat. Biotechnol.* **33,** 73–80 (2014).

4. Nagy, A. Cre Recombinase: The Universal Reagent for Genome Tailoring. *Genesis* **26,** 99–109 (2000).

5. Marschall, A. L. J., Frenzel, A., Schirrmann, T., Schüngel, M. & Dübel, S. Targeting antibodies to the cytoplasm. *mAbs* **3,** 3–16 (2011).

6. Stewart, M. P. *et al.* In vitro and ex vivo strategies for intracellular delivery. *Nature* **538,** 183–192 (2016).

7. Du, J., Jin, J., Yan, M. & Lu, Y. Synthetic nanocarriers for intracellular protein delivery. *Curr. Drug Metab.* **13,** 82–92 (2012).

8. Gu, Z., Biswas, A., Zhao, M. & Tang, Y. Tailoring nanocarriers for intracellular protein delivery. *Chem. Soc. Rev.* **40,** 3638 (2011).

9. Fu, A., Tang, R., Hardie, J., Farkas, M. E. & Rotello, V. M. Promises and Pitfalls of Intracellular Delivery of Proteins. *Bioconjug. Chem.* **25,** 1602–1608 (2014).

10. Choi, Y. S. & David, A. E. Cell penetrating peptides and the mechanisms for intracellular entry. *Curr. Pharm. Biotechnol.* **15,** 192–199 (2014).

11. Gräslund, A., Madani, F., Lindberg, S., Langel, Ü. & Futaki, S. Mechanisms of cellular uptake of cell-penetrating peptides. *J. Biophys.* **2011,** (2011).

12. Letchford, K. & Burt, H. A review of the formation and classification of amphiphilic block copolymer nanoparticulate structures: micelles, nanospheres, nanocapsules and polymersomes. *Eur. J. Pharm. Biopharm.* **65,** 259–269 (2007).

13. Zhang, Y. & Yu, L. C. Single-cell microinjection technology in cell biology. *BioEssays* **30,** 606–610 (2008).

14. Zhang, Y. & Yu, L. C. Microinjection as a tool of mechanical delivery. *Curr. Opin. Biotechnol.* **19,** 506–510 (2008).

15. Zhang, Y. & C, L. A. Microinjections to study the specific role of proapoptotic proteins in neurons. 83–106 (2002).

16. Zhang, Y., Goodyer, C. G. & LeBlanc, A. Selective and protracted apoptosis in human primary neurons microinjected with active caspase-3, -6, -7, and -8. *J. Neurosci.* **20,** 8384–8389 (2000).

17. Zhang, Y. *et al.* Estrogen and Androgen Protection of Human Neurons against Intracellular Amyloid b1-42 Toxicity through Heat Shock Protein 70. *J Neurosci* **24,** 5315–5321 (2004).

18. Cuevas, C. *et al.* Overcoming chemoresistance of non-small cell lung carcinoma through restoration of an AIF-dependent apoptotic pathway. *Oncogene* **27,** 1981–92 (2008).

19. Theiss, C. & Meller, K. Microinjected anti-actin antibodies decrease gap junctional intercellular commmunication in cultured astrocytes. *Exp. Cell Res.* **281,** 197–204 (2002).

20. Lim, S. N., Zeenathul, A. N., Mohd Azmi, M. L., Abas Mazni, O. & Fauziah, O. Effect of protein concentration and injection pressure in microinjection delivery of maltose binding protein into breast cancer cells. *Pertanika J. Sci. Technol.* **19,** 273–283 (2011).

21. Le Gac, S. & Uitert, I. Van. *Handbook of Electroporation*. (Springer International Publishing, 2017). doi:10.1007/978-3-319-32886-7

22. Geng, T. & Lu, C. Microfluidic electroporation for cellular analysis and delivery. *Lab Chip* **13,** 3803–3821 (2013).

23. Schumann, K. *et al.* Generation of knock-in primary human T cells using Cas9 ribonucleoproteins. *Proc. Natl. Acad. Sci. U. S. A.* **112,** 10437–10442 (2015).

24. Hendel, A. *et al.* Chemically modified guide RNAs enhance CRISPR-Cas genome editing in human primary cells. *Nat. Biotechnol.* **33,** 985–989 (2015).

25. Eksioglu-Demiralp, E. *et al.* A method for functional evaluation of caspase activation pathways in intact lymphoid cells using electroporation-mediated protein delivery and flow cytometric analysis. *J. Immunol. Methods* **275,** 41–56 (2003).

26. Todorova, R. Estimation of methods of protein delivery into mammalian cells--a comparative study by electroporation and bioporter assay. *Prikl Biokhim Mikrobiol* **45,** 493–496 (2009).

27. Schakowski, F. *et al.* Novel non-viral method for transfection of primary leukemia cells and cell lines. *Genet. Vaccines Ther.* **2,** 1 (2004).

28. Miersch, S., Sidhu, S. S., Miersch, S. & Sidhu, S. S. Intracellular targeting with engineered proteins. *F1000Research* **5,** 1947 (2016).

29. Kooijmans, S. A. A. *et al.* Electroporation-induced siRNA precipitation obscures the efficiency of siRNA loading into extracellular vesicles. *J. Control. Release* **172,** 229–238 (2013).

30. Hallow, D. M. *et al.* Shear-induced intracellular loading of cells with molecules by controlled microfluidics. *Biotechnol. Bioeng.* **99,** 846–854 (2008).

31. Sharei, A. *et al.* A vector-free microfluidic platform for intracellular delivery. *Proc. Natl. Acad. Sci.* **110,** 2082–2087 (2013).

32. Lee, J. *et al.* Nonendocytic delivery of functional engineered nanoparticles into the cytoplasm of live cells using a novel, high-throughput microfluidic device. *Nano Lett.* **12,** 6322–6327 (2012).

33. Szeto, G. L. *et al.* Microfluidic squeezing for intracellular antigen loading in polyclonal B-cells as cellular vaccines. *Sci. Rep.* **5,** 10276 (2015).

34. Tan, M. L., Choong, P. F. M. & Dass, C. R. Recent developments in liposomes, microparticles and nanoparticles for protein and peptide drug delivery. *Peptides* **31,** 184–193 (2010).

35. Nakamura, T. *et al.* Octaarginine-modified liposomes enhance cross-presentation by promoting the c-terminal trimming of antigen peptide. *Mol. Pharm.* **11,** 2787–2795 (2014).

36. Liguori, L., Marques, B., Villegas-Mendez, A., Rothe, R. & Lenormand, J. L. Liposomes-mediated delivery of pro-apoptotic therapeutic membrane proteins. *J. Control. Release* **126,** 217–227 (2008).

37. Simão, A. M. S. *et al.* Liposomal systems as carriers for bioactive compounds. *Biophys. Rev.* **7,** 391–397 (2015).

38. Petersen, A. L., Hansen, A. E., Gabizon, A. & Andresen, T. L. Liposome imaging agents in personalized medicine. *Adv. Drug Deliv. Rev.* **64,** 1417–1435 (2012).

39. Yang, N. J. & Hinner, M. J. in *Site-Specific Protein Labeling: Methods and Protocols* 29–53 (2015). doi:10.1007/978-1-4939-2272-7_3

40. Shete, H. K., Prabhu, R. H. & Patravale, V. B. Endosomal escape: a bottleneck in intracellular delivery. *J. Nanosci. Nanotechnol.* **14,** 460–74 (2014).

41. Wang, M. *et al.* Efficient delivery of genome-editing proteins using bioreducible lipid nanoparticles. *Proc. Natl. Acad. Sci.* **113,** 2868–2873 (2016).

42. Nair, S., Zhou, F., Reddy, R., Huang, L. & Rouse, B. T. Soluble proteins delivered to dendritic cells via pH-sensitive liposomes induce primary cytotoxic T lymphocyte responses in vitro. *J. Exp. Med.* **175,** 609–612 (1992).

43. Nakamura, T., Moriguchi, R., Kogure, K., Shastri, N. & Harashima, H. Efficient MHC class I presentation by controlled intracellular trafficking of antigens in octaarginine-modified liposomes. *Mol Ther* **16,** 1507–1514 (2008).

44. Knudsen, K. B. *et al.* In vivo toxicity of cationic micelles and liposomes. *Nanomedicine Nanotechnology, Biol. Med.* **11,** 467–477 (2015).

45. Almeida, A. J. & Souto, E. Solid lipid nanoparticles as a drug delivery system for peptides and proteins. *Adv. Drug Deliv. Rev.* **59,** 478–490 (2007).

46. Martins, S., Sarmento, B., Ferreira, D. C. & Souto, E. B. Lipid-based colloidal carriers for peptide and protein delivery - Liposomes versus lipid nanoparticles. *Int. J. Nanomedicine* **2,** 595–607 (2007).

47. Reithmeier, H., Herrmann, J. & Go, A. Development and characterization of lipid microparticles as a drug carrier for somatostatin. **218,** 133–143 (2001).

48. Reithmeier, H., Herrmann, J. & Göpferich, A. Lipid microparticles as a parenteral controlled release device for peptides. *J. Control. Release* **73,** 339–350 (2001).

49. Schubert, M. A. & Müller-Goymann, C. C. Characterisation of surface-modified solid lipid nanoparticles (SLN): Influence of lecithin and nonionic emulsifier. *Eur. J. Pharm. Biopharm.* **61,** 77–86 (2005).

50. Nagaraju, K., Reddy, R. & Reddy, N. A review on protein functionalized carbon nanotubes. *J. Appl. Biomater. Funct. Mater.* **13,** 0–0 (2015).

51. Kam, N. W. S., Jessop, T. C., Wender, P. A. & Dai, H. Nanotube molecular transporters: Internalization of carbon nanotube-protein conjugates into mammalian cells. *J. Am. Chem. Soc.* **126,** 6850–6851 (2004).

52. Chakrabarti, M., Kiseleva, R., Vertegel, A. & Ray, S. K. Carbon Nanomaterials for Drug Delivery and Cancer Therapy. *J Nanosci Nanotechnol* **15,** 5501–5511 (2015).

53. Vashist, S. K. *et al.* Delivery of drugs and biomolecules using carbon nanotubes. *Carbon N. Y.* **49,** 4077–4097 (2011).

54. Pantarotto, D., Briand, J.-P., Prato, M. & Bianco, A. Translocation of bioactive peptides across cell membranes by carbon nanotubesElectronic supplementary information (ESI) available: details of the synthesis and characterization, cell culture, TEM, epifluorescence and confocal microscopy images of CNTs 1, . *Chem. Commun.* 16 (2004). doi:10.1039/b311254c

55. Kam, N. W. S. & Dai, H. Carbon nanotubes as intracellular protein transporters: Generality and biological functionality. *J. Am. Chem. Soc.* **127,** 6021–6026 (2005).

56. Bilan, R., Nabiev, I. & Sukhanova, A. Quantum Dot-Based Nanotools for Bioimaging, Diagnostics, and Drug Delivery. *ChemBioChem* **17,** 2103–2114 (2016).

57. Zrazhevskiy, P., Sena, M. & Gao, X. Designing multifunctional quantum dots for bioimaging, detection, and drug delivery. *Chem. Soc. Rev.* **39,** 4326 (2010).

58. Martin, I., Teixido, M. & Giralt, E. Intracellular Fate of Peptide-Mediated Delivered Cargoes. *Curr. Pharm. Des.* **19,** 2924–2942 (2013).

59. Bentzen, E. L. *et al.* Surface modification to reduce nonspecific binding of quantum dots in live cell assays. *Bioconjug. Chem.* **16,** 1488–1494 (2005).

60. Cui, B. *et al.* One at a time, live tracking of NGF axonal transport using quantum dots. *Proc. Natl. Acad. Sci.* **104,** 13666–13671 (2007).

61. Koshman, Y. E. *et al.* Delivery and visualization of proteins conjugated to quantum dots in cardiac myocytes. *J. Mol. Cell. Cardiol.* **45,** 853–856 (2008).

62. Delehanty, J. B., Mattoussi, H. & Medintz, I. L. Delivering quantum dots into cells: Strategies, progress and remaining issues. *Anal. Bioanal. Chem.* **393,** 1091–1105 (2009).

63. Bradburne, C. E. *et al.* Cytotoxicity of quantum dots used for in vitro cellular labeling: Role of QD surface ligand, delivery modality, cell type, and direct comparison to organic fluorophores. *Bioconjug. Chem.* **24,** 1570–1583 (2013).

64. Wang, C., Zhu, W. & Wang, B. Z. Dual-linker gold nanoparticles as adjuvanting carriers for multivalent display of recombinant influenza hemagglutinin trimers and flagellin improve the immunological responses in vivo and in vitro. *Int. J. Nanomedicine* **12,** 4747–4762 (2017).

65. Khoshnevisan, K. *et al.* The promising potentials of capped gold nanoparticles for drug delivery systems. *J Drug Target* 1–8 (2017). doi:10.1080/1061186X.2017.1387790

66. Connor, E. E., Mwamuka, J., Gole, A., Murphy, C. J. & Wyatt, M. D. Gold nanoparticles are taken up by human cells but do not cause acute cytotoxicity. *Small* **1,** 325–327 (2005).

67. Mout, R. *et al.* General Strategy for Direct Cytosolic Protein Delivery via Protein-Nanoparticle Co-engineering. *ACS Nano* **11,** 6416–6421 (2017).

68. Tang, R. *et al.* Direct delivery of functional proteins and enzymes to the cytosol using nanoparticle-stabilized nanocapsules. *ACS Nano* **7,** 6667–6673 (2013).

69. Mout, R., Ray, M., Lee, Y. W., Scaletti, F. & Rotello, V. M. In Vivo Delivery of CRISPR/Cas9 for Therapeutic Gene Editing: Progress and Challenges. *Bioconjug. Chem.* **28,** 880–884 (2017).

70. Kim, J., Cao, L., Shvartsman, D., Silva, E. A. & Mooney, D. J. Targeted delivery of nanoparticles to ischemic muscle for imaging and therapeutic angiogenesis. *Nano Lett.* **11,** 694–700 (2011).

71. Lai, C. Y. *et al.* A mesoporous silica nanosphere-based carrier system with chemically removable CdS nanoparticle caps for stimuli-responsive controlled release of neurotransmitters and drug molecules. *J. Am. Chem. Soc.* **125,** 4451–4459 (2003).

72. Giri, S., Trewyn, B. G., Stellmaker, M. P. & Lin, V. S. Y. Stimuli-responsive controlled-release delivery system based on mesoporous silica nanorods capped with magnetic nanoparticles. *Angew. Chemie - Int. Ed.* **44,** 5038–5044 (2005).

73. Huang, D.-M. *et al.* Highly efficient cellular labeling of mesoporous nanoparticles in human mesenchymal stem cells: implication for stem cell tracking. *FASEB J.* **19,** 2014–6 (2005).

74. Slowing, I., Trewyn, B. G. & Lin, V. S.-Y. Effect of Surface Functionalization of MCM-41-Type Mesoporous Silica Nanoparticles on the Endocytosis by Human Cancer Cells. *J. Am. Chem. Soc.* **128,** 14792–14793 (2006).

75. Santra, S. *et al.* TAT conjugated, FITC doped silica nanoparticles for bioimaging applications. *Chem. Commun.* 2810 (2004). doi:10.1039/b411916a

76. Slowing, I. I., Trewyn, B. G. & Lin, V. S. Y. Mesoporous silica nanoparticles for intracellular delivery of membrane-impermeable proteins. *J. Am. Chem. Soc.* **129,** 8845–8849 (2007).

77. Bale, S. S. *et al.* Nanoparticle-Mediated Cytoplasmic Machinery. *ACS Nano* **4,** 1493–1500 (2010).

78. Prasetyanto, E. A. *et al.* Breakable Hybrid Organosilica Nanocapsules for Protein Delivery. *Angew. Chemie - Int. Ed.* **55,** 3323–3327 (2016).

79. Deodhar, G. V., Adams, M. L. & Trewyn, B. G. Controlled release and intracellular protein delivery from mesoporous silica nanoparticles. *Biotechnol. J.* **12,** (2017).

80. Yu, M., Wu, J., Shi, J. & Farokhzad, O. C. Nanotechnology for protein delivery: Overview and perspectives. *J. Control. Release* **240,** 24–37 (2016).

81. Chorny, M., Hood, E., Levy, R. J. & Muzykantov, V. R. Endothelial delivery of antioxidant enzymes loaded into non-polymeric magnetic nanoparticles. *J. Control. Release* **146,** 144–151 (2010).

82. Naqvi, S. *et al.* Concentration-dependent toxicity of iron oxide nanoparticles mediated by increased oxidative stress. *Int. J. Nanomedicine* **5,** 983–989 (2010).

83. Thompson, D. B., Cronican, J. J. & Liu, D. R. in *Methods in Enzymology* **503,** 293–319 (2012).

84. Lawrence, M. S., Phillips, K. J. & Liu, D. R. Supercharging proteins can impart unusual resilience. *J. Am. Chem. Soc.* **129,** 10110–10112 (2007).

85. Cronican, J. J. *et al.* Potent delivery of functional proteins into mammalian cells in vitro and in vivo using a supercharged protein. *ACS Chem. Biol.* **5,** 747–752 (2010).

86. McNaughton, B. R., Cronican, J. J., Thompson, D. B. & Liu, D. R. Mammalian cell penetration, siRNA transfection, and DNA transfection by supercharged proteins. *Proc. Natl. Acad. Sci. U. S. A.* **106,** 6111–6 (2009).

87. Cronican, J. J. *et al.* A class of human proteins that deliver functional proteins into mammalian cells in vitro and in vivo. *Chem. Biol.* **18,** 833–838 (2011).

88. Lim, Y. T., Cho, M. Y., Lee, J. M., Chung, S. J. & Chung, B. H. Simultaneous intracellular delivery of targeting antibodies and functional nanoparticles with engineered protein G system. *Biomaterials* **30,** 1197–1204 (2009).

89. Molino, N. M., Neek, M., Tucker, J. A., Nelson, E. L. & Wang, S. W. Viral-mimicking protein nanoparticle vaccine for eliciting anti-tumor responses. *Biomaterials* **86,** 83–91 (2016).

90. Molino, N. M., Anderson, A. K. L., Nelson, E. L. & Wang, S. W. Biomimetic protein nanoparticles facilitate enhanced dendritic cell activation and cross-presentation. *ACS Nano* **7,** 9743–9752 (2013).

91. Johnsen, K. B. *et al.* A comprehensive overview of exosomes as drug delivery vehicles - Endogenous nanocarriers for targeted cancer therapy. *Biochim. Biophys. Acta - Rev. Cancer* **1846,** 75–87 (2014).

92. EL Andaloussi, S., Mäger, I., Breakefield, X. O. & Wood, M. J. A. Extracellular vesicles: biology and emerging therapeutic opportunities. *Nat. Rev. Drug Discov.* **12,** 347–357 (2013).

93. Shimoda, A. *et al.* Exosomes as nanocarriers for systemic delivery of the Helicobacter pylori virulence factor CagA. *Sci Rep* **6,** 18346 (2016).

94. Sterzenbach, U., Putz, U., Low, L. H., Silke, J. & Tan, S. S. Engineered exosomes as vehicles for biologically active proteins. *Mol. Ther.* (2017).

95. Yim, N. *et al.* Exosome engineering for efficient intracellular delivery of soluble proteins using optically reversible protein–protein interaction module. *Nat. Commun.* **7,** 12277 (2016).

96. Akishiba, M. *et al.* Cytosolic antibody delivery by lipid-sensitive endosomolytic peptide. *Nat. Chem.* **9,** 751–761 (2017).

97. Kaczmarczyk, S. J., Sitaraman, K., Young, H. a, Hughes, S. H. & Chatterjee, D. K. Protein delivery using engineered virus-like particles. *Pnas* **108,** 16998–17003 (2011).

98. Herrera Estrada, L. P. & Champion, J. A. Protein nanoparticles for therapeutic protein delivery. *Biomater. Sci.* **3,** 787–799 (2015).

99. Kondo, E., Seto, M., Yoshikawa, K. & Yoshino, T. Highly efficient delivery of p16 antitumor peptide into aggressive leukemia/lymphoma cells using a novel transporter system. *Mol. Cancer Ther.* **3,** 1623–1630 (2004).

100. Voelkel, C. *et al.* Protein transduction from retroviral Gag precursors. *Proc. Natl. Acad. Sci.* **107,** 7805–7810 (2010).

101. Wu, D. T. & Roth, M. J. MLV based viral-like-particles for delivery of toxic proteins and nuclear transcription factors. *Biomaterials* **35,** 8416–8426 (2014).

102. Aoki, T., Miyauchi, K., Urano, E., Ichikawa, R. & Komano, J. Protein transduction by pseudotyped lentivirus-like nanoparticles. *Gene Ther.* **18,** 936–941 (2011).

103. Schneider-Schaulies, J. Cellular receptors for viruses: Links to tropism and pathogenesis. *J. Gen. Virol.* **81,** 1413–1429 (2000).

104. Beilhartz, G. L., Sugiman-Marangos, S. N. & Melnyk, R. A. Repurposing bacterial toxins for intracellular delivery of therapeutic proteins. *Biochem. Pharmacol.* **142,** 13–20 (2017).

105. Rabideau, A. E. & Pentelute, B. L. Delivery of Non-Native Cargo into Mammalian Cells Using Anthrax Lethal Toxin. *ACS Chem. Biol.* **11,** 1490–1501 (2016).

106. Ballard, J. D., John Collier, R. & Starnbach, M. N. Anthrax toxin as a molecular tool for stimulation of cytotoxic T lymphocytes: Disulfide-linked epitopes, multiple injections, and role of CD4+ cells. *Infect. Immun.* **66,** 4696–4699 (1998).

107. Fischer, R., Köhler, K., Fotin-Mleczek, M. & Brock, R. A Stepwise Dissection of the Intracellular Fate of Cationic Cell-penetrating Peptides. *J. Biol. Chem.* **279,** 12625–12635 (2004).

108. Jones, S. W. *et al.* Characterisation of cell-penetrating peptide-mediated peptide delivery. *Br. J. Pharmacol.* **145,** 1093–1102 (2005).

109. Liao, X., Rabideau, A. E. & Pentelute, B. L. Delivery of antibody mimics into mammalian cells via anthrax toxin protective antigen. *ChemBioChem* **15,** 2458–2466 (2014).

110. Auger, A. *et al.* Efficient Delivery of Structurally Diverse Protein Cargo into Mammalian Cells by a Bacterial Toxin. *Mol. Pharm.* **12,** 2962–2971 (2015).

111. Mitchell, D. J., Kim, D. T., Steinman, L., Fathman, C. G. & Rothbard, J. B. Polyarginine enters cells more efficiently than other polycationic homopolymers. *J. Pept. Res.* **56,** 318–325 (2000).

112. Wender, P. A. *et al.* The design, synthesis, and evaluation of molecules that enable or enhance cellular uptake: peptoid molecular transporters. *Proc. Natl. Acad. Sci.* **97,** 13003–13008 (2000).

113. Milletti, F. Cell-penetrating peptides: Classes, origin, and current landscape. *Drug Discov. Today* **17,** 850–860 (2012).

114. Sgolastra, F., deRonde, B. M., Sarapas, J. M., Som, A. & Tew, G. N. Designing mimics of membrane active proteins. *Acc. Chem. Res.* **46,** 2977–2987 (2013).

115. deRonde, B. M. & Tew, G. N. Development of protein mimics for intracellular delivery. *Biopolymers* **104,** 265–280 (2015).

116. Stanzl, E. G., Trantow, B. M., Vargas, J. R. & Wender, P. A. Fifteen years of cell-penetrating, guanidinium-rich molecular transporters: Basic science, research tools, and clinical applications. *Acc. Chem. Res.* **46,** 2944–2954 (2013).

117. Brooks, H., Lebleu, B. & Vivès, E. Tat peptide-mediated cellular delivery: Back to basics. *Adv. Drug Deliv. Rev.* **57,** 559–577 (2005).

118. Heitz, F., Morris, M. C. & Divita, G. Twenty years of cell - penetrating peptides : from molecular mechanisms to therapeutics. *Br. J. Pharmacol.* **157,** 195–206 (2009).

119. Morris, M. C., Depollier, J., Mery, J., Heitz, F. & Divita, G. A peptide carrier for the delivery of biologically active proteins into mammalian cells. *Nat. Biotechnol.* **19,** 1173–1176 (2001).

120. Pooga, M. *et al.* Cellular translocation of proteins by transportan. *FASEB J.* **15,** 1451–1453 (2001).

121. Meade, B. R. & Dowdy, S. F. Exogenous siRNA delivery using peptide transduction domains/cell penetrating peptides. *Advanced Drug Delivery Reviews* **59,** 134–140 (2007).

122. Ramakrishna, S. *et al.* Gene disruption by cell-penetrating peptide-mediated delivery of Cas9 protein and guide RNA. *Genome Res.* **24,** 1020–1027 (2014).

123. Barbas, C. F. Cell-penetrating peptide-mediated delivery of TALEN proteins via bioconjugation for genome engineering. *PLoS One* **9,** e85755 (2014).

124. Guelen, L. *et al.* TAT-apoptin is efficiently delivered and induces apoptosis in cancer cells. *Oncogene* **23,** 1153–1165 (2004).

125. Murata, H. *et al.* Denatured and reversibly cationized p53 readily enters cells and simultaneously folds to the functional protein in the cells. *Biochemistry* **45,** 6124–6132 (2006).

126. Yoon, H. Y. *et al.* TAT-mediated delivery of human glutamate dehydrogenase into PC12 cells. *Neurochem. Int.* **41,** 37–42 (2002).

127. Wheeler, D. S., Dunsmore, K. E. & Wong, H. R. Intracellular delivery of HSP70 using HIV-1 Tat protein transduction domain. *Biochem. Biophys. Res. Commun.* **301,** 54–59 (2003).

128. Kristensen, M., Birch, D. & Nielsen, H. M. Applications and challenges for use of cell-penetrating peptides as delivery vectors for peptide and protein cargos. *Int. J. Mol. Sci.* **17,** (2016).

129. Kristensen, M. *et al.* Conjugation of Cell-Penetrating Peptides to Parathyroid Hormone Affects Its Structure, Potency, and Transepithelial Permeation. *Bioconjug. Chem.* **26,** 477–488 (2015).

130. Treat, N. J. *et al.* Guanidine-Containing Methacrylamide (Co)polymers via a RAFT: Toward a Cell-Penetrating Peptide Mimic. *ACS Macro Lett.* **1,** 100–104 (2012).

131. McKinlay, C. J., Waymouth, R. M. & Wender, P. A. Cell-Penetrating, Guanidinium-Rich Oligophosphoesters: Effective and Versatile Molecular Transporters for Drug and Probe Delivery. *J. Am. Chem. Soc.* **138,** 3510–3517 (2016).

132. Tezgel, A. O. Ö., Jacobs, P., Backlund, C. M., Telfer, J. C. & Tew, G. N. Synthetic Protein Mimics for Functional Protein Delivery. *Biomacromolecules* **18,** 819–825 (2017).

133. Kolonko, E. M. & Kiessling, L. L. A polymeric domain that promotes cellular internalization. *J. Am. Chem. Soc.* **130,** 5626–5627 (2008).

134. Sgolastra, F. *et al.* Sequence segregation improves non-covalent protein delivery. *J. Control. Release* **254,** 131–136 (2017).

135. Ozay, E. I. *et al.* Intracellular Delivery of Anti-pPKCθ (Thr538) via Protein Transduction Domain Mimics for Immunomodulation. *Mol. Ther.* **24,** 2118–2130 (2016).

136. Backlund, C. M., Takeuchi, T., Futaki, S. & Tew, G. N. Relating structure and internalization for ROMP-based protein mimics. *Biochim. Biophys. Acta - Biomembr.* **1858,** 1443–1450 (2016).

137. Akash, M. S. H., Rehman, K. & Chen, S. Polymeric-based particulate systems for delivery of therapeutic proteins. *Pharm. Dev. Technol.* **21,** 367–378 (2016).

138. Wani, T. U. *et al.* Targeting Aspects of Nanogels: An Overview. *Int J Pharm Sci Nanotech Vol* **7,** 2612–2630 (2014).

139. Sahdev, P., Ochyl, L. J. & Moon, J. J. Biomaterials for Nanoparticle Vaccine Delivery Systems. *Pharm. Res.* **31,** 2563–2582 (2014).

140. Ventura, J. *et al.* Reactive Self-Assembly of Polymers and Proteins to Reversibly Silence a Killer Protein. *Biomacromolecules* **16,** 3161–3171 (2015).

141. Zhao, M. *et al.* Redox-responsive nanocapsules for intracellular protein delivery. *Biomaterials* **32,** 5223–5230 (2011).

142. Yuhua, H. *et al.* Cytosolic delivery of membrane-impermeable molecules in dendritic cells using pH-responsive core-shell nanoparticles. *Nano Lett.* **7,** 3056–3064 (2007).

143. Priftis, D., Laugel, N. & Tirrell, M. Thermodynamic characterization of polypeptide complex coacervation. *Langmuir* **28,** 15947–15957 (2012).

144. Coué, G., Freese, C., Unger, R. E., James Kirkpatrick, C. & Engbersen, J. F. J. Bioresponsive poly(amidoamine)s designed for intracellular protein delivery. *Acta Biomater.* **9,** 6062–6074 (2013).

145. Walter, M. V. & Malkoch, M. Simplifying the synthesis of dendrimers: accelerated approaches. *Chem. Soc. Rev.* **41,** 4593 (2012).

146. Markovsky, E. *et al.* Administration, distribution, metabolism and elimination of polymer therapeutics. *J. Control. Release* **161,** 446–460 (2012).

147. Bayele, H. K. *et al.* Protein transduction by lipidic peptide dendrimers. *J. Pharm. Sci.* **95,** 1227–1237 (2006).

148. Hamilton, S. K., Ikizler, M. R., Wallen, C., Wright, P. F. & Harth, E. Effective delivery of IgG-antibodies into infected cells via dendritic molecular transporter conjugate IgGMT. *Mol. Biosyst.* **4,** 1209–11 (2008).

149. Avvakumova, S., Colombo, M., Tortora, P. & Prosperi, D. Biotechnological approaches toward nanoparticle biofunctionalization. *Trends Biotechnol.* **32,** 11–20 (2014).

150. Kim, C. S. *et al.* Co-delivery of protein and small molecule therapeutics using nanoparticle-stabilized nanocapsules. *Bioconjug. Chem.* **26,** 950–954 (2015).

151. Yang, X. C. *et al.* Drug delivery using nanoparticle-stabilized nanocapsules. *Angew. Chemie - Int. Ed.* **50,** 477–481 (2011).

152. Liu, G. *et al.* The highly efficient delivery of exogenous proteins into cells mediated by biodegradable chimaeric polymersomes. *Biomaterials* **31,** 7575–7585 (2010).

153. Lu, L. *et al.* Anisamide-decorated pH-sensitive degradable chimaeric polymersomes mediate potent and targeted protein delivery to lung cancer cells. *Biomacromolecules* **16,** 1726–1735 (2015).

154. Chu, D. S. H. *et al.* Application of Controlled Radical Polymerization for Nucleic Acid Delivery. *Acc Chem Res.* **45,** 1089–1099 (2013).

155. Mo, R. H., Zaro, J. L. & Shen, W. C. Comparison of cationic and amphipathic cell penetrating peptides for siRNA delivery and efficacy. *Mol. Pharm.* **9,** 299–309 (2012).

156. Kitazoe, M. *et al.* Protein transduction assisted by polyethylenimine-cationized carrier proteins. *J. Biochem.* **137,** 693–701 (2005).

157. Murata, H. *et al.* Intracellular delivery of glutathione S-transferase-fused proteins into mammalian cells by polyethylenimine-glutathione conjugates. *J. Biochem.* **144,** 447–455 (2008).

158. Apostolopoulos, V. *et al.* Delivery of tumor associated antigens to antigen presenting cells using penetratin induces potent immune responses. *Vaccine* **24,** 3191–3202 (2006).

159. Lackey, C. A., Press, O. W., Hoffman, A. S. & Stayton, P. S. A biomimetic pH-responsive polymer directs endosomal release and intracellular delivery of an endocytosed antibody complex. *Bioconjug. Chem.* **13,** 996–1001 (2002).

160. Ye, M., Kim, S. & Park, K. Issues in long-term protein delivery using biodegradable microparticles. *J. Control. Release* **146,** 241–260 (2010).

161. Morris, M. C., Deshayes, S., Heitz, F. & Divita, G. Cell-penetrating peptides: from molecular mechanisms to therapeutics. *Biol. Cell* **100,** 201–217 (2008).

162. Pooga, M. & Langel, Ü. Classes of Cell-Penetrating Peptides. *Methods Mol. Biol.* **1324,** 3–28 (2015).

163. Frankel, A. D. & Pabo, C. O. Cellular uptake of the tat protein from human immunodeficiency virus. *Cell* **55,** 1189–1193 (1988).

164. Green, M. & Loewenstein, P. M. Autonomous functional domains of chemically synthesized human immunodeficiency virus tat trans-activator protein. **55,** 1179–1188

165. Vivès, E., Brodin, P. & Lebleu, B. A truncated HIV-1 Tat protein basic domain rapidly translocates through the plasma membrane and accumulates in the cell nucleus. *J. Biol. Chem.* **272,** 16010–16017 (1997).

166. Lindgren, M. & Langel, U. Classes and prediction of cell-penetrating peptides. *Methods Mol. Biol.* **683,** 3–19 (2011).

167. Futaki, S. *et al.* Arginine-rich peptides. An abundant source of membrane-permeable peptides having potential as carriers for intracellular protein delivery. **276,** 5836–5840

168. Oehlke, J. *et al.* Cellular uptake of an a-helical amphipathic model peptide with the potential to deliver polar compounds into the cell interior non-endocytically. *Biochim. Biophys. Acta - Biomembr.* **1414,** 127–139 (1998).

169. Nakase, I., Tanaka, G. & Futaki, S. Cell-penetrating peptides (CPPs) as a vector for the delivery of siRNAs into cells. *Mol. Biosyst.* **9,** 855–61 (2013).

170. Wadia, J. S., Stan, R. V & Dowdy, S. F. Transducible TAT-HA fusogenic peptide enhances escape of TAT-fusion proteins after lipid raft macropinocytosis. *Nat. Med.* **10,** 310–315 (2004).

171. Nakase, I. *et al.* Cellular uptake of arginine-rich peptides: Roles for macropinocytosis and actin rearrangement. *Mol. Ther.* **10,** 1011–1022 (2004).

172. Conner, S. D. & Schmid, S. L. Regulated portals of entry into the cell. *Nature* **422,** 37–44 (2003).

173. Jones, A. T. Macropinocytosis: Searching for an endocytic identity and role in the uptake of cell penetrating peptides. *J. Cell. Mol. Med.* **11,** 670–684 (2007).

174. El-Sayed, A., Futaki, S. & Harashima, H. Delivery of Macromolecules Using Arginine-Rich Cell-Penetrating Peptides: Ways to Overcome Endosomal Entrapment. *AAPS J.* **11,** 13–22 (2009).

175. Thorén, P. E. G. *et al.* Uptake of analogs of penetratin, Tat(48-60) and oligoarginine in live cells. *Biochem. Biophys. Res. Commun.* **307,** 100–107 (2003).

176. Rothbard, J. B., Jessop, T. C., Lewis, R. S., Murray, B. a. & Wender, P. a. Role of membrane potential and hydrogen bonding in the mechanism of translocation of guanidinium-rich peptides into cells. *J. Am. Chem. Soc.* **126,** 9506–9507 (2004).

177. Kosuge, M., Takeuchi, T., Nakase, I., Jones, A. T. & Futaki, S. Cellular internalization and distribution of arginine-rich peptides as a function of extracellular peptide concentration, serum, and plasma membrane associated proteoglycans. *Bioconjug. Chem.* **19,** 656–664 (2008).

178. Herce, H. D., Garcia, A. E. & Cardoso, M. C. Fundamental molecular mechanism for the cellular uptake of guanidinium-rich molecules. *J. Am. Chem. Soc.* **136,** 17459–17467 (2014).

179. Herce, H. D. *et al.* Arginine-rich peptides destabilize the plasma membrane, consistent with a pore formation translocation mechanism of cell-penetrating peptides. *Biophys. J.* **97,** 1917–1925 (2009).

180. Fretz, M. M. *et al.* Temperature-, concentration- and cholesterol-dependent translocation of L- and D-octa-arginine across the plasma and nuclear membrane of CD34+ leukaemia cells. *Biochem. J.* **403,** 335–342 (2007).

181. Brock, R. The uptake of arginine-rich cell-penetrating peptides: Putting the puzzle together. *Bioconjug. Chem.* **25,** 863–868 (2014).

182. Schmidt, N. W. *et al.* Molecular basis for nanoscopic membrane curvature generation from quantum mechanical models and synthetic transporter sequences. *J. Am. Chem. Soc.* **134,** 19207–19216 (2012).

183. Madani, F. *et al.* Modeling the endosomal escape of cell-penetrating peptides using a transmembrane pH gradient. *Biochim. Biophys. Acta - Biomembr.* **1828,** 1198–1204 (2013).

184. Pae, J. *et al.* Translocation of cell-penetrating peptides across the plasma membrane is controlled by cholesterol and microenvironment created by membranous proteins. *J. Control. Release* **192,** 103–113 (2014).

185. Som, A., Tezgel, A. O., Gabriel, G. J. & Tew, G. N. Self-activation in de novo designed mimics of cell-penetrating peptides. *Angew. Chemie - Int. Ed.* **50,** 6147–6150 (2011).

186. Som, A., Reuter, A. & Tew, G. N. Protein transduction domain mimics: The role of aromatic functionality. *Angew. Chemie - Int. Ed.* **51,** 980–983 (2012).

187. Tezgel, A. Ö., Telfer, J. C. & Tew, G. N. De novo designed protein transduction domain mimics from simple synthetic polymers. *Biomacromolecules* **12,** 3078–3083 (2011).

188. Tezgel, A. Ö. *et al.* Novel Protein Transduction Domain Mimics as Nonviral Delivery Vectors for siRNA Targeting NOTCH1 in Primary Human T cells. *Mol. Ther.* **21,** 201–209 (2012).

189. Hennig, A., Gabriel, G. J., Tew, G. N. & Matile, S. Stimuli-responsive polyguanidino-oxanorbornene membrane transporters as multicomponent sensors in complex matrices. *J. Am. Chem. Soc.* **130,** 10338–10344 (2008).

190. Gabriel, G. J. *et al.* Synthetic mimic of antimicrobial peptide with nonmembrane-disrupting antibacterial properties. *Biomacromolecules* **9,** 2980–2983 (2008).

191. Sgolastra, F., Minter, L. M., Osborne, B. A. & Tew, G. N. Importance of sequence specific hydrophobicity in synthetic protein transduction domain mimics. *Biomacromolecules* **15,** 812–820 (2014).

192. Lienkamp, K. & Tew, G. N. Synthetic mimics of antimicrobial peptides-a versatile ring-opening metathesis polymerization based platform for the synthesis of selective antibacterial and cell-penetrating polymers. *Chem. - A Eur. J.* **15,** 11784–11800 (2009).

193. Takayama, K. *et al.* Effect of the attachment of a penetration accelerating sequence and the influence of hydrophobicity on octaarginine-mediated intracellular delivery. *Mol. Pharm.* **9,** 1222–1230 (2012).

194. Takayama, K. *et al.* Enhanced intracellular delivery using arginine-rich peptides by the addition of penetration accelerating sequences (Pas). *J. Control. Release* **138,** 128–133 (2009).

195. Richard, J. P. *et al.* Cell-penetrating peptides. A reevaluation of the mechanism of cellular uptake. *J. Biol. Chem.* **278,** 585–590 (2003).

196. Suk Choi, Y. *et al.* Cell Penetrating Peptides for Tumor Targeting. *Curr. Pharm. Biotechnol.* **12,** 1166–1182 (2011).

197. Zorko, M. & Langel, Ü. Cell-penetrating peptides: mechanism and kinetics of cargo delivery. *Adv. Drug Deliv. Rev.* **57,** 529–545 (2005).

198. Dupont, E., Prochiantz, A. & Joliot, A. Identification of a Signal Peptide for Unconventional Secretion. *J. Biol. Chem.* **282,** 8994–9000 (2007).

199. Derossi, D., Chassaing, G. & Prochiantz, A. Trojan peptides: the penetratin system for intracellular delivery. *Trends Cell Biol.* **8,** 84–87 (1998).

200. McKinlay, C. J., Waymouth, R. M. & Wender, P. A. Cell-Penetrating, Guanidinium-Rich Oligophosphoesters: Effective and Versatile Molecular Transporters for Drug and Probe Delivery. *J. Am. Chem. Soc.* **138,** 3510–3517 (2016).

201. Joliot, A., Pernelle, C., Deagostini-Bazin, H. & Prochiantz, A. Antennapedia homeobox peptide regulates neural morphogenesis. *Proc. Natl. Acad. Sci. U. S. A.* **88,** 1864–8 (1991).

202. Elmquist, A., Lindgren, M., Bartfai, T. & Langel, Ü. VE-Cadherin-Derived Cell-Penetrating Peptide, pVEC, with Carrier Functions. *Exp. Cell Res.* **269,** 237–244 (2001).

203. Pooga, M., Hällbrink, M., Zorko, M. & Langel, U. Cell penetration by transportan. *FASEB J.* **12,** 67–77 (1998).

204. Alhakamy, N. A. *et al.* Charge Type, Charge Spacing, and Hydrophobicity of Arginine-Rich Cell-Penetrating Peptides Dictate Gene Transfection. *Mol. Pharm.* **13,** 1047–1057 (2016).

205. Jones, S., Uusna, J., Langel, Ü. & Howl, J. Intracellular Target-Specific Accretion of Cell Penetrating Peptides and Bioportides: Ultrastructural and Biological Correlates. *Bioconjug. Chem.* **27,** 121–129 (2016).

206. Blum, A. P., Kammeyer, J. K. & Gianneschi, N. C. Activating Peptides for Cellular Uptake via Polymerization into High Density Brushes. *Chem. Sci.* **7,** 989–994 (2016).

207. Gasparini, G. & Matile, S. Protein delivery with cell-penetrating poly(disulfide)s. *Chem. Commun.* **51,** 17160–17162 (2015).

208. Gasparini, G., Bang, E.-K. K., Montenegro, J. & Matile, S. Cellular uptake: lessons from supramolecular organic chemistry. *Chem. Commun. (Camb)*. **51,** 10389–10402 (2015).

209. Sakai, N., Takeuchi, T., Futaki, S. & Matile, S. Direct observation of anion-mediated translocation of fluorescent oligoarginine carriers into and across bulk liquid and anionic bilayer membranes. *ChemBioChem* **6,** 114–122 (2005).

210. Takeuchi, T. *et al.* Direct and rapid cytosolic delivery using cell-penetrating peptides mediated by pyrenebutyrate. *ACS Chem. Biol.* **1,** 299–303 (2006).

211. Deshayes, S., Morris, M., Divita, G. & Heitz, F. Interactions of amphipathic carrier peptides with membrane components in relation with their ability to deliver therapeutics. *J Pept. Sci Off. Publ Eur. Pept. Soc* **12,** 758–765 (2006).

212. Wimley, W. C. & White, S. H. Experimentally determined hydrophobicity scale for proteins at membrane interfaces. *Nat. Struct. Mol. Biol.* **3,** 842–848 (1996).

213. Sengupta, D., Smith, J. C. & Ullmann, G. M. Partitioning of amino-acid analogues in a five-slab membrane model. *Biochim. Biophys. Acta - Biomembr.* **1778,** 2234–2243 (2008).

214. Yau, W. M., Wimley, W. C., Gawrisch, K. & White, S. H. The preference of tryptophan for membrane interfaces. *Biochemistry* **37,** 14713–14718 (1998).

215. Perret, F. *et al.* Anionic Fullerenes, Calixarenes, Coronenes, and Pyrenes as Activators of Oligo/Polyarginines in Model Membranes and Live Cells. *J. Am. Chem. Soc.* **127,** 1114–1115 (2005).

216. Witte, K., Olausson, B. E. S., Walrant, A., Alves, I. D. & Vogel, A. Structure and dynamics of the two amphipathic arginine-rich peptides RW9 and RL9 in a lipid environment investigated by solid-state NMR and MD simulations. *Biochim. Biophys. Acta - Biomembr.* **1828,** 824–833 (2013).

217. Walrant, A. *et al.* Different membrane behaviour and cellular uptake of three basic arginine-rich peptides. *Biochim. Biophys. Acta - Biomembr.* **1808,** 382–393 (2011).

218. Katayama, S., Hirose, H., Takayama, K., Nakase, I. & Futaki, S. Acylation of octaarginine: Implication to the use of intracellular delivery vectors. *J. Control. Release* **149,** 29–35 (2011).

219. Loudet, A. *et al.* Non-covalent delivery of proteins into mammalian cells. *Org. Biomol. Chem.* **6,** 4516 (2008).

220. Wender, P. a., Galliher, W. C., Goun, E. a., Jones, L. R. & Pillow, T. H. The design of guanidinium-rich transporters and their internalization mechanisms. *Adv. Drug Deliv. Rev.* **60,** 452–472 (2008).

221. deRonde, B. M., Birke, A. & Tew, G. N. Design of Aromatic-Containing Cell-Penetrating Peptide Mimics with Structurally Modified π Electronics. *Chem. - A Eur. J.* **21,** 3013–3019 (2015).

222. Lienkamp, K., Madkour, A. E., Kumar, K.-N. N., Nüsslein, K. & Tew, G. N. Antimicrobial polymers prepared by ring-opening metathesis polymerization: manipulating antimicrobial properties by organic counterion and charge density variation. *Chem. - A Eur. J.* **15,** 11715–11722 (2009).

223. Zorko, M. & Langel, Ü. Cell-penetrating peptides: Mechanism and kinetics of cargo delivery. *Adv. Drug Deliv. Rev.* **57,** 529–545 (2005).

224. Dinca, A., Chien, W.-M. & Chin, M. Intracellular Delivery of Proteins with Cell-Penetrating Peptides for Therapeutic Uses in Human Disease. *Int. J. Mol. Sci.* **17,** 263 (2016).

225. Eguchi, A. & Dowdy, S. F. siRNA delivery using peptide transduction domains. *Trends Pharmacol. Sci.* **30,** 341–345 (2009).

226. Maeder, M. L. & Gersbach, C. A. Genome-editing Technologies for Gene and Cell Therapy. *Mol. Ther.* **24,** 430–446 (2016).

227. Rehman, Z. U., Zuhorn, I. S. & Hoekstra, D. How cationic lipids transfer nucleic acids into cells and across cellular membranes: Recent advances. *J. Control. Release* **166,** 46–56 (2013).

228. Simeoni, F., Morris, M. C., Heitz, F. & Divita, G. Insight into the mechanism of the peptide-based gene delivery system MPG: Implications for delivery of siRNA into mammalian cells. *Nucleic Acids Res.* **31,** 2717–2724 (2003).

229. Backlund, C. M. *et al.* Increased hydrophobic block length of PTDMs promotes protein internalization. *Polym. Chem.* **7,** (2016).

230. deRonde, B. M., Torres, J. A., Minter, L. M. & Tew, G. N. Development of Guanidinium-Rich Protein Mimics for Efficient siRNA Delivery into Human T Cells. *Biomacromolecules* **16,** 3172–3179 (2015).

231. Sarapas, J. M., Backlund, C. M., deRonde, B. M., Minter, L. M. & Tew, G. N. ROMP- and RAFT-Based Guanidinium-Containing Polymers as Scaffolds for Protein Mimic Synthesis. *Chem. - A Eur. J.* **23,** 6858–6863 (2017).

232. deRonde, B. M. *et al.* Optimal Hydrophobicity in Ring-Opening Metathesis Polymerization-Based Protein Mimics Required for siRNA Internalization. *Biomacromolecules* **17,** 1969–1977 (2016).

233. Walker, P. R., Belnoue, E., Dietrich, P. & Derouazi, M. Cell-penetrating peptides—the Swiss Army knife of cancer vaccines. *Oncoimmunology* **5,** e1095435 (2016).

234. Foster, S., Duvall, C. L., Crownover, E. F., Hoffman, A. S. & Stayton, P. S. Intracellular delivery of a protein antigen with an endosomal-releasing polymer enhances CD8 T-cell production and prophylactic vaccine efficacy. *Bioconjug. Chem.* **21,** 2205–2212 (2010).

235. Krishnamachari, Y., Geary, S. M., Lemke, C. D. & Salem, A. K. Nanoparticle delivery systems in cancer vaccines. *Pharm. Res.* **28,** 215–236 (2011).

236. Irvine, D. J., Hanson, M. C., Rakhra, K. & Tokatlian, T. Synthetic Nanoparticles for Vaccines and Immunotherapy. *Chemical Reviews* **115,** 11109–11146 (2015).

237. Kapadia, C. H., Perry, J. L., Tian, S., Luft, J. C. & DeSimone, J. M. Nanoparticulate immunotherapy for cancer. *J. Control. Release* **219,** 167–180 (2015).

238. Murphy, K., Travers, P., Walport, M., & Janeway, C. *Janeway's Immunobiology*. (Garland Science, Taylor & Franscis Group LLC, 2012).

239. Curtsinger, J. M. & Mescher, M. F. Inflammatory cytokines as a third signal for T cell activation. *Curr. Opin. Immunol.* **22,** 333–340 (2010).

240. Pulendran, B. & Ahmed, R. Immunological mechanisms of vaccination. *Nat. Immunol.* **131,** 509–517 (2011).

241. Lin, M. L. *et al.* Selective suicide of cross-presenting CD8+ dendritic cells by cytochrome c injection shows functional heterogeneity within this subset. *Proc. Natl. Acad. Sci. U. S. A.* **105,** 3029–34 (2008).

242. Kelly, C., Jefferies, C. & Cryan, S. Targeted Liposomal Drug Delivery to Monocytes and Macrophages. *J. Drug Deliv.* **2011,** 1–11 (2011).

243. Ueno, H. *et al.* Targeting human dendritic cell subsets for improved vaccines. *Semin. Immunol.* **23,** 21–27 (2011).

244. Johansen, P. T. *et al.* Monocyte targeting and activation by cationic liposomes formulated with a TLR7 agonist. *Expert Opin. Drug Deliv.* **12,** 1045–1058 (2015).

245. Tacken, P. J., Torensma, R. & Figdor, C. G. Targeting antigens to dendritic cells in vivo. *Immunobiology* **211,** 599–608 (2006).

246. Tacken, P. J. *et al.* No advantage of cell-penetrating peptides over receptor-specific antibodies in targeting antigen to human dendritic cells for cross-presentation. *J. Immunol.* **180,** 7687–7696 (2008).

247. Cros, J. *et al.* Human CD14dim Monocytes Patrol and Sense Nucleic Acids and Viruses via TLR7 and TLR8 Receptors. *Immunity* **33,** 375–386 (2010).

248. Kwon, Y. J., Standley, S. M., Goh, S. L. & Fréchet, J. M. J. Enhanced antigen presentation and immunostimulation of dendritic cells using acid-degradable cationic nanoparticles. *J. Control. Release* **105,** 199–212 (2005).

249. Kapadia, C. H., Tian, S., Perry, J. L., Luft, J. C. & Desimone, J. M. Reduction Sensitive PEG Hydrogels for Codelivery of Antigen and Adjuvant to Induce Potent CTLs. *Mol. Pharm.* **13,** 3381–3394 (2016).

250. Jiang, Y., Li, M., Zhang, Z., Gong, T. & Sun, X. Cell-Penetrating Peptides as Delivery Enhancers for Vaccine. *Curr. Pharm. Biotechnol.* **15,** 256–266 (2014).

251. Chikh, G., Bally, M. & Schutze-Redelmeier, M. P. Characterization of hybrid CTL epitope delivery systems consisting of the Antennapedia homeodomain peptide vector formulated in liposomes. *J. Immunol. Methods* **254,** 119–135 (2001).

252. Shibagaki, N. & Udey, M. C. Dendritic cells transduced with TAT protein transduction domain-containing tyrosinase-related protein 2 vaccinate against murine melanoma. *Eur. J. Immunol.* **33,** 850–860 (2003).

253. Mitsui, H., Inozume, T., Kitamura, R., Shibagaki, N. & Shimada, S. Polyarginine-mediated protein delivery to dendritic cells presents antigen more efficiently onto MHC class I and class II and elicits superior antitumor immunity. *J. Invest. Dermatol.* **126,** 1804–1812 (2006).

254. Schutze-Redelmeier, M. P. M., Kong, S., Bally, M. B. & Dutz, J. P. Antennapedia transduction sequence promotes anti tumour immunity to epicutaneously administered CTL epitopes. *Vaccine* **22,** 1985–1991 (2004).

255. Kim, D. T. *et al.* Introduction of soluble proteins into the MHC class I pathway by conjugation to an HIV tat peptide. *J. Immunol.* **159,** 1666–1668 (1997).

256. Lu, J., Higashimoto, Y., Appella, E. & Celis, E. Multiepitope Trojan antigen peptide vaccines for the induction of antitumor CTL and Th immune responses. *J. Immunol.* **172,** 4575–4582 (2004).

257. Pouniotis, D. S., Apostolopoulos, V. & Pietersz, G. A. Penetratin tandemly linked to a CTL peptide induces anti-tumour T-cell responses via a cross-presentation pathway. *Immunology* **117,** 329–339 (2006).

258. Derouazi, M. *et al.* Novel cell-penetrating peptide-based vaccine induces robust CD4+ and CD8+ T cell-mediated antitumor immunity. *Cancer Res.* **75,** 3020–3031 (2015).

259. deRonde, B. M., Torres, J. A., Minter, L. M. & Tew, G. N. Development of Guanidinium-Rich Protein Mimics for Efficient siRNA Delivery into Human T Cells. *Biomacromolecules* **16,** 3172–3179 (2015).

260. Madkour, A. E., Koch, A. H. R., Lienkamp, K. & Tew, G. N. End-functionalized ROMP polymers for biomedical applications. *Macromolecules* **43,** 4557–4561 (2010).

261. van Helden, S. F. G. G., van Leeuwen, F. N. & Figdor, C. G. Human and murine model cell lines for dendritic cell biology evaluated. *Immunol. Lett.* **117,** 191–7 (2008).

262. Dewitte, H. *et al.* Choose your models wisely: How different murine bone marrow-derived dendritic cell protocols influence the success of nanoparticulate vaccines in vitro. *J. Control. Release* **195,** 138–146 (2014).

263. Daigneault, M., Preston, J. A., Marriott, H. M., Whyte, M. K. B. & Dockrell, D. H. The identification of markers of macrophage differentiation in PMA-stimulated THP-1 cells and monocyte-derived macrophages. *PLoS One* **5,** e8668 (2010).